Andreia Sofia da Costa de Mónica Ferreira

# Oxidoreductase protein family interaction with DJ-1 and oxidative stress-induced modulation of HADHA interactome

Dissertação de Mestrado em Biologia Celular e Molecular,
orientada pelo Doutor Bruno Manadas e pelo Professor Doutor Carlos Duarte,
apresentada ao Departamento de Ciências da Vida da Universidade de Coimbra.

Junho 2016

· U C ·

UNIVERSIDADE DE COIMBRA

**Andreia Sofia da Costa de Mónica Ferreira**

# Oxidoreductase protein family interaction with DJ-1 and oxidative stress-induced modulation of HADHA interactome

Dissertação de Mestrado em Biologia Celular e Molecular, orientada pelo Doutor Bruno Manadas (Centro de Neurociências e Biologia Celular, Universidade de Coimbra) e pelo Professor Doutor Carlos Duarte (Departamento de Ciência das Vida, Universidade de Coimbra) e apresentada ao Departamento de Ciências da Vida da Universidade de Coimbra

**Junho 2016**

· U C ·

UNIVERSIDADE DE COIMBRA

Este projecto foi realizado no grupo Life Sciences Mass Spectrometry do Centro de Neurociências e Biologia Celular (Universidade de Coimbra, Portugal), orientado pelo Doutor Bruno Manadas.

O trabalho foi financiado pela Fundação para a Ciência e Tecnologia (FCT), Portugal, com o projecto PTDC/NEU-NMC/0205/2012, UID/NEU/04539/2013 e PEstC/SAU/LA0001/2013-2014, e co-financiado pelo Programa COMPETE (Programa Operacional Factores de Competitividade), pelo QREN, a União Europeira (FEDER – Fundo Europeu de Desenvolvimento Regional), e pela Rede Nacional de Espectrometria de Massa (RNEM), sob o contracto REDE/1506/REM/2005.

The present work was performed in the Life Sciences Mass Spectrometry group of Center for Neuroscience and Cell Biology (University of Coimbra, Portugal), and under scientific guidance of Doctor Bruno Manadas.

The work was supported by Fundação para a Ciência e Tecnologia (FCT), Portugal, projects reference PTDC/NEU-NMC/0205/2012, UID/NEU/04539/2013 and PEstC/SAU/LA0001/2013-2014, and cofinanced by "COMPETE Programa Operacional Factores de Competitividade, QREN, the European Union (FEDER – Fundo Europeu de Desenvolvimento Regional) and by The National Mass Spectrometry Network (RNEM) under contract REDE/1506/REM/2005.

*“So many people along the way, whatever it is you aspire to do, will tell you it can't be done. But all it takes is imagination. You dream. You plan. You reach. There will be obstacles. There will be doubters. There will be mistakes. But with hard work, with belief, with confidence and trust in yourself and those around you, there are no limits.”*

— Michael Phelps with Alan Abrahamson, No Limits: The Will To Succeed

# AGRADECIMENTOS

Antes de mais, gostaria de começar por agradecer ao meu orientador Doutor Bruno Manadas. Não porque é da praxe agradecer ao orientador, mas porque de facto são uns agradecimentos mais do que merecidos. Queria agradecer por me ter acolhido no seu grupo e por me ter dado a oportunidade de fazer este projeto que, para mim, é espetacular. Quero agradecer por todo o apoio, conhecimentos transmitidos, entusiasmo (muito entusiasmo) e inspiração. Um obrigada por fazer de mim uma futura cientista, pela amizade e pela confiança.

Quero também dar um agradecimento muito, mas mesmo muito, especial à Sandra que foi um Anjo que apareceu na minha vida. Não há palavras que descrevam o quão agradecida estou, apenas que tenho a certeza que se este Anjo não existisse, muito provavelmente neste momento não teria agradecimentos para escrever. Obrigada pela orientação, pela ajuda, por todos os conhecimentos que me foram transmitidos, pelo *tough love*, mas especialmente pelos momentos de descontração, pelo divertimento e pela amizade que vou guardar comigo.

A toda a equipa do grupo Life Sciences Mass Spectrometry. À Cátia, à Guida, à Joana e à Vera por toda a ajuda que também me deram quando pedi. À Karolina por me ter poupado umas valentes horas na sala de cultura e…bem e por tudo! Mas especialmente pela diversão, por nunca me deixarem desistir (ou pelo menos apoiar o movimento que se desiste uma, desistimos todas), por todos os momentos "vê-se mesmo que hoje é sexta-feira" e pelas degustações que foram feitas por vários sítios. Agradecer também aos mestres do ano letivo passado, Carolina, Vanessa, Diogo e Nuno por todo o companheirismo, especialmente ao Nuno por ter sido um *partner in crime* neste projeto. No entanto, o que eu vos quero mesmo agradecer é por terem tornado a minha saída do grupo algo que me custa verdadeiramente e por se terem tornado pessoas a quem me custa dizer adeus. Mas não será um adeus, será um até já.

Ao Doutor Mário Grãos por ter cedido aquela que foi por vezes a minha segunda casa, a sala de cultura, e também pela simpatia. Assim, gostaria também de agradecer às meninas da Biologia Celular, Tânia, Heloísa e Daniela por toda a ajuda que também disponibilizaram, pela simpatia e pela diversão.

Às minhas princesas do mestrado, Ana Rafaela, Beatriz, Carina, Inês, Joana, Laetitia, Madalena, Marta, Rafaela e Raquel por significarem o que significam e por terem tornado todo este processo mais fácil e divertido, e por terem feito tudo valer a pena. A todos os meus colegas do mestrado por compreenderem melhor que ninguém aquilo que passei e ultrapassei ao longo destes dois anos e por se terem também tornado aquelas pessoas a quem custa dizer adeus. E porque afinal #aculpaédomestrado.

A todos os meus amigos que me apoiaram, nunca duvidaram de mim, aceitaram o facto de não estar presente tanto quanto queria e aturaram os meus devaneios. Finalmente, e não menos importante, à minha família e especialmente aos meus pais. Por tudo e por nada. Por fazerem o que acharem ser a sua obrigação e que para mim é mais do que um ato de amor. Por serem aqueles que tiveram de lidar com o meu lado menos bom que todo este processo despertou. Por me tornarem a pessoa determinada que sou hoje. Por me amarem como amam! Que isto me possibilite um dia poder retribuir-vos, nem que seja um terço, do que vocês fizeram por mim.

Um enorme obrigada a todos que, de certa forma, me ajudaram a concluir esta etapa!

# ABSTRACT

Parkinson's disease (PD) is the second most common neurodegenerative disease and the most common movement disorder, characterized by massive loss of dopaminergic neurons in the substantia nigra pars compacta (SNpc), leading to degeneration of nigrostriatal dopaminergic pathways. Evidence suggest several cellular dysfunctions important for pathogenesis in PD, including oxidative stress. Even though several efforts have been made to obtain a deeper knowledge of this disease, the etiology and pathogenesis still remain unclear. Nevertheless, there is an agreement that the majority of PD cases are sporadic and some rare cases have familial background. Indeed, mutations in several genes have been reported to cause hereditary forms of the disease, leading to valuable insights into the molecular mechanisms of neurodegeneration.

Among the genetic forms, *Dj1* gene was identified as an autosomal recessive gene responsible for familial early-onset PD, meaning that deeper knowledge on its physiological functions will provide important insights into molecular mechanisms of PD. Several functions have been attributed to DJ-1 protein, being its putative role in neuroprotection the most relevant, probably due to its involvement in protection against oxidative stress. Evidence indicate that DJ-1 operates at multiple levels and interact, directly or indirectly, with several partners. Although the mechanisms through which DJ-1 mediates neuroprotection is not fully understood, it seems to play a pivotal role in the mediation of signaling pathways and modulation of the oxidative metabolism. Several studies reported that indeed oxidative stress is the trigger condition for DJ-1 neuroprotective function, in a way that conformational changes to an oxidized form were pointed out as protein's active form. Moreover, the stability of the majority of the interactions reported is also influenced by the oxidation state of DJ-1. A dynamic DJ-1 interactome screening was previously made in order to provide a comprehensive characterization of DJ-1 binding partners under oxidative stress conditions, leading to the identification of several binding partner. From those, proteins belonging to oxidoreductase family were identified, which are mainly associated with cellular response to oxidative stress, such as NDUFA4, PGDH and HADHA. However, such interactions still require validation.

Based on this, complementary assays were performed to validate DJ-1 interaction with oxidoreductase proteins, such as immunoprecipitation, pull down assay, and immunocytochemistry followed by confocal analysis, in normal and oxidative stress conditions. iImunocytochemistry assay followed by confocal analysis of SH-SY5Y cells revealed that DJ-1 interacts with both PGDH and HADHA proteins *in situ*, thus confirming they are indeed binding partners. Moreover, pull down approach results suggested an interaction between HADHA and PGDH with recombinant WT DJ-1, which is modulated by oxidative stress., thus corroborating previous assumptions.

After confirming HADHA as a DJ-1 bindings partner, an AP-SWATH approach was used to study HADHA interactome in SH-SY5Y cells exposed to normal and oxidative stress conditions, to assess this protein's involvement in cellular response to oxidative stress, and to expand DJ-1's dynamic interactome. With this methodology, it was possible to conclude that HADHA has a dynamic interactome that it is modulated by oxidative stress conditions. Several proteins were identified as binding proteins, like cytoskeleton proteins, motor proteins, proteins involved in DNA repair and gene expression, and in different signaling pathways. Moreover, some of the identified HADHA putative interactors were previously also identified as DJ-1 interactors. The majority of

proteins quantified showed an increased interaction with HADHA in oxidative stress conditions, thus providing insights into their biological functions in cellular response to such insult, pointing to a new HADHA role in neuronal protection against oxidative stress. Such results, also contribute to deeper knowledge on PD pathogenesis, the distinct pathways involved in the establishment and progression of the disease, highlighting potential new targets for PD prognosis, therapy and prevention.

**Keywords:** Parkinson's disease, DJ-1, interactomics, oxidative stress, 3PGDH, HADHA, AP-SWATH, neuroprotection pathways.

# RESUMO

A doença de Parkinson (DP) é a segunda doença neurodegenerativa mais comum, sendo a mais incidente dentro das doenças do movimento, e caracterizada por uma drástica perca de neurónios dopaminérgicos na região cerebral *substantia nigra pars compacta* (SNpc), levando à degeneração dos circuitos dopaminérgicos nigroestriatais. Várias evidências apontam para diversas disfunções celulares importantes na patogénese da DP, incluindo o stress oxidativo. Apesar de vários estudos na área terem sido realizados para uma maior elucidação sobre a doença, a etiologia e patogénese da Doença de Parkinson continuam por estar esclarecidas. No entanto, é sabido que a causa da maioria dos casos de DP são esporádicos, e que alguns casos raros têm uma componente genética, hereditária. De facto, diversas mutações em diversos genes têm sido identificadas como causadoras da forma hereditária da doença, o que contribuiu com importantes conhecimentos sobre os mecanismos moleculares que levam à neurodegeneração.

O gene *dj1*, associado às formas genéticas da DP, foi identificado como sendo um gene autossómico recessivo responsável pela DP familiar, que se desenvolve em idades mais novas, o que o torna um candidato para ser estudado de forma a fornecer importantes conhecimentos sobre os mecanismos moleculares da doença. Várias funções foram atribuídas à proteína DJ-1, no entanto o seu papel de neuroprotecção é o mais relevante, provavelmente devido ao seu envolvimento na proteção contra o stress oxidativo. Estudos indicam que a proteína DJ-1 opera em diversos níveis interagindo, direta ou indiretamente, com várias proteínas. Apesar dos mecanismos através dos quais a proteína exerce a sua função neuroprotetora não serem completamente conhecidos, esta aparenta ter uma importante função na mediação de vias de sinalização e na modelação do metabolismo oxidativo. Vários estudos demonstraram que de facto o stress oxidativo é a condição que despoleta a função neuroprotectiva da DJ-1, alterando a conformação da proteína para uma forma oxidada, que é considerada a sua forma ativa. Além do mais, a estabilidade da maioria das interações estudadas entre a DJ-1 e outras proteínas é influenciada pelo seu estado oxidativo. Tendo isto em mente, o interatoma dinâmico da DJ-1 foi anteriormente estudado, de forma a fornecer uma caracterização abrangente dos interatores da proteína em condições do stress oxidativo. Este estudo possibilitou a identificação de diversas proteínas que interagem com a DJ-1, nomeadamente proteínas pertencentes à família das oxidoredutases, que estão relacionadas com a resposta celular ao stress oxidativo, como a NDUFA4, PGDH e a HADHA. No entanto, as interações da DJ-1 com essas proteínas estão ainda por serem validadas.

Dentro deste contexto, diversas análises complementares foram realizadas de forma a validar a interação da DJ-1 com as proteínas pertencentes à família das oxidoredutases, incluindo imunoprecipitação, *pull down* e imunocitoquímica seguida de uma análise por microscopia confocal, em condições fisiológicas e de stress oxidativo. através do ensaio de imunocitoquímica seguido de análise por confocal das células SH-SY5Y, foi possível validar a interação entre as proteínas *in situ*, o que parece confirmar que tanto a HADHA como a PGDH são interatores da DJ-1. Além disso, os resultados obtides através da análise por *pull down* sugerem uma interação das proteínas HADHA e PGDH com a proteína DJ-1 recombinante, na sua forma nativa, sendo essa interação aparentemente modelado pelo stress oxidativo, o que vem corroborar a os esukltados anteriores.

Após a confirmação de que a proteína HADHA é um interator da DJ-1, o método AP-SWATH foi utilizado de forma a estudar o interatoma da proteína em células SH-SY5Y em células expostas ao stress oxidativo ou em condições fisiológicas, de forma a aferir o envolvimento desta proteína na resposta celular ao stress oxidativa, e para expandir o interactoma dinâmico da DJ-1. Com esta metodologia, foi possível concluir que a proteína HADHA tem um interatoma dinâmico que é modelado pelo stress oxidativo. Diversas proteínas foram identificadas como interatores, pertencendo a diversos grupos funcionais, tais como proteínas do citoesqueleto, proteínas motoras, proteínas envolvidas na reparação do DNA e expressão de genes, e proteínas envolvidas em diferentes vias de sinalização. Além disso, muitas das proteínas identificadas como potenciais interatores da HADHA foram também anteriormente identificadas como interatores da DJ-1. A generalidade das proteínas quantificadas apresentou um aumento de interação com a HADHA em condições de stress oxidativo, fornecendo informações fundamentais sobre as suas funções biológicas associada à resposta celular a essa patologia, apontando para uma nova função da proteína HADHA relacionada com a proteção neuronal contra o stress oxidativo. Estes resultados contribuíram também para o aprofundar dos conhecimentos sobre a patogénese da doença de Parkinson, as potenciais vias envolvidas no despoletar da doença e a sua progressão, podendo fornecer novos potenciais alvos para o prognóstico, terapia e progressão da DP.

**Palavras-chave:** Doença de Parkinson, DJ-1, interatómica, stress oxidativo, 3PGDH, HADHA, AP-SWATH, vias de neuroprotecção.

# TABLE OF CONTENTS

# LIST OF ABBREVIATIONS

| | |
|---|---|
| **3PGDH (PGDH)** | 3-phosphoglycerate dehydrogenase |
| **Ab** | Antibody |
| **ACN** | Acetonitrile |
| **AD** | Autosomal dominant |
| **AO** | Adult onset |
| **AP** | Affinity purification |
| **AP-MS** | Affinity purification followed by mass spectrometry |
| **AR** | Autosomal recessive |
| **BSA** | Bovine serum albumin |
| **Co-IP** | Co-immunoprecipitation |
| **Cys** | Cysteine |
| **DA** | Dopamine |
| **DJ-1** | Protein deglycase DJ-1 |
| **EO** | Early onset |
| **EOPD** | Early onset Parkinson's disease |
| **ERK** | extracellular-signal-regulated kinase |
| **ESI** | Electrospray ionization |
| **FA** | Formic acid |
| **FBS** | Fetal bovine serum |
| **$H_2O_2$** | Hydrogen Peroxide |
| **HADHA** | Trifunctional enzyme subunit α, mitochondrial; TP-α |
| **IDA** | Information-dependent acquisition |
| **IgG** | Immunogloblin G |
| **IP** | Immunoprecipitation |
| **JP** | Juvenile *Parkinsonism* |
| **kDa** | Kilodalton |
| **LB** | Lewy Bodies |
| **LC** | Liquid Chromatography |
| **LOPD** | Late onset Parkinson's disease |
| **LRRK2** | leucine-rich repeat kinase 2 |

| | |
|---|---|
| **m/z** | Mass to charge ratio |
| **MALDI** | Matrix-assisted laser desorption ionization |
| **MAPK** | Mitogen-activated protein kinase |
| **MEM** | Minimum essential media |
| **MPTP** | 1-methyl-4-phenyl-1,2,3,6-tetrahydropyridine |
| **MS** | Mass spectrometry |
| **MS/MS** | Tandem mass spectrometry |
| **NDUFA4** | NADH dehydrogenase [ubiquinone] 1 α subcomplex subunit 4 |
| **NDUFA4L2** | NADH dehydrogenase [ubiquinone] 1 α subcomplex subunit 4-like 2 |
| **Nrf2** | Nuclear factor erythroid 2-related factor |
| ***p*** | p-value |
| **PD** | Parkinson's disease |
| **PDL** | Poly-D-lysine |
| **PINK1** | PTEN-induced putative kinase 1 |
| **ROS** | Reactive oxygen species |
| **SD** | Standard deviation |
| **SDS-PAGE** | Sodium dodecyl sulfate – Polyacrylamide gel electrophoresis |
| **SNpc** | Substantia nigra pars compacta |
| **SWATH** | Sequential windowed data independent acquisition of the total high-resolution mass spectra |
| **TOF** | Time-of-flight |
| **WB** | Western Blot |
| **WT** | Wild type |

# 1 INTRODUCTION

## 1.1 PARKINSON'S DISEASE

Neurodegenerative diseases, as multifactorial conformational disorders, may arise, not only due to genetic or environmental factors, but also as a consequence of aging. These factors may result in abnormal protein dynamics, with defective protein degradation and aggregation, oxidative stress and reactive oxygen species (ROS) formation, thus, impaired bioenergetics and mitochondrial dysfunction, and toxic exposure to metals, as schematized in Figure 1.1 [1].

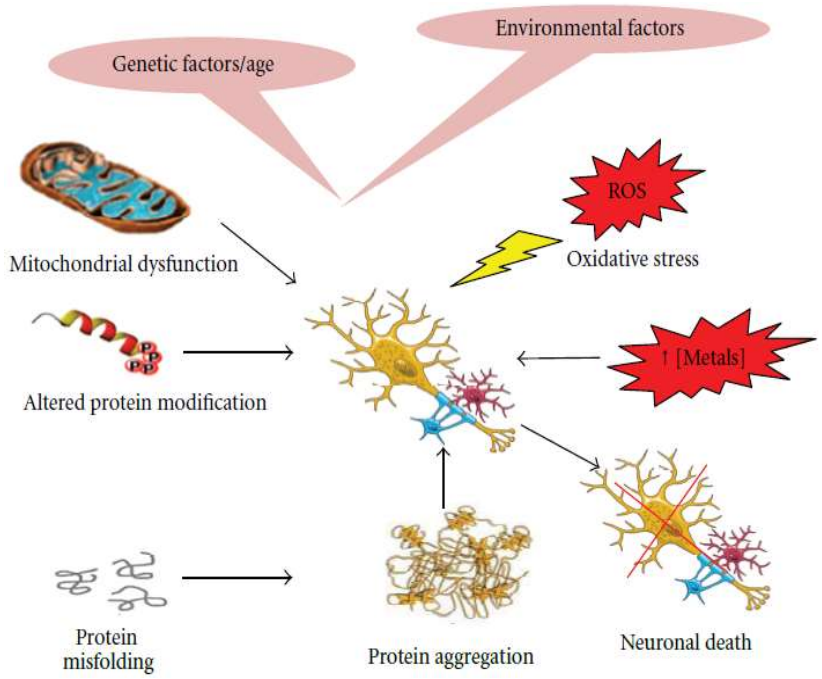


***Figure 1.1*** – Neurodegenerative disorders may arise due to genetic/aging or environmental factors. Such factors can lead to pathologies such as mitochondrial dysfunction, altered protein modification, aggregation, increased oxidative stress, or lethal metal concentration, which leads to neuronal death characteristic of neurodegenerative diseases [1].

Parkinson's Disease (PD) is the second most common age-related neurodegenerative disorder, following Alzheimer's Disease, being the most common movement disorder, with a prevalence of 160/100 000 in Western Europe [2,3]. This disease affects 1-2% of the population older than 65 years old, rising to 4% on the population older than 80 years old, in which 90-95% of the cases are sporadic, whereas the remaining cases have a familial (genetic) background [2–5]. In Germany, it is estimated that the mean total annual cost of PD is 20,095€ per patient [6], and $22,800 in USA [7] (Disability-adjusted life year (DALY) indicator of PD shown in Figure 1.2). However, with the increase in lifespans, it is expected an increase in the prevalence of this disease, which will increase this social and economic burden for society, thus proving the importance of the studies in this area [2,5].

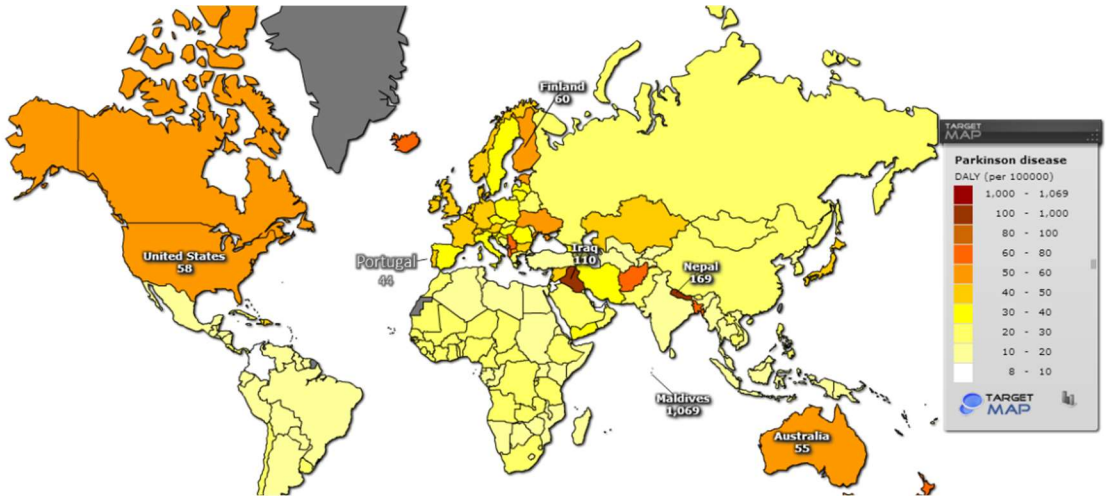


***Figure 1.2*** **–** Disability-Adjusted Life Year (DALY) indicator of Pakinson's Disease. DALY indicator, as a measure of overall disease burden, expresses the number years lost due to ill-healthy, disability or early death. Light-colored countries represent the ones with 8-10 disability-adjusted life years out of 10,000 lost due to PD, whereas the dark-colored countries represent the ones with 1,000-1,069 disability-adjusted life years out of 10,000 lost due to PD (taken from: http://www.targetmap.com/).

PD is characterized by a massive loss of dopaminergic nigrostriatal pathways, more specifically, the loss of neuromelanin-containing neurons in the substantia nigra pars compacta (SNpc) (Figure 1.3 a, b), which consists the primary hallmark of this disease. This loss will lead to a depletion of dopamine (DA) in the striatum, which will cause the motor symptoms known to be associated with this disease: tremor at rest, rigidity, bradykinesia, postural instability, and freezing [2,4,8,9]. Moreover, there are some clinical non-motor symptoms that also result from this depletion of DA and are linked to PD, which become enhanced with the progression of the disease. The most common are dementia, sleep disorders and depression [2,8,10]. Another characteristic of this disease is that by the time the onset of motor symptoms becomes evident, approximately 70% of nigral DA neurons are already lost [2,4,11]. However, similarly to what happens with another neurodegenerative disease, the neuropathology is not confined to this specific brain area and such histological abnormalities may also be visible in other dopaminergic and non-dopaminergic cell groups [11].

The second hallmark of PD is the presence of eosinophilic, cytoplasmic inclusions of fibrillary, misfolded proteins, the so-called Lewy Bodies (LB) (Figure 1.3c). LB are extensively ubiquitinylated and are mainly composed of α-synuclein, but they may also have in their constitution parkin, synphilin, neurofilaments and synaptic vesicle proteins [9].

There are numerous distinct pathologies that share features with PD, meaning that the definitive diagnosis of this disease can only be accomplished with *post-mortem* analysis, through autopsy, which is not only based on the loss of striatal DA neurons but also in the presence of Lewy Bodies [12].

The current treatment in use is the administration of L-DOPA, a precursor in dopamine metabolism, which will increase the production of dopamine, however, this only provides symptomatic relief, as do other current treatments, without altering the neurodegenerative process and disease progression. Moreover, some studies show that the administration for long periods of time (5-10 years) will lead to the development of adverse events. Thus, some research groups have directed their studies effort towards extending the knowledge of the etiology and pathogenesis of PD for the development of a more effective therapy that would allow the slow

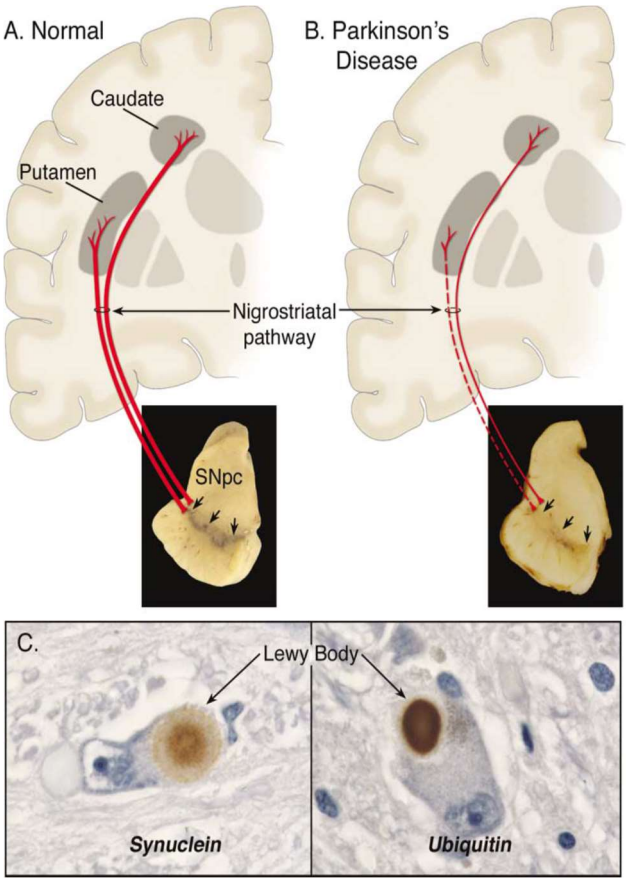


***Figure 1.3*** **-** Neuropathology of PD. (A) Schematic representation of the normal nigrostriatal pathway (in red). It is composed of dopaminergic neurons whose cell bodies are located in the SNpc (see arrows). These neurons project their axons (thick solid red lines) to the basal ganglia and synapse in the striatum (i.e., putamen and caudate nucleus). The image shows the normal pigmentation of the SNpc. (B) Schematic representation of the diseased nigrostriatal pathway (in red). In PD, the nigrostriatal pathway degenerates. There is a marked loss of dopaminergic neurons that project to the putamen (dashed line) and a much more modest loss of those that project to the caudate (thin red solid line). The image shows depigmentation (i.e., loss of dark-brown pigment; arrows) of the SNpc due to the marked loss of dopaminergic neurons. (C) Immunohistochemical labeling of intraneuronal inclusions, termed Lewy bodies, in a SNpc dopaminergic neuron. Immunostaining with an antibody against α-synuclein reveals a LB (black arrow) with an intensely immunoreactive central zone surrounded by a faintly immunoreactive peripheral zone (left image) [9].

progression of the disease, or even cease it [2,13,14]. Indeed, a recent study, reported a DJ-1 based peptide, which was able to attenuate dopaminergic degeneration in experimental models of PD by enhancing Nrf2 pathway, as a therapeutic target in PD and a disease-modifying drug candidate [15], although there are still some parameters to be assessed in this study before moving to clinical trials, this report already shows the potential of this peptide, and how the research in the area of PD disease-modifying therapies is evolving.

### 1.1.1 Etiology

The specific etiology of Parkinson's Disease remains unknown, but the determination of this disorder's cause has been the focus of research efforts for many decades [12,16].

As mentioned before, the majority of PD cases arises spontaneously, but in the minority of the cases arises in an inherited, mendelian, way. Although both sporadic and familial cases of PD

are quite similar, the genetic forms of the disease normally have an earlier onset and are associated with atypical clinical features [5,12].

The sporadic forms of PD develop due to environmental factors, individual's lifestyle and exposure to some toxins, and the discovery of these toxins as enhancers of such pathology helped in the determination of PD's animal models. As for the genetic forms of PD, they arise from mutations on specific PD-associated genes. Moreover, it can also occur a synergetic effect between environmental and genetic factors that will modify the propensity of the individual to develop PD [12,17]. However, one factor that strongly correlates with the onset is age or aging process [10]. Until recently, the hypothesis regarding the cause and mechanisms of PD neurodegeneration derived from information obtained from autopsy tissues from individuals with PD, such situation changed with the identification of mutations in genes associated with the disease [12,16].

#### 1.1.1.1 Environmental Factors

PD is characterized as a slow progression sporadic and idiopathic disease, but although significant insights and hypothesis have been proposed in recent years, the origin of sporadic PD remains undetermined, thus the specific etiology of PD is still a subject under thorough studies. Some epidemiological studies have reported that PD incidence may differ internationally, with North America and Europe showing high rates of the disease [18], clearly proving that environmental factors play an important role in the onset of the disease. This and many other epidemiological studies have, thus, enhanced the impact of environmental factors in PD's etiology. In fact, there were several reports showing that lifestyles, like rural living with exposure to pesticides, drinking well water, certain occupations like mining and welding, or even a high caloric intake diet, appears to confer an increased risk for PD [9,18–20].

The environmental hypothesis states that the neurodegeneration is mediated by the exposure to a dopaminergic neurotoxin. In theory, the progressive neurodegeneration could be produced by chronic neurotoxin exposure, or by limited exposure, initiating a cascade of deleterious events [21,22].

The first evidence of an exogenous toxin that could mimic the clinical and pathological features of PD came in 1983 when Langston and his collegues[21] discovered, by chance, the neurotoxin 1-methyl-4-phenyl-1,2,3,6-tetrahydropyridine (MPTP), a byproduct of the illicit manufacture of a synthetic meperidine derivative [21,23]. This report studied a group of people with drug addiction problems that used a drug contaminated by MPTP and observed that one week after the injection they start developing *Parkinsonism*, a syndrome in which patients develop PD-like syndromes [21]. Since then, several studies have been made in order to understand the mechanism through which MPTP induces cytotoxicity. It was reported that MPTP by itself is not toxic, but it has an active form, 1-methyl-4-phenylpyridinium ($MPP^+$), which is responsible for its toxic effect. However, contrary to MPTP, which is a lipophilic component, $MPP^+$ is not able to cross the blood-brain barrier (BBB) (Figure 1.4). Thus, MPTP will enter the brain, where it will be internalized by glial cells and metabolized into its active toxic form, $MMP^+$, by the enzyme MAOB. $MMP^+$ is then released by astrocytes and will compete with dopamine for the dopamine transporter (DAT), consequently, the transporter will allow the entrance of the toxin into dopaminergic neurons where it will interfere with mitochondrial complex I, which will cause the

formation of ROS and bioenergetics impairments, leading to cell death, similarly to what is observed in PD cases [9,23].

The environmental hypothesis was reinforced by similar studies in two different molecules: paraquat and rotenone [22,24], which are two of the most widely used pesticides worldwide. Paraquat, which is structurally similar to $MPP^+$, is an herbicide, and rotenone is a pesticide, which is also largely used to kill unwanted lake fish. Paraquat-mediated toxicity seems to be derived from the production of superoxide radicals, functioning as an oxidative stressor, whereas rotenone-mediated toxicity comes from its function as mitochondrial complex I inhibitor, which, for both cases, will result in dopaminergic neurons degeneration accompanied by an increase in α-synuclein-containing inclusions [22,24].

Although these studies show that these toxins are related to PD, no convincing data seems to suggest that they are the specific cause of sporadic PD onset, as no MPTP-like factor has, to date, been identified in PD patients, and both paraquat and rotenone, even with chronic exposure, are unlikely to cause the disease. However, acute administration of related neurotoxins has been useful for providing experimental models of the disease [13,19].

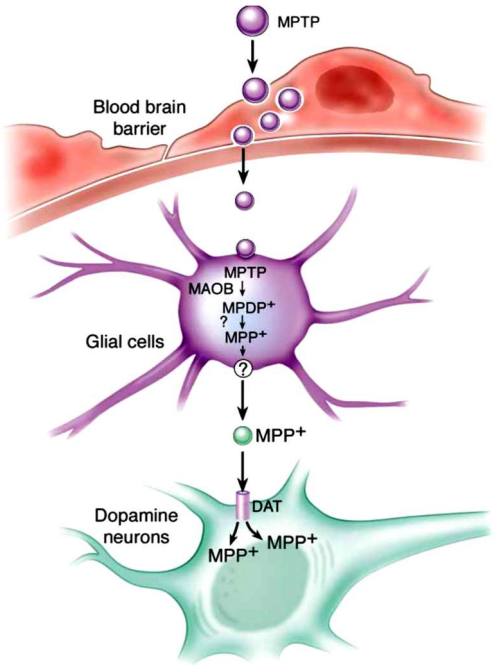


***Figure 1.4*** – MPTP metabolism. After crossing the blood brain barrier, MPTP is uptaken by glial cells where it will be transformed into $MPP^+$, the toxic form of the compound, that will compete with DA for DAT transporter and enter DA neurons (adapted from Dauer & Przedborski, 2003 [9]).

On the other hand, other studies, have reported that cigarette smoking, coffee drinking and alcohol intake are inversely associated with the risk for development of PD, reinforcing this way the concept that environmental factors are associated with PD, being able to, at least, modify susceptibility to this disorder [9,17].

This seems to indicate that both environmental and genetic factors contribute to the onset of the illness to a point now where increasingly genetic predisposition must be seen as a major contributor to the underlying cause [9,19,20].

#### 1.1.1.2 Genetic Factors

Since the mid-1990's, with the discovery of an Italian kindred with a family history of Parkinson's disease associated with a mutation in α-synuclein-encoding gene (*snca*), the theory of PD's relating gene arose [12,25]. This and other studies allowed a better understanding of the disease pathogenesis, which is becoming clearer with the identification of several other gene mutations associated with PD [5,9].

Even though PD is characterized as a sporadic disease, in which the majority of the cases have an idiopathic cause, there is a small part of the cases that occur due to mutations in PD-associated genes, transmitted in either an autosomal-dominant or autosomal-recessive pattern [26,27]. The regions of the genome in which these genes map are known as PARK loci [26,27].

Since the discovery of the first gene linked to PD (*snca*, PARK1 locus), a total of 18 PD loci have been reported through linkage analysis (PARK1-PARK15) or genome-wide association studies (GWAS) (PARK16-PARK18) (Table 1.1) [4,26,27].

***Table 1.1*** **– Gene/Loci Underlying Monogenic *Parkinsonism*** (Adapted from Bekris *et al*., 2010 [26])

| PARK Locus | Gene | Inheritance | Type of *Parkinsonism* |
|---|---|---|---|
| **PARK1/PARK4** | *snca* | AD | EOPD |
| **PARK2** | *prkn* | AR | Juveline and EOPD |
| **PARK3** | *Unknown* | AD | LOPD |
| **PARK5** | *uchl1* | AD | LOPD |
| **PARK6** | *pink1* | AR | EOPD |
| **PARK7** | *dj1* | AR | EOPD |
| **PARK8** | *lrrk2* | AD | LOPD |
| **PARK9** | *atp13a2* | AR | Kufor-Rakeb syndrome |
| **PARK10** | *Unknown* | Not clear | LOPD |
| **PARK11** | *gigyf2* | AD | LOPD |
| **PARK12** | *Unknown* | Not clear | Not clear |
| **PARK13** | *omi/htra2* | Not clear | Not clear |
| **PARK14** | *plag6* | AR | AO dystonia – *Parkinsonism* |
| **PARK15** | *fbxo7* | AR | EO parkinsonian-pyramidal syndrome |
| **PARK16** | *Unknown* | NA | NA |
| **PARK17** | *gak* | NA | NA |
| **PARK18** | *hla-dra* | NA | NA |

Abbreviations: AD (autosomal dominant), AR (autosomal recessive), AO (adult onset), EO (early onset), EOPD (early onset Parkinson disease), LOPD (late-onset Parkinson disease), NA (not assigned).

Although follow-up genetic studies are inconsistent for some of those genes, there is an ample evidence that five of those (*snca*, *lrrk2*, *prkn*, *pink1*, *dj-1*) cause familial *Parkinsonism*, resulting in a disease that closely resembles the clinical features of idiopathic PD (Table 1.2) [5,25–27].

These monogenic forms of PD can be classified according to its inheritance pattern. The autosomal recessive form is linked to mutations in *prkn*, *pink1,* and *dj-1,* and are characterized by an early onset of the disease. As for the autosomal dominant form, there have been identified mutations in *snca* and *lrrk2* genes [4,5]. Mutations in these susceptibility genes are known to affect biochemical processes involved in PD pathogenesis, such as mitochondrial activity (*dj1* and *pink1*),

oxidative stress (*snca* and *dj-1*), intracellular signaling (*dj1* and *lrrk2*) and, in particular, protein aggregation (*parkin* and *snca*) [4].

***Table 1.2* – Overview of the mutations in the five major PD genes and proteins' feature** (Adapted from references [5,27])

| Gene | Protein | Function | Inheritance | Mutation | Phenotype/onset |
|---|---|---|---|---|---|
| ***snca*** | α-synuclein | Enriched in synaptic terminals; vesicle trafficking | AD | Missense | EOPD<br>Lewy bodies |
| ***lrrk2*** | Dardarin | Kinase/GTPase | AD | Missense | Late-onset |
| ***parkn*** | Parkin | Ubiquitin E3 ligase | AR | Nonsense<br>frameshift<br>missense | *Parkinsonism*<br>Juvenil < 40 years |
| ***pink1*** | PINK1 | Mitochondrial kinase | AR | Nonsense<br>frameshift<br>missense | *Parkinsonism*<br>30-50 years |
| ***dj1*** | DJ-1 | Redox-sensitive chaperone | AR | Missense | *Parkinsonism*<br>20-40 years |

Abbreviations: AD (autosomal dominant), AR (autosomal recessive), EOPD (early onset Parkinson's disease), LOPD (late onset Parkinson's disease).

*Snca*, the α-synuclein protein codifying-gene, was the first gene associated with familial onset of PD, when the mutation Ala53Thr was discovered in an Italian family and in another three unrelated Greek families, around 1996 [25]. Studies underlying this susceptibility gene were carried out and two more single point mutations were found, in which one (Ala30Pro) was found in a German family [28], and the other (E46K) was found in a Spanish family [29]. These studies seem to suggest that a single mutation in human *snca* gene is sufficient to account for PD phenotype. These mutant forms are often associated with an early-onset forms of PD, which is usually more aggressive, progress more rapidly and in some cases present atypical clinical features [26,28,29]. Besides these three missense mutations, there are also duplications and triplications of *snca*, indicating toxicity of wild-type (WT) forms of the protein is sufficient to trigger the disease [4,26,27]. Phenotype comparison analyses indicate that patients with duplications show features resembling idiopathic PD, with late age-of-onset, slow progression, and no atypical features, whereas those with triplications have earlier onset, faster disease progression, marked dementia, and frequent dysautonomia, suggesting that *snca* gene dosage might play a role in age-of-onset, disease duration, and severity [26,27].

SNCA is a small protein, composed of approximately 140 amino acids, which is typically found as a natively unfolded, soluble protein in the cytoplasm or associated with lipid membranes, although it can adopt partially folded structures. It is a major constituent of LBs, where it assumes a fibrillary, β-pleated-sheet conformation and binds to other proteins such as chaperonins or antiapoptotic factors. The exact biological function of this proteins still remains controversial, although there is evidence that implicates α-synuclein in neurotransmitter release and vesicle turnover at the presynaptic terminals [4,5,27].

α-synuclein is widely expressed throughout the nervous system and enriched in presynaptic nerve terminals, in close association with synaptic vesicles and the plasma membrane, where it binds reversibly to brain vesicle and components of the vesicular trafficking machinery. More specifically, in striatal dopaminergic terminals, this protein participates in the modulation of synaptic function, possibly by regulating DA release through modulation of the cycling rate of

readily releasable pools [26,27]. A study published in 2000 revealed that the downregulation of *snca*, using an antisense oligonucleotide, in hippocampal cell culture, decreased the distal pool of synaptic vesicles and altered expression of vesicular-associated proteins[30], thus showing this protein might have a synaptic vesicle-related role.

The second gene belonging to the autosomal dominant form of inheritance is *leucine-rich repeat kinase 2* gene (*lrrk2*), which has been only recently added to the list of genes implicated in PD. Mutations in this gene have a relatively high frequency, up to 2% in sporadic late-onset PD patients, being the most frequently mutated gene of the five major susceptibility PD genes. The initial publications underlying mutations in *lrrk2* [31,32] identified four different pathogenic missense mutations segregating in families of European and North-American origin. However, subsequent mutation analyzes identified a total of 80 missense mutations, in which five were proven to be pathogenic; two substitutions have been associated with an increased risk for sporadic PD. Clinically, mutations in this gene result in the more typical late-onset form of PD, being difficult to distinguish from sporadic PD cases, even though LB pathology is sometimes absent [5,31–33].

*Lrkk2* codes the protein dardarin, a 2.527 amino acids protein with a molecular weight of 280 kDa. This protein is expressed in most brain regions, including the substantia nigra, caudate nucleus, and putamen but also outside the CNS, however, immunocytochemistry has so far failed to highlight any specific neurodegenerative lesion, thus being unclear how protein mutations result in neuropathology. Dardarin protein contains LRR and WD40 domains, responsible for a protein-protein interaction function, as well as GTPase and kinase domains, responsible for proteins phosphorylation. However, the exact biological function of this protein remains largely unknown, thus, further genetic and functional studies are necessary to identify dardarin modifiers, either genetic or environmental, that might influence age-of-onset and contrasting clinical and pathological presentations [5,31,33].

The first of the three recessive PD genes identified is *prkn*. Mutations in this genes were first reported in Japanese families with autosomal recessive, juvenile *Parkinsonism* (AR-JP) [34], with age-of-onset typically between childhood and 40 years. Point mutations are the most frequent lesions in *prkn*, with at least 57 being reported, in a total of more than 100 mutations already described, which can alter WT *prkn*-codified protein cellular localization, solubility or propensity to aggregate or event result in loss-of-function of the protein. Such mutations account for over 50% of patients with juvenile onset *Parkinsonism*, however mutations frequency diminishes substantially with increasing age of onset. Nevertheless, this is the most prevalent gene associated with early-onset *Parkinsonism*. Clinically, patients with a mutation in this gene present dystonia, slow progression of the disease and are L-DOPA responsive. Pathologically, although patients exhibit loss of pigmented nigral dopamine neurons, LBs are usually absent [19,26,35].

*Prkn* codes a 465 amino acids protein, Parkin, which is thought to function as an E3- ligase, conjugating ubiquitin to proteins to target them for degradation, thus, playing a role in the ubiquitin-proteasome system [35]. It is present predominantly in the cytosol and cellular vesicle; however, part of the cellular Parkin pool associates with the outer mitochondrial membrane (OMM) of depolarized mitochondria, promoting ubiquitination of OMM proteins involved in upregulation of mitochondrial fusion, and consequent removal of such proteins [36]. This shifts the equilibrium between fission and fusion towards increased fission, thus promoting mitochondrial fragmentation, stimulating cellular autophagic machinery to degrade impaired mitochondria through mitophagy. Moreover, overexpression of this protein in model systems seems to be neuroprotective, indicating that disruption of this ligase function in mutants may evoke cellular

damage. Nonetheless, further investigation is necessary to establish the exact physiological functions of Parkin and how a mutation in the gene induces selective degeneration of nigral neurons in AR-JP without LB formation [19].

The second most common cause of autosomal recessive PD, after Parkin, was first associated with PARK6, in studies carried out with a large consanguineous Italian family with AR-JP [37]. Further studies identified *P-TEN-induced putative kinase 1 (pink1)* as the disease-causing gene [38]. *Pink1* mutations have been reported to account for approximately 1-3% of early-onset PD in population of European ancestry. The majority of the mutations are either missense or nonsense, and most of them are located in a highly conserved amino acid position in the protein kinase domain. Defects in this gene seem to affect protein stability, location and kinase activity, and also to disrupt mitochondrial membrane potential under stress conditions. Although age-of-onset for *pink1*-related PD is usually around 40-50 years old, clinical features are similar to those of late-onset PD, showing slow progression, excellent response to L-DOPA and, in some cases, dementia [19,26].

PINK1, the protein coded by *pink1* gene, has 581 amino acids and is a putative serine/threonine kinase involved in the mitochondrial response to cellular and oxidative stress [38], playing a role in PINK1/Parkin pathway. As a mitochondrial protein, it is located in the matrix and the intermembrane space, being ubiquitously expressed throughout the brain and systemic organs [38,39]. Once located at the OMM of damaged mitochondria, PINK1 initiates the process of mitophagy and mitochondrial degradation by recruiting parkin to the mitochondria. The WT form of the protein appears to be important in neuroprotection against mitochondrial dysfunction and proteasome-induced apoptosis, whereas the majority of its mutations seem to impair this protective effect, as their kinase activity is inhibited. It is, thus, clear the pivotal role of PINK1 in maintaining mitochondrial homeostasis and protecting the cell against stress-induced apoptosis by regulating mitochondrial networks, decreasing mitochondrial oxidative stress and modulating autophagy, together with Parkin [5]. However, the neuropathology caused by PINK1 mutations still remains unknown, as no autopsy resulted from *pink1*-causing disease has been reported, thus, kinase activity assays and substrate identification will be particularly important for unraveling the role of this protein in dopamine cell death and *Parkinsonism* [19].

The last member of the autosomal recessive form of PD was associated to PARK7 locus, after studies in consanguineous families from genetically isolated communities in the Netherlands and Italy [40], that was further reported to be *dj1* gene [41]. Mutations in this gene are associated with AR-JP and cause rare familial PD, as the recessively inherited deletions and missense mutations that have been identified are associated with less than 1% of early-onset *Parkinsonism*, putatively resulting in protein loss of function [19,36]. Clinically, age-of-onset is usually around the third decade with a slow progression and a good response to L-DOPA, however, some patients present other clinical features like psychiatric symptoms, short statue and brachydactyly [26]. Although *dj1* mutations are very rare, recent studies suggest that mutations in this gene may also play an important role in sporadic late-onset PD, as altered levels of DJ-1 or isoforms have been reported in brains [42], cerebrospinal fluid [43] and plasma [44] of sporadic PD patients, providing a common role between idiopathic and hereditary disease. However, very few patients carrying *dj1* mutations have been reported in the literature, meaning there is a limited knowledge of the clinical features, neuropathology and genotype-phenotype correlation of *dj1*-related PD, and further studies are needed[5,26,36].

This gene encodes DJ-1, an 189 amino acids protein that belongs to the family of molecular chaperones, which are induced during oxidative stress. DJ-1 is ubiquitously expressed and abundant in most mammalian tissues, including the brain where it is found in both neuronal and glial cells. It is localized in both the nucleus and cytoplasm, where it exists as a dimer, but it can also translocate into the mitochondria where it appears to act as an antioxidant [26,42]. This protein seems to be an oxidative stress sensor and ROS scavenger, which might play a particularly important role in nigral dopamine neurons that are exposed to high levels of oxidative stress [26]. Functional studies reported that the WT protein has a pivotal role in cellular survival, which is mediated through the phosphorylation of PKB/Akt by PTEN. The L166P mutant protein, the most aggressive mutation identified so far, has been shown to be associated with loss of nuclear localization and translocation to mitochondria, which is suggested to be a requirement for neuroprotection [19]. DJ-1 is thought to protect neurons from oxidative stress, although exactly how it exerts its protective effects remains to be elucidated.

### 1.1.2 Pathophysiology

The identification of genes related to the onset of the disease that contributes to PD susceptibility is of obvious importance. Studies regarding such genes would help to understand the pathogenic of the disease and the molecular pathways that lead to neuronal death. However, it is worth noting that genes and their protein products, do not work alone in the cell but are, rather, organized into pathways, meaning that proteins can have multiple functions within cells depending on the signaling context of the pathway. Moreover, the existence of these PD-associated genes suggests that even sporadic PD has a significant genetic component, and the shared phenotypes associated with different mutations, are consistent with the likely existence of different pathological mechanisms that could lead to *Parkinsonism* [45,46]. Among a variety of mechanistic hypothesis, available data seems to favor impaired protein degradation and accumulation of misfolded protein as the unifying factor linking genetic alterations to dopaminergic neurodegeneration in familial PD. However, there are at least two more types of cellular dysfunction that also have a crosslink in the pathway promoting pathogenesis in PD: mitochondrial respiration defect and oxidative stress. These dysfunctions are not mutually exclusive, and one of the key aims of current PD research is to understand the sequence in which they act and which points of interaction in these pathways result in the neuronal damage characteristic of PD [9,12,26]. Figure 1.5 illustrates a proposed mechanism through which these pathways may crosslink with each other [47].

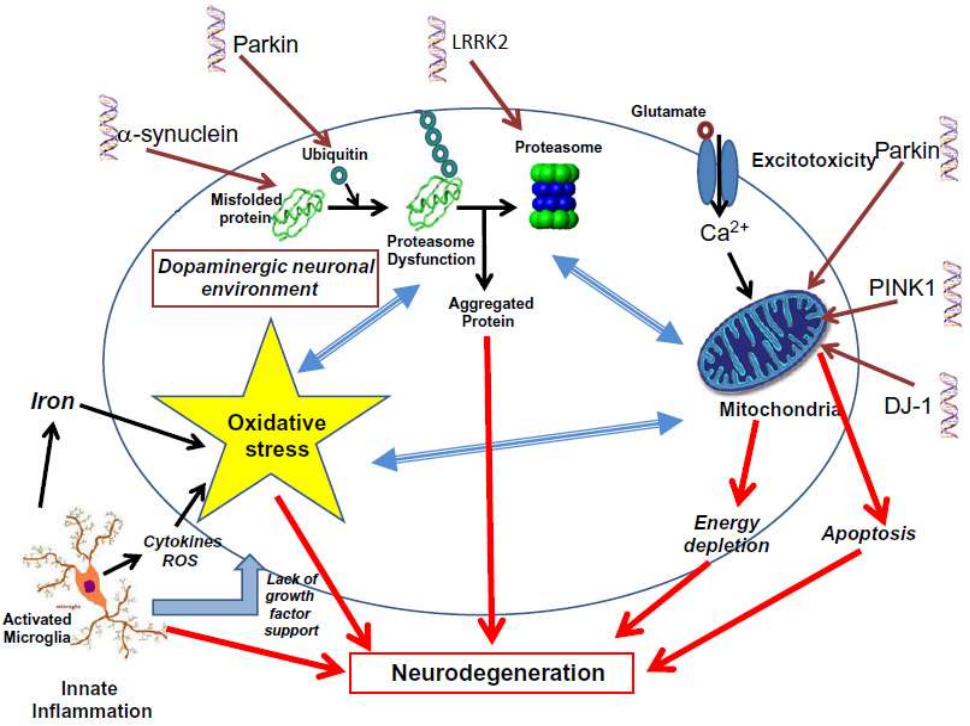


***Figure 1.5*** - Key molecular mechanisms that contribute to neurodegenerative process in Parkinson disease. Blue double-headed arrows indicate molecular mechanisms that may not only be toxic in their own right but importantly may also influence other molecular mechanisms known to be features in Parkinson disease. Double helix structures identify some of the common gene mutations found in familial PD and brown arrows indicate where the altered protein may interfere with cell function and overlap with known mechanisms of cell death in sporadic Parkinson disease (Adapted from Dexter & Jenner, 2013 [47]).

#### 1.1.2.1 Misfolding and Aggregation of Proteins

The aggregation of misfolded proteins has for long been associated with age-related neurodegenerative diseases, as the abnormal deposition of proteins has been tracked in brain tissue of patients affected by such disorders [9]. Truncated translational polypeptide products, misfolded intermediates, and unassembled subunits of oligomeric proteins complexes frequently expose hydrophobic regions. Hence, due to the hydrophilic nature of cellular medium, hydrophobic surfaces from different misfolded proteins tend to interact with each other and form cellular aggregates. Although the composition and location of protein aggregates differ between diseases, this common feature suggests that protein deposition *per se* might be toxic to neurons [1].

The mechanisms through which these aggregates exert their neurotoxicity are quite variable. These aggregates could directly cause damage to the cell by interfering with intracellular trafficking in neurons, or even by sequestering proteins important for cell survival [9]. Curiously, inclusion formation, while possibly indicative of a cell under attack that causes neurotoxicity, may be a defensive mechanism aimed to remove toxic soluble misfolded proteins [48]. In PD, this neurotoxicity evoked by proteins aggregation arises from direct protein-damaging modification or from dysfunctions of chaperones or proteasome that may indirectly contribute to the accumulation of misfolded proteins. The inability of the cell to detect and degrade misfolded proteins might occur due to mutations in *prkn*, whereas *snca* and *dj1* mutations seem to be the

cause of abnormal protein conformations that lead to the overwhelming of the main cellular protein degradation system [49,50]. Under physiological conditions, cells respond to misfolded proteins by inducing chaperones that will promote the refolding process, however if proteins are not properly refolded, they will be targeted for proteasomal degradation. It is known that activity of the proteasome and the ability to induce a variety of chaperones is decreased with aging, which will lead to the accumulation of misfolded proteins and provokes a vicious cycle, with excess buildup of unwanted proteins, which should have been cleared, inhibiting an already compromised clearance pathway. These defects in the protein turnover machinery may lead to a slow degeneration of dopaminergic neurons, which may explain progressive nature of PD [4,50].

#### 1.1.2.2 Mitochondrial Dysfunction

The discovery of environmental toxins, such as MPTP, rotenone, or paraquat as disturbers of mitochondrial complex I, causing dopaminergic cell death and inducing the formation of LB-like filamentous inclusions, thus leading to *Parkinsonism*, suggested an involvement of mitochondria in PD.

The presence of the previously mentioned proteins aggregates has been widely reported to permeabilize both cell and mitochondrial membranes, indicating they might be responsible for processes such as calcium dysregulation, membrane depolarization, and impairment of mitochondrial functions, which have been identified as the common feature of most neurodegenerative disorder [47,49,51,52]. In fact, inhibition of complex I was shown to be present in SNpc [53], that was further proven to be tissue and disease specific [54]. Although it is unclear why neurons in this region are preferentially lost in PD, mitochondria in these neurons seem to be particularly vulnerable to mitochondrial stress and damage. Turnover of dopamine itself may lead to oxidative damage and these neurons are subject to particularly high fluxes of calcium, which drive their basal firing activity [47,51]. Thus, due to such stresses, probably mitochondria in SNpc have higher mtDNA mutation rate (sign of oxidative stress) than in any other region [52]. Mitochondrial defects could subject cells to oxidative stress, due to a toxic production of superoxide radical. It could even contribute to cell degeneration through decreased ATP synthesis (since complex I is dysfcuntional) and consequent bioenergetics defect, thus promoting apoptosis. This seems to be problematic as neurons are post-mitotic cells, meaning any mitochondrial damage acquired will accumulate over the individual's lifetime, leading to progressive mitochondrial dysfunction [55]. Moreover, a study using cytoplasmic hybrid cell lines (cybrids) from patients with sporadic PD revealed deficits in complex I to be stably transmitted, raising even more the concern about mitochondrial role in the disease and the crosslink between idiopathic and familial PD [56].

Remarkably, mutations in α-synuclein, Parkin, PINK1, and DJ-1, and at some instances LRRK2, have been associated with altered mitochondrial function. These mutations can be responsible for altered protein localization in mitochondria, abnormalities in mitochondrial structure and function, and a decrease in complex I assembly and activity. Loss of function of DJ-1, Parkin and PINK1 decreases mitochondrial protection against oxidative stress, which in turn increases mitochondrial dysfunction [47]. Another important role of Parkin and PINK1 is the turnover of mitochondria by autophagy (mitophagy), in which they act together to regulate this process. When mitochondrial membrane potential is low, PINK1 is requested to the mitochondrial membrane, which will then recruit Parkin leading to the ubiquitination and ultimately to

autophagy [55]. Defects in these processes may be critical as they will reduce cell's ability to remove damaged mitochondria, leading to the issues mentioned before [45,47,55].

#### 1.1.2.3 Oxidative Stress

The role of oxidative stress in the pathogenesis of PD has been receiving increased attention with the discovery of dopamine itself as a source of oxidative stress, contributing to the explanation of selective degeneration of DA neurons in SNpc [57]. Whenever there is an excess amount of cytosolic DA outside the synaptic vesicle in damaged neurons, it is easily metabolized, via monoamine oxidase (MAO), or by auto-oxidation, into DA-quinone, a cytotoxic ROS able to damage proteins. Moreover, the presence of ROS-generating enzymes, such as tyrosine hydroxylase (TH) and MAO, increase DAergic neurons susceptibility to oxidative stress [57,58]. In both sporadic and familial PD, oxidative stress is thought to be the common underlying mechanism that leads to cellular dysfunction and neurodegeneration. As such, studies in *post-mortem* tissue revealed the presence of increased levels of oxidized lipids, proteins, and DNA, decreased levels of reduced glutathione (GSH), increased levels of iron, and reduction of ferritin concentrations in the substantia nigra of PD patients [58,59]. Also, defects within the respiratory chain and dopamine metabolism, as mentioned before, contribute to free radical production [57–59].

The source of oxidative stress remains quite controversial, with both neuronal and glial cells being implicated as possible sources, but there are still questions raised about which is the most likely contributor. Nevertheless, it is known that the induction of oxidative stress in PD occurs through accumulation of iron in SNpc, changes in calcium channel activity, altered proteolysis, changes in α-synuclein aggregation, and the presence of mutant proteins (such as DJ-1, for example) [47]. This oxidative damage can directly impair protein ubiquitination and degradation systems leading to cell death mechanisms through the accumulation of toxic products. DJ-1 is, indeed, known to have a pivotal role in oxidative stress, as when exposed to such conditions, the protein will associate with parkin, potentially linking these proteins into a common molecular pathway that lead to nigral degeneration and PD [36,47]. Moreover, there are some studies relating the oxidative state of DJ-1 and the cell fate in response to oxidative stress. Ji Cao and colleagues in 2014 reported that under mild oxidative stress, a moderate oxidation state of DJ-1 is recruited to apoptosis signal-regulating kinase 1 (ASK1) pathway and this interaction inhibits its activity, keeping the cell alive by activating, instead, autophagy. However, under lethal levels of oxidative stress, excessively oxidized DJ-1 is dissociated from AKS1, thereby activating it, which initiates an apoptotic pathway that will result in cell death [60].

## 1.2 DJ-1

DJ-1 was first identified, in 1997, as an oncogene able to transform cells in cooperation with H-Ras [61], suggesting its involvement in ras-related signal transduction pathways. Moreover, the same group proposed DJ-1 expression in a mitogen-dependent manner and its translocation in part from the cytoplasm to nuclei in S phase of the cell cycle, and that this process might be due to the translocation of other proteins associated with DJ-1 [61].

Since then, putative roles for this protein have been proposed and, although precise biochemical role is still unknown, some studies suggest it binds to multiple protein targets involved in transcriptional regulation [62,63], RNA binding [64], SUMOylation [62,65], protein folding [66] and apoptosis [63,67], showing multifunctionality of DJ-1 being involved in multiple cellular functions [68]. DJ-1 is a small protein (~20 KDa), member of the DJ-1 superfamily that has homologs distributed across all biological kingdoms [69]. In fact, a homology was attributed between DJ-1 and proteins belonging to the ThiJ/Pfpl family of bacterial proteases [70], suggesting this protein probably also has a putative chaperone function. Other studies underlying DJ-1 rodent homolog, contraception associated protein 1 (CAP1), suggest this protein enhances male rodent fertility [71], perhaps by binding to and modulating an androgen receptor inhibitor. Several functions of DJ-1 seem to be cell-type specific, but in general the net result is cytoprotection, all the way to distant microbial organism [72].

DJ-1 seems to display an isoelectric pH shift upon induction of oxidative stress, shifting to more acidic (oxidized) forms in PD brains. Indeed, oxidative modifications have been found not only in brain samples of PD and Alzheimer's disease patients but also in inclusion body myositis muscle fibers. This seems to indicate that oxidative modifications of DJ-1 are specifically linked to age-related amyloidosis, establishing the role of the redox-reactive protein DJ-1 with age-related disorders. Moreover, some studies have shown that DJ-1 confers protection against oxidative stress enhancing cell survival when challenged with pro-apoptotic stimuli [73], although the mechanisms by which DJ-1 accomplishes this are not well known [69,72].

### 1.2.1 Structural Biology

The characterization of DJ-1 crystal structure came as a helpful framework for the molecular understanding of this redox-reactive protein mode of action. DJ-1 is an homomeric protein with a six-strand parallel β-sheet sandwiched by α-helical arrangements (the so-called flavodoxin fold, which is similar to PH1704 protease and chaperone Hsp31 [74]). The tertiary structure belongs to a superfamily that includes the archetypical bacterial ThiJ and Pfpl structures, as already mentioned [72,74]. Although there are some structural similarities between DJ-1 and members belonging to

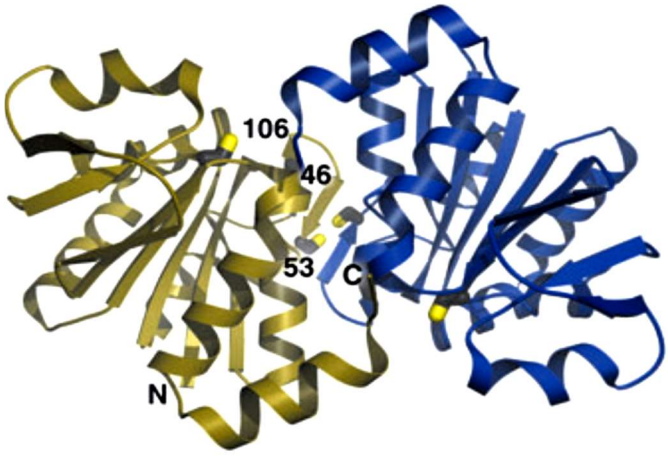


***Figure 1.6*** – A view of the DJ-1 dimer. A ribbon diagram of dimeric DJ-1 is shown with the molecular twofold axis perpendicular to the plane of the page. One monomer is shown in gold and the other in blue. The three cysteine residues in DJ-1 are shown in stick representation. C – carboxy terminus; N – amino terminus (Adapted from Wilson, 2011[69]).

latter protease family, there are some significant differences: (1) DJ-1 has a distorted catalytical triad that is essential for protease activity, and (2) the putative active site of DJ-1 is occluded by an additional C-terminal helix. Moreover, the quaternary structure of the dimeric DJ-1 differs from that of the other superfamily. This explains why DJ-1 has no protease activity [70,72,75]. The crystal structure of DJ-1 also reports the presence of a highly conserved residue, Cys-106 (C106), located at the "nucleophile elbow" region, which was suggested to be a site of regulation of DJ-1 activity by oxidation, making the protein a potential sensor for the presence of certain types of ROS in the cell [70]. Even though DJ-1 contains three cysteine residues located at amino acid positions 46, 53 and 106 (C46, C53 and 106) [76] (Figure 1.6), residue C106 stood out because of its easily oxidizable characteristic, which is thought to be the key residue involved in oxidative activation of DJ-1. However, further oxidation of C106 is thought to cause DJ-1 inactivity, and such oxidized form of DJ-1 has been observed in patients with sporadic PD [42,77]. In addition, the peripheral cysteine residues C53 and C46 in the dimer interface might also constitute a second redox center of DJ-1, which could regulate its oxidizability and, hence, activation[78]. Despite the prominent biological implications of C106 oxidation, the overall structures of oxidized DJ-1 forms do not differ from the reduced form[73].

The PD-associated DJ-1 point mutations E64D, E163K, and M261I (Figure 1.7) crystal and nuclear magnetic resonance spectroscopy (NMR) structures display only slight local changes [68]. On the contrary, the severe L166P mutation is able to disrupt α-helix 8 of structurally important C-terminal helix-kink-helix motif [79], leading to a dramatic destabilization and thereby functional loss of the protein, suggesting that dimer formation is required for its physiological function [80,81]. Nevertheless, it remains to be shown which conformational changes link C106 oxidation with cytoprotective and/or antioxidative effectors, and how the more subtle PD-associated point mutations affect these processes [72,78].

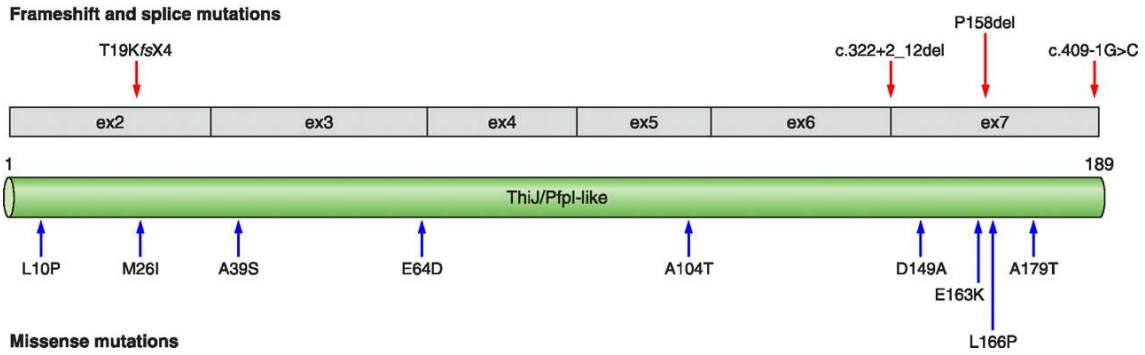


***Figure 1.7*** **-** Schematic representation of DJ-1 on transcript level and the functional domains of the DJ-1 protein with pathogenic frameshift mutations above the transcript and protein organization and missense mutations below the protein. Only homozygous or compound heterozygous mutations are listed (adapted from Corti *et al.*, 2011 [82]).

### 1.2.2 Cellular Functions

As already mentioned, DJ-1 is a multifunctional protein that is expressed throughout the body without any clues of tissue or organ specificity roles, showing a wide range of biological functions, from fertility, to oncogenesis, and neuroprotection. DJ-1 is mostly localized in the cytosol, showing some pools in the nucleus and in mitochondria, existing also some evidence of

extracellular localization [73,83,84]. Such subcellular localization is related to signal transduction, transcriptional regulation, mitochondrial dysfunction and others [72]. Nevertheless, physiological functions of DJ-1 remain unclear but altogether the several studies converge towards a neuroprotective role under oxidative stress conditions, by acting at multiples levels.

DJ-1 is an important regulator of antioxidative gene induction, such that it might influence the expression of particular antioxidative enzyme in a cell-type-specific manner. Furthermore, studies reported DJ-1 indirectly stabilizes the antioxidant transcriptional master regulator, nuclear factor erythroid 2-related factor 2 (Nrf2), enhancing its cellular antioxidant response [85,86]. The first DJ-1 binding partner identified was PIASx-α, an inhibitor of activated signal transducers and activators of transcription, also known as androgen receptor-interacting protein. DJ-1 was found to modulate this protein in a highly cell-type-specific manner. This suggests that cell type/context and nuclear localization of DJ-1 are important factors for the sensitive androgen receptor modulation [87].

A study reported a synergistic activity of DJ-1 and PGC-1α in the activation of human MnSOD promoter [88]. Moreover, as PGC-1α is an important mediator of mitochondrial biogenesis, they suggested that abnormal mitochondrial gene expression may contribute to the development of sporadic PD, and indeed this synergistic transcriptional activity is suggestive of a DJ-1 role in general mitochondrial maintenance. In fact, the effects of DJ-1 on mitochondria have been intensively studied. As this organelle is the major source of ROS in eukaryotes, DJ-1 has been reported to promote proper mitochondrial function and defense against damage caused by complex I inhibition [73,89]. The fact that mitochondrial dysfunction has long been suspected of playing an important role in etiology of *Parkinsonism*, and that oxidative stress can both cause and result from mitochondrial damage, explains the importance of DJ-1 association with this organelle [69]. To corroborate this information, a study published in 2004 [73] reported an oxidation-dependent translocation of DJ-1 to the mitochondrial outer membrane. Moreover, they stated that C106 residue was pivotal for this translocation, showing C106A-mutant DJ-1 abolished the cytoprotective effect of DJ-1 against mitochondrial toxin $MPP^+$ [73]; in fact, DJ-1 PD-associated point mutations (discussed below) do not show an altered subcellular localization [89,90], on the other hand, oxidation-facilitating mutations enhanced mitochondrial recruitment of DJ-1. Nevertheless, and although there are still questions remaining the extent and mechanisms of DJ-1 mitochondrial localization, there is solid evidence that the protein protects cells against mitochondrial damage and can partially localize to this organelle under oxidative stress conditions [69,72].

The cytoprotective functions of DJ-1 against mitochondrial ROS were originally related to a direct quenching effect of DJ-1 [91], meaning that although this easily oxidizable protein has a biochemical reactivity and its three-dimensional structure has the flavodoxin fold as core secondary structure arrangement, it does not act as a direct antioxidative enzyme *in vivo*. It is much more probable that DJ-1 exerts its antioxidative effects by influencing antioxidative gene regulation (by indirect or direct interaction with antioxidative enzymes) [85].

A promising model for DJ-1's cytoprotective function in higher organisms has emerged from several studies that identified ASK1 as a target for DJ-1 action [67,92,93]. DJ-1 was first implicated in the ASK1/p38/mitogen-activated protein kinase (MAPK) pathway, by binding to the pro-apoptotic protein Daxx and preventing its translocation from the nucleus into the cytoplasm, thus preventing Daxx from activating ASK1 and, ultimately, initiating apoptosis [67]. Further studies reported DJ-1 ability to inhibit ASK1 activity in an oxidation-dependent manner that requires the C106 residue [78,93]. They detected a direct physical interaction between DJ-1 and ASK1,

demonstrating DJ-1 recruitment to the ASK1 signalosome, under oxidative stress conditions, where it inhibits the mitogen-activated protein kinase (MAPK) cascade and apoptosis. Moreover, the recruitment of such oxidized DJ-1 to an inhibitory site near N-terminus of ASK1 could be recapitulated by C106 specific point mutations, suggesting an oxidative modification of C106 is important for this cytoprotective function [78]. Moreover, PD-relevant neurotoxic pathways mediated by oxidative dopamine stress also involve apoptotic kinase signaling via MAPK modules. DJ-1 was reported to be induced by dopamine intoxication, via extracellular signal-regulated kinases, and to activate this neuroprotective pathway [94]. On the other hand, DJ-1 suppresses the stress-activated $p38^{MAPK}$ and c-Jun N-terminal kinase (JNK) pathways, which are implicated in ROS-dependent signaling of upstream MAPKKK. DJ-1 suppresses UV-light-stimulated MEKK1 and thereby the JNK signaling cascade leading to cell death [95]. Altogether, these results demonstrate that ASK1/p38/MAPK signaling cascade appears to be an important target of DJ-1, showing this protein is exerting its neuroprotective function by promoting the inhibition of apoptotic pathways.

However, DJ-1 might also accomplish its purpose by activating the major pro-survival signaling pathways, ERK1/2, under oxidative stress. A study reported that DJ-1 may regulate ERK1/2 pathway by decreasing the expression of protein phosphatase 2A (PP2A), which is known to dephosphorylate (inactivate) MEK 1/2, which is an upstream effector of ERK1/2, leading to this pro-apoptotic pathway activation [96]. This then suggests that DJ-1 indeed does affect the ERK1/2 signaling pathways and changes the susceptibility of the cells to oxidative stress. Additionally, another group studied the influence of DJ-1 oxidation state in its interaction with the regulator of ERK1/2, p53. They reported that oxidized DJ-1 at cysteine 106, induced by oxidative stress, strongly binds to p53, which is required to suppress p53-dependent transcriptional activation of DUSP1 gene, thus inhibiting its phosphatase activity that, if active, would inactivate ERK1/2. Meaning that, in this specific example, DJ-1 activates cell survival pathways under oxidative stress conditions through downregulation of DUSP1 expression. Furthermore, they suggest that DJ-1 suppresses the expression of p53 target genes by preventing promoter recognition of p53 in a DNA-binding affinity-dependent manner [97].

Some other studies have shown that DJ-1 has also a signaling regulation in astrocytes. It was observed that abolished expression of DJ-1 in astrocytes lead to less neuroprotection on cocultured primary neurons exposed to rotenone, suggesting DJ-1 may not only act as an antioxidative and anti-apoptotic regulator within neurons but also, it may play an important transcellular role in the control of astrocytic neuroinflammation damage [98].

Altogether, these results seem to suggest that DJ-1 protein accomplishes its functions by interacting, directly or indirectly, with other proteins, its binding partners.

### 1.2.3 Mutations

As previously mentioned, DJ-1 mutations are associated with an autosomal recessive inherited form of early-onset familial PD. Although *Parkinsonism* caused by these mutations is very rare, the study of pathophysiological consequences of DJ-1 deficiency and its diverse functions may provide insights into the molecular and cellular mechanisms of neurodegeneration characteristic of PD. Thus, understanding how the causative DJ-1 mutations interfere with the structure, function and localization of the protein is of critical importance. Meaning, further basic

and applied research on DJ-1 should continue in order to shed more light on this universal cytoprotective protein and its mechanisms of action that lead to PD pathology [69].

The link between DJ-1 and neurodegeneration became apparent when it was identified as the PARK7 gene causing autosomal recessive juvenile *Parkinsonism*. Afterwards, several mutations were reported: three homozygous mutations and a deletion segregating with the disease in families, while several other heterozygous and less definitively casual mutations have been identified in studies of early-onset *Parkinsonism* patients (Table 1.3) (Figure 1.7) [41,69,72].

***Table 1.3* – Genetic sequence variants of DJ-1** (adapted from Kahle *et al.,* 2009 [72])

| Mutation | Inheritance | Effect |
|---|---|---|
| L166P | Homozygous | Protein instability |
| 14-kb deletion | Homozygous | Loss of protein |
| M26I | Homozygous | Decreased stability |
| D149A | Heterozygous | Unknown |
| IVS6-1 G-C | Heterozygous | Altered transcript |
| c.5delC | Heterozygous | Frameshift |
| c.57G->A | | |
| g.168_185del | Both | Polymorphism |
| A104T | Heterozygous | Unknown |
| Ex5-7del | Heterozygous | Altered transcript |
| IVS5+2-12del | Heterozygous | Altered transcript |
| R98Q | Heterozygous | Polymorphism |
| E64D | Homozygous | Unknown |
| E163K | Compound | Altered activity |
| g.168_185dup | Homozygous | Unknown |
| P158del | Homozygous | Unknown |
| A179T | Heterozygous | Unknown |
| Ex1.5dup | Heterozygous | Unknown |

The natural occurring L166P, E64D, E163K and M26I mutation have been shown to create structural perturbations on DJ-1 protein that lead to global destabilization, unfolding of protein structure, heterodimer formation, and reduced antioxidant activity. These PD-associated mutations and even artificial mutants have in common their loss of cytoprotection function against oxidative damage [68,89,99]. Crystal structure and NMR analysis of these mutations indicated most of the structural differences with WT DJ-1 to be modest, and none of these mutant proteins display profound structural defects, contrary to L166P, which is known to be the most aggressive form of DJ-1 mutation [68,100]. These findings suggest that even minor structural defects introduced by these disease-related mutations are able to cause considerable loss of DJ-1 functions. However, more studies are needed to determine the detailed biophysical basis of the pathogenicity of these mutants, and how DJ-1 inactivation takes place in and contributes to PD.

M26I mutation will induce a destabilization and aggregation by enhanced oxidation of the protein, meaning this substitution of methionine to isoleucine leads to decreased thermal stability and promote propensity for aggregation, resulting in packing defects in the core of the protein [68,101]. A mutation of glutamic acid in residue 163, resulting in a substitution to lysine (E163K) leads to a disruption of a key stabilizing salt bridge, resulting in destabilization of the mutated DJ-1 [68,102]. Moreover, these mutations seem to impair protein protection against oxidative stress and to translocate to mitochondria, showing a reduced distribution towards the organelle [103]. One

common feature of these two PD-associated mutations is their location near the junctions between secondary structural elements, which is known to exert considerable influence on protein folding and unfolding kinetics [104].

Besides the previously mentioned natural occurring mutations, there are also some engineered mutations being studied. Such mutations take advantage of C106 DJ-1 residue pivotal role in oxidation stress sensoring and allow a deeper knowledge of this residue function. Examples of such engineered mutations are C106A mutation, which lacks the ability to operate as a stress sensor, and C106DD mutation, which mimics a constitutively oxidized protein. C106A mutation, besides preventing the formation of an oxidized isoform, due to the impaired sensoring function, it also blocks oxidation-induced mitochondrial localization and protection against $MPP^+$ toxicity in neuronal cells, suggesting C106 residue has a role in the neuroprotective function of DJ-1 [73]. C106DD mutant is of great importance, as it is one of the first mutations at C106 residue to preserve DJ-1 protective function, providing a powerful tool for DJ-1 biochemistry study. This DJ-1 mutation was protective during oxidative stress and, additionally, enhanced binding of DJ-1 to ASK1, proving the importance of oxidized C106 for cytoprotection [78]. It is important to notice, that these results suggest that the interaction of DJ-1 with its binding partners is dependent on, or at least influenced by, its oxidation state.

### 1.2.4 Binding Partners

Several proteins interact with each other to accomplish their functions. When the function of a specific protein is unknown, a characterization of the proteins they partner with can provide insights into its physiological role. Several investigators relied on this assumption to perform such studies with DJ-1 and cumulatively reported several putative interactors, including the already mentioned PIASx-α protein[87], an uncharacterized DJ-1 binding protein (DJBP) [105], Daxx [67], parkin [106], α-synuclein [107], Hipk1 [108], androgen receptor [109], HDAC6 [110], PTEN [111] or more recently, paraoxonase-2 [112] and PRAK [113], both responsible for neuronal survival under oxidative stress, and c-raf [114]. Furthermore, DJ-1, due to its pivotal role in PD, seems to be an interesting protein target for interactome investigations with the purpose to (i) address whether this protein exists as a part of a larger complex, (ii) elucidate the relative influence of the cellular context and (iii) explore whether acute exposure to oxidative stressors alters the molecular environment of DJ-1 [115].

As already mentioned, the interactions between DJ-1 and its interactors are dependent on its oxidation state. Thus, a study [66] provided a comprehensive analysis of DJ-1 interactome in the presence and absence of rotenone (that was already classified as an oxidative stressor), which allowed the identification of several different proteins interacting with DJ-1 under oxidative stress conditions, however the absence of a negative control made it difficult to distinguish between interactors and unspecific binders [115]. Therefore, a previous project in our laboratory aimed to do a similar DJ-1 interactome analysis, considering the oxidation state of the protein, and in the presence of a negative control, which allowed the identification of several DJ-1 interactors (unpublished data) as present in Table 1.4.

***Table 1.4*** **- Functional grouping of proteins co-immunoprecipitated with DJ-1 in SH-SY5Y cell exposed to different stimulation periods of $H_2O_2$ (1 mM)** (adapted from Sandra Anjo dissertation. Identification of DJ-1 Binding Partners Under Oxidative Stress Conditions: Finding New Targets For Parkinson's disease, 2011).

| Functional Grouping | No. Protein ID | | | | |
|---|---|---|---|---|---|
| Time (min): | 0 | 10 | 15 | 20 | 40 |
| **ATPase** | | | | 1 | |
| **Carbohydrate-binding proteins** | | 1 | | | |
| **Chaperone** | 1 | 1 | 1 | | |
| **Cytoskeleton proteins** | 1 | 11 | 8 | 5 | 1 |
| **DNA repair proteins** | | 1 | 1 | 2 | |
| **DNA/RNA binding proteins** | 1 | | | 1 | |
| **G-protein coupled receptors** | | 1 | 1 | 1 | |
| **Histone proteins** | 2 | 2 | 1 | 1 | |
| **Calcium transporter proteins** | | | 2 | | |
| **Metabolic protein** | | | | 1 | |
| **Modulator proteins** | 1 | | 1 | | |
| **Motor proteins** | | 6 | 4 | 5 | |
| **Neuropeptide** | | 1 | | 1 | |
| **Oxireductases** | 1 | 1 | | 1 | |
| **Peptidylprolyl isomerase** | 1 | | | | |
| **Phosphatases** | | 2 | | | |
| **Ribossomal proteins** | | | | 1 | |
| | 4 | 2 | | 1 | |
| **Scaffold proteins** | 1 | | | | |
| **Transcription factor** | | | | 1 | |
| **Transmembranal proteins** | 1 | | | 1 | |
| **Ubiquitin ligase** | 1 | | | | |

With this project, they were able to identify a larger number of proteins interacting with DJ-1, in cells exposed to oxidative stress, which is consistent with the protein's stress-dependent activation. Under such conditions, it was possible to identify more cytoskeleton and motor proteins when compared with resting conditions, which suggests DJ-1 involvement in cytoskeleton and cell reorganization in response to oxidative stress. They also identified proteins related with gene expression, involved in distinct mechanisms, such as ribosomal proteins, histones,

transcription factors and other DNA/RNA-interacting proteins. Moreover, a proteins belonging to DNA repairing functional group were also present in oxidative stress conditions, which seems to suggest a new DJ-1 neuroprotection mechanism through DNA repair. Besides, this study also allowed the identification of proteins associated with protein folding, mediation of signaling pathways, mitochondria, calcium ions transport among others. In general, several new putative DJ-1 binding partners were identified, which presented a broad range of biological functions, mainly associated with cellular response to oxidative stress, pointing to new mechanisms through which DJ-1 mediates its neuronal protection function. Moreover, from the wide range of proteins identified, oxidoreductase functional group received great attention due to its association with cellular response to oxidative stress. From those proteins, D-3-phosphoglycerate dehydrogenase (PGDH), NADH dehydrogenase [ubiquinone] 1 alpha subcomplex subunit 4 (NDUFA4), and Trifunctional enzyme subunit alpha, mitochondrial (HADHA) proteins were identified as being part of oxidoreductases family. PGDH is a cytosolic protein involved in the early steps of L-serine synthesis in animal cells, which serves as a precursor for the synthesis of proteins, membrane lipids, and the neuromodulators glycine and D-serine [116], playing a central role in cellular proliferation [117]. PGDH deficiency has shown to induce a neurometabolic disorder associated with reduced L-serine synthesis [117]. NDUFA4 is an accessory subunit of cytochrome C oxidase, complex IV of mitochondrial respiratory chain that catalyzes the reduction of oxygen to water [118]. NADUFA4 impairments lead to dysfunction in cytochrome c oxidase subunit linked to Leigh syndrome neurological phenotype[119]. HADHA is a mitochondrial protein that catalyzes mitochondrial β-oxidation of long chain fatty acids, to produce Acetyl-CoA for TCA cycle, resulting in NADH to fuel electron transport chain activity and, consequently, production of ATP needed for cellular basic functions [120]. HADHA deficiency has been shown to be associated with progressive neuropathy and myopathy[121]. All three proteins are also known to be involved in the $NAD^+$/NADH balance.

However, they emphasized the fact that the large number of proteins identified in these groups might be a result of the higher expression of this type of proteins, meaning that validation of these interactions is needed and its significance remains to be studied.

## 1.3 INTERACTOMICS

The explosion in genome sequencing over the past few years has brought many exciting opportunities to biological research, which led to the complete sequencing of several eukaryotic genomes, providing a comprehensive inventory of predicted proteins for many different species. However, although complete genome sequences provide lists of tens of thousands of predicted unique proteins, the sequences *per se* do not provide knowledge of their biological/physiological role in the cellular system, being insufficient to describe biological processes. Thus, molecular biology has entered in the “post-genome era”, which aims to address questions using more global approaches, such as the use of nearly complete sets of proteins rather than one or few genes at a time. However, expectations of such approaches have remained relatively modest so far, as the majority of predicted genes and proteins are currently completely uncharacterized [122].

Vital cellular functions such as DNA replication and transcription, and mRNA translation require the coordinated action of a large number of proteins that are assembled into an array of multiprotein complexes [122–125]. In fact, the majority of the proteins accomplish their functions by

interacting, directly or indirectly, with other proteins, meaning a detailed description of the cellular signaling pathway might greatly benefit from the elucidation of protein-protein interactions in the cell, thus unraveling the interactome of those proteins. It has become clear that a large number of proteins exist in dynamic protein complexes that orchestrate and regulate several biological processes, and that identifying binding partners of such proteins of unknown function might provide insights into their functions, which is of central importance in biological research [122,125,126]. Moreover, an important task of proteomics is to elucidate protein-protein interaction in normal and diseased state, because disturbances in such interactions within a cell can lead to many diseases, namely cancer or even Parkinson's disease. Since modulation of protein-protein interaction represents an emerging therapeutic paradigm, it is of great biomedical interest to identify proteins that bind to certain target protein and consequently help to modulate its function. Also, evidence now reveals that protein interaction interfaces describe a new class of attractive target for drug development [123,127].

A number of experimental methods, based on distinct physical principles, have been developed to characterize protein complexes and protein-protein interaction networks. They fit in two main types of approaches: (i) techniques that measure direct physical interactions between protein pairs (binary approaches), and (ii) those that measure interactions among a group of proteins that may not form direct physical contacts (co-complex methods). The first interactome map was obtained using the most frequently used binary method, the yeast two-hybrid method (Y2H) [128]. More recently, a combination of affinity purification and mass spectrometry (AP-MS) has been used to greatly advance of the knowledge on protein complex composition (more in-depth information presented below) [125,129].

Y2H system [130] has variations involving different reagents and has been adapted to high-throughput screening. The strategy uses two proteins, called bait and prey, coupled to two halves of a transcription factor, and is expressed in yeast. If the proteins interact, they reconstitute a transcription factor that activates a reporter gene (Figure 1.8) [131]. Currently, this is the only technique that requires manipulation of DNA exclusively [122]. However, the sensitivity, specificity, efficiency, versatility and accuracy provided by affinity purification makes this strategy the method of choice for mapping system-wide scale, *in vivo* protein interaction networks in various

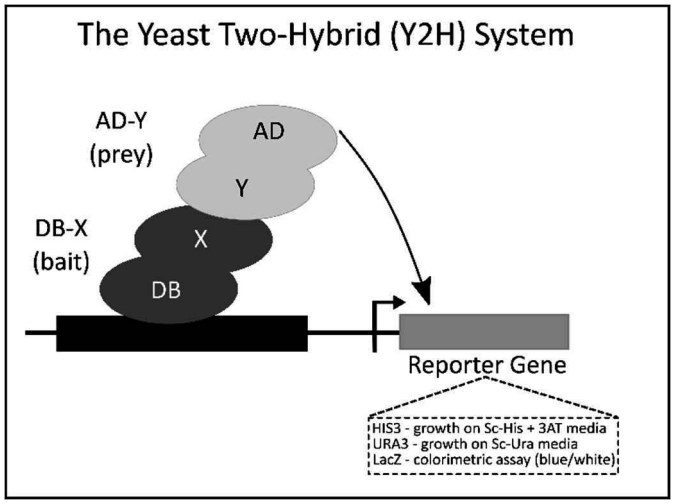


***Figure 1.8*** **-** The yeast two-hybrid system. The scheme represents the Y2H system, in which there is the Binding Domain (BD) coupled to the bait protein (X) and the Activation Domain (AD) coupled to the prey protein (Y). Upon their interaction, a functional transcription factor is reconstituted, activating the expression of the reporter gene (adapted from Walhout & Boulton, 2006 [131]).

organisms. Furthermore, similar strategies have also been applied to study protein interaction of protein complexes and protein interaction networks within the context of cellular pathways [127].

### 1.3.1 Affinity-based Strategies

The second major approach to study protein-protein interaction, AP-MS, is particularly suited to identify and map multi-protein complexes under near to physiological conditions, being, therefore, complementary to Y2H method. This approach is based on immuno-affinity purification methods, such as tandem affinity purification (TAP) or other single affinity tags, in conjugation with mass spectrometric protein identification strategies. Alternatively, specific antibodies can be employed, instead of tags, to purify endogenous protein complexes under physiological and pathophysiological conditions [124,129].

Affinity purification (AP) constitutes a category of protein enrichment strategies used for analysis of protein complexes. In order to identify and quantify proteins present in such complexes, AP is frequently coupled to mass spectrometry (MS). One method of affinity purification is immunoprecipitation (IP) (Figure 1.9), in which an antibody is coupled to a solid phase (often sepharose beads) and incubated with the biological sample of interest. The bound proteins are removed through elution or denaturation. The final co-immunoprecipitated sample contains the antibody, the protein of interest, and any associated proteins [132]. AP coupled with quantitative MS has become the primary method for studying *in vivo* protein interaction of whole organism proteomes, allowing the identification and quantification of protein's interactors in complexes that are stable, dynamic, transient and/or weak. Moreover, in contrast to Y2H and related methods, AP-MS can be performed under near physiological conditions, in the relevant organism and cell type. This is because this approach does not perturb the typically relevant post-translational modifications (PTM), which are often crucial for the organization and/or activity of complexes, and can also be identified by MS. Another advantage of AP-MS, besides providing real-time insights of protein assemblies, is its ability to probe dynamic changes in the composition of protein complexes, especially when used in combination with quantitative techniques [125,127,129,132].

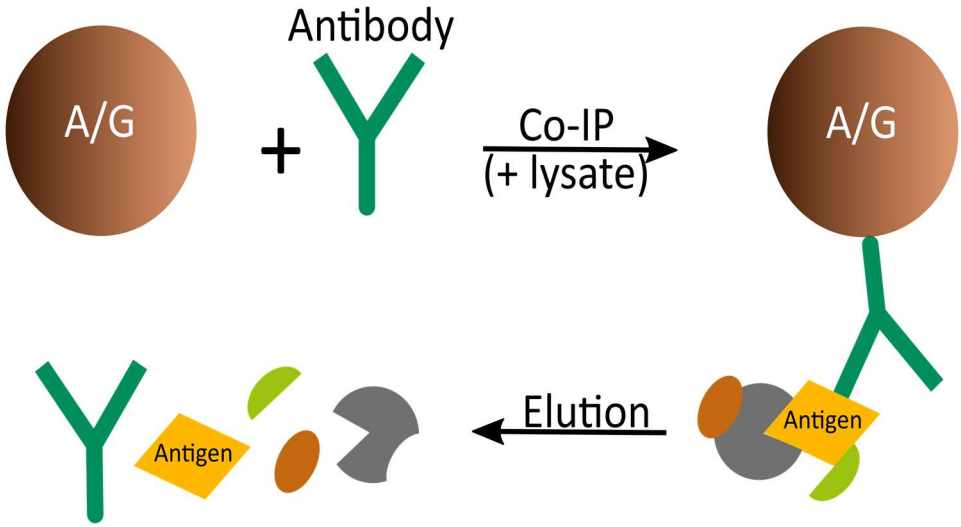


***Figure 1.9 –*** Immunopurification standard experiment. In a standard IP experiment, protein A or protein G coupled sepharose beads are combined with an antibody and a sample lysate. The antibody binds to both the beads and its target antigen, which may also affinity enrich a variety of interacting proteins. Proteins are eluted from the beads leaving the antibody in solution with the antigen and interacting proteins (adapted from Rogstad *et al.*, 2013 [132]).

The first step in an AP-MS approach (workflow described in Figure 1.10) is the generation and clearance of a suitable extract derived from cultured cells or tissue. Next, an immunoaffinity matrix, generated by immobilizing a target-specific antibody or specific tags to a matrix, for easy recovery of antibody or tag, is added to the extract, and protein complexes containing bait proteins are immunocaptured. After extensive washes, proteins are eluted from the immunoaffinity matrix and are reduced, alkylated, and trypsinized with or without prior gel separation. The resulting peptide mixture is then subjected to tandem mass spectrometry (MS/MS). Finally, processing of MS/MS peptide fragmentation spectra by protein identification algorithms reveals the identity of the proteins that are putatively engaged in interactions with the target protein [133]. Nevertheless, it is important to understand that AP-MS technique alone only generates a list of proteins detected and does not necessarily reveals the composition of individual protein complexes. The data from a single AP-MS experiment represents an average of binding partners and protein complexes, meaning that if bait protein is a component of multiple alternative complexes, a single AP-MS analysis cannot be used to unravel the multiplicity of association, which is of great importance as proteins can have dramatically different roles as components of different types of complexes. So, analyzing the composition of an intact protein complex with defined biochemical properties can be used to reveal the composition of a given complex, and this can be accomplished by coupling AP-MS with different strategies such as biochemical fractionation in protein complex analysis or guilt by association analysis [125].

### 1.3.2 Mass Spectrometry (MS)

Mass spectrometry (MS), measures the mass to charge ratios (*m/z*) of gas-phase ions, and has increasingly become the method of choice for analysis of complex protein samples. MS-based proteomics is a discipline made possible by the availability of gene and genome sequence databases, and technical and conceptual advances in many areas, most notably the discovery and development of protein ionization methods. A mass spectrometer consists of an ion source, to produce ions from the sample; one or more mass analyzers, to separate the ions according to their *m/z* ratios; a detector, to register the number of ions emerging from the last analyzer; and a computer, to process data, to produce the mass spectrum in a suitable form, and to control the instrument through feedback. Each mass spectrometer also has an inlet device to introduce the analyte into the ion source, such as liquid chromatograph or a direct insertion probe (Figure 1.10) [134,135]. One of the techniques often used to volatilize and ionize the proteins or peptides for mass spectrometric analyzes is electrospray ionization (ESI), which produces gaseous ions from solution phase samples that can be easily coupled to a liquid-based separation, such as liquid chromatography, allowing the analysis of complex samples [135].

The general mass spectrometry-based proteomic experiment starts with the electrophoretic separation of the samples using SDS-PAGE. Bands generated with the technique are then excised into small pieces in order to perform in-gel digestion of the proteins, through trypsin, which will generate a mixture of peptides with C-terminal protonated amino acids, providing an advantage in subsequent peptide sequencing. This is because MS of whole protein is less sensitive than peptide MS, and the mass of the intact protein by itself is insufficient for identification. Peptide mixture is then subjected to high-pressure liquid chromatography, in very fine capillaries, and eluted into an electrospray ion source, where they are nebulized into small, highly charged droplets. After evaporation, multiply protonated peptides enter mass

spectrometer, and a mass spectrum of the peptides eluting at this time point is taken. The computer generates a list of such peptides for fragmentation, a given peptide ion is then isolated, fragmented by energetic collision with gas, and a MS/MS spectrum is recorded. The MS and MS/MS spectra are typically acquired and stored for matching against protein sequence database. The outcome of the experiment is the identity of the peptides and, therefore, the proteins present in the protein extract [136] (Figure 1.10). Protein quantification can be achieved using SWATH (sequential window acquisition of all theoretical spectra)-MS method. With this method, a mass range relevant for peptide-based proteomics (400-1200 m/z) is scanned in 25 m/z windows, in which all ions that fall into that window are simultaneously fragmented (MS/MS). Quantification is then conducted based on the chromatographic peak areas of extracted ion chromatrograms (XIC), which are computationally reconstituted. This method, uses a *priori* information contained in spectral libraries (obtained with previous peptide identification) to query the acquired fragment ion maps for the presence and quantity of specific peptides of interest [137].

MS is the current method of choice to identify peptide sequence due to its sensitivity; it routinely allows the identification of peptides present at femtomole levels. MS is also rapid, the identification of individual peptides can be achieved within hundreds of milliseconds, and thousands of peptides can, therefore, be identified in a single LC-MS analysis. Moreover, MS is compatible with high-throughput strategies and is easily automated. It also allows, as previously mentioned, the characterization of peptide modification, including naturally occurring PTM, such as phosphorylation, and exogenously added modifications, like chemical crosslinkers. Additionally, MS can also be adapted to quantitatively measure peptide abundance, not requiring pre-existing knowledge on proteins to be analyzed [125]. Finally, MS-based proteomics can be applied to resolve three types of biological or clinical questions: (1) generation of protein-protein linkage maps, (2) use of protein identification technology to annotate and, if necessary, correct genomic DNA sequences, and (3) use quantitative methods to analyze protein expression profiles as a function of cellular state as an aid to infer cellular function [136].

Indeed, MS is at the core of proteomics today. It has an extensive range of applications, which includes identification, characterization, and quantification of proteins, their interactions and modifications. However, this subject is only standing at the tip of the iceberg, meaning it is still very much a nascent technology, where change is still possible. Advances in instrumentation, experimental design and data handling will ensure that MS continues to play a pivotal role in life sciences research in the future [125,134,135].

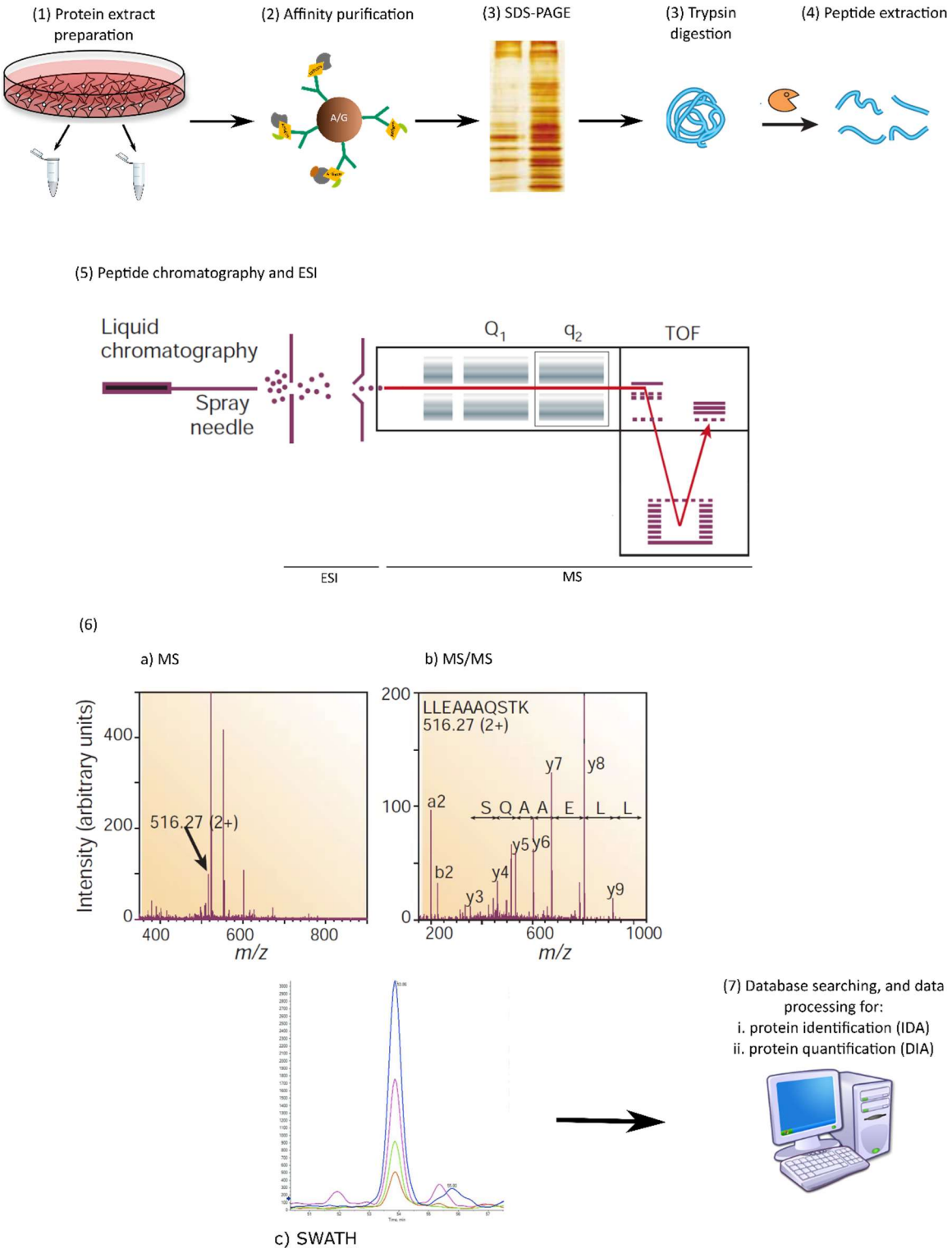


***Figure 1.10*** – Generic AP-MS experiment. (1) Proteins are first isolated from cell or tissues lysates and are (2) immunopurified. Eluates from immunopurification are subjected to (3) SDS-PAGE, followed by (4) enzymatic digestion with trypsin and (4) peptide extraction. (5) Peptide mixture is separated using one or more stages of liquid chromatography. LC eluate is directed into an electrospray source and (6 - a) peptides are analyzed first by full-scan MS and (6 - b) then by MS/MS. (7) Peptide MS/MS spectra are searched against a protein database using a search algorithm which assigns peptide identifications based on match criteria, which also allows the quantification of the proteins from SWATH Data (6-c).

## 1.4 OBJECTIVES

Although PD is a sporadic idiopathic disorder, several genes are known to be PD-associated, such as *dj1* gene. Mutations in DJ-1 are responsible for an inherited form of *Parkinsonism*, and the study of pathophysiological consequences of DJ-1 deficiency and its diverse function has already provided important insights into the mechanisms of oxidative stress-induced neurodegeneration. DJ-1 is a multifunction protein involved in several mechanisms, but its role in neuroprotection against oxidative stress it the most relevant in PD context. Moreover, several studies indicated that oxidative stress itself seems to be a trigger condition for DJ-1 activity. In this context, a previous DJ-1 interatomic study under oxidative stress conditions was accomplished, from which it was identified several new putative binding partners. The validation of such interactions and the study of the putative interactors themselves would elucidate into molecular mechanisms of PD.

Therefore, this project aims to study oxidoreductase family proteins, which are closely related to oxidative stress, more specifically 3PGDH, NDUFA4, and HADHA proteins, having two major goals. First, to validate the interaction between DJ-1 and the three representative oxidoreductase proteins, through immunoprecipitation, pull down, and immunocytochemistry, followed by confocal microscopy analysis. Second, if HADHA interaction with DJ-1 is confirmed, to expand DJ-1 dynamic interactome to its binding partner, namely HADHA, by characterizing HADHA interactome under oxidative stress conditions, through AP-SWATH-MS methodology, to assess this protein's involvement in cellular response to oxidative stress. Such study will help to elucidate the cellular response mechanisms to oxidative stress and how this correlates with Parkinson's disease potential progression.

# 2 EXPERIMENTAL PROCEDURES

## 2.1 REAGENTS

All reagents used in cell culture were cell culture-tested. The Minimum Essential Medium (MEM) with L-glutamine, fetal bovine serum (FBS), MEM-non essential aminoacids (NEAA) solution, trypsin-EDTA 0.05% solution (1x), amphotericin B solution, penincilin-streptomycin solution and Dulbecco's phosphate buffer saline (DPBS, 10x) were obtained from Gibco® (Life Technologies™). Hydrogen peroxide ($H_2O_2$) used for redox stimulus was obtained from Sigma-Aldrich®.

As for the reagents used for procedures such as SDS-PAGE, immunoblotting or protein extraction, tris(hydroxymethyl)aminomethane (Tris) was obtained from Calbiochem® (Merck™), and hydrogen chloride (HCl) from JT Baker® (Avantor™). Sodium dodecyl sulfate (SDS), dithiothreitol (DTT), acrylamide/vis-acrylamide solution (37.5%:40%), Tween 20, and Transfer buffer were obtained from Biorad. Glycine, ammonium persulfate, glyceral, bromophenol blue, and ECF reagent from GE Healthcare. Magnesium chloride ($MgCl_2$) and potassium phosphate dibasic trihydrate ($K_2HPO_4.3H_2O$) were from Merck™, and sodium chloride (NaCl), potassium chloride (KCl), sodium dihydrogen phosphate monohydrate ($NaH_2PO4.H_2O$), sodium hydroxide (NaOH), tetramethylethylenediamine (TEMED) from Sigma-Aldrich®.

Antibodies used were: anti-HADHA (E-8, sc-374497, Santa Cruz Biotechnology, Inc.), anti-3PGDH (6B2, sc-100318, Santa Cruz Biotechnology, Inc.uz), anti-NDUFA4L2 (C-12, sc-131987, Santa Cruz Biotechnology, Inc.), anti-DJ-1 (C-16, sc-27006, Santa Cruz Biotechnology, Inc.), and mouse IgG Isotype Control (10400C, Invitrogen).

The reagents used for mass spectrometry analysis were high quality chemical or reagents (ACS Reagent Chemicals & Lab Grades). Formic acid (FA) was obtained from AMRESCO® and acetonitrile (ACN) from VWR. Ortho-phosphoric acid and ammonium sulfate were obtained from Fisher Chemical and ammonium bicarbonate from Fluka (Sigma-Aldrich).

The Trypsin Modified Sequencing Grade used in protein digestion and the Complete Mini Protease inhibitor mixture and Complete Mini Phosphatase inhibitor mixture were obtained from Roche Diagnostics.

The origin of the remaining reagents, antibodies, kits and material used during this project is referred throughout the text.

## 2.2 ANTIBODIES OPTIMIZATION

Antibodies used in the present project were anti-HADHA (sc-374497, Santa Cruz Biotechnology. Inc.), anti-3PGDH (sc-100317, Santa Cruz Biotechnology. Inc.), and anti-NDUFA4L2 (sc-131987. Santa Cruz Biotechnology) antibodies.

### 2.2.1 SH-SY5Y cell culture

Human neuroblastoma SH-SY5Y (ATTC® CRL-2266™) cells were cultured in a 1:1 mixture of Minimum Essential Medium (MEM, Gibco), supplemented with 1% NEEA (Gibco), and F12 Medium (Gibco) supplemented with 10% fetal bovine serum (Gibco), 1.25 µg/mL amphotericin B

solution (Invitrogen), and 1% penincillin-streptomycin solution (Pen-Strep). Cells were maintained at 37 °C, 5% $CO_2$ / 95% air atmosphere, in a humidified incubator (Shel Lab 35172, Sheldon Manufacturing, Inc.).

For cells passage, Dulbecco's phosphate buffered saline (DPBS) was used for cells washing, followed by trypsin-EDTA (0.05% solution in phosphate buffered saline (PBS)) (Invitrogen) to detach cells.

### 2.2.2 Preparation of Protein Extracts

SH-SY5Y cells were seeded at $75\times10^3$ cells/$cm^2$ in 55 $cm^2$ culture plates (Corning, USA), in 1:1 mixture of MEM-F12 supplemented with 10% FBS culture medium for 48h, until high confluency was reached.

Forty-eight hours after platting, culture medium was completely removed, cells were washed with PBS (8 mM $K_2HPO_4.3H_2O$, 2 mM $NaH_2PO4.H_2O$, 150 mM NaCl, pH 7.4), and RIPA buffer (50 mM Tris-HCl, pH 7.4; 1% (v/v) Igepal; 0.25% (v/v) sodium-deoxycholate; 150 mM NaCl; 1 mM DTT; 1 mM EDTA, Complete Mini protease inhibitor mixture and Complete Mini phosphatase inhibitor mixture, Roche) was added. After addition of the lysis buffer, cell culture plates were placed on ice and cell lysates was obtained by scrapping the plate twice with a cell scraper (TPP, Switzerland). Cell lysates were collected to microcentrifuge tubes, followed by sonication (Sonicator model Vibra cell 75041 from Bioblock Scientific, France) for 30 seconds, 1 second on-off cycles, 40% amplitude, and 20 minutes centrifugation at 20,000×g and 4 °C. After centrifugation, supernatant (protein extract) was collected to new tubes. A sample of the protein extract was used for protein quantification and remaining extract was frozen at -20 °C until further use.

### 2.2.3 Protein Quantification - 2D Quant Kit

Protein concentration in protein extracts was then quantified using 2D Quant Kit (GE Healthcare®) assay. The procedure works by quantitatively precipitating proteins while leaving interfering substances in solution. The assay is based on the specific binding of cooper ions to proteins, in such a way that precipitated proteins are resuspended in a cooper-containing solution and unbound copper is measured with a colorimetric agent. Thus, color intensity is inversely related to the protein concentration.

Bovine serum albumin (BSA) was used as standard and the assay was performed following manufacturer standard protocol. Briefly, the set of protein standards was prepared by pipetting specific volumes of BSA stock solution (2 mg/mL), in a working range of 0-60 µg of protein, to microcentrifuge tubes. Then, samples and standards were mixed with "*Precipitant*", which renders proteins insoluble, and "*Co-precipitant*", which contains reagents that co-precipitate with protein and enhance their removal from solution, followed by centrifugation for 5 minutes at 14,100×g. After centrifugation, supernatant was discarded and pellet was resuspended in cooper solution, followed by incubation for 15 minutes with Working Color Reagent (100 parts of color reagent A to 1 part color reagent B), at room temperature. In every step of this procedure,

thorough homogenization was achieved by intense vortexing followed by short-spins. Sample's absorbance was measured at 480 nm in a Microplate Spectrophotometer (PowerWave XS, BioTek, Bad Friedrichshall, Germany). Finally, results from protein standards were used to design a calibration curve, which allowed the interpolation of protein extract concentration.

### 2.2.4 Antibody Peptide Neutralization

Antibody against NDUFA4L2 (sc-131987, Santa Cruz Biotechnology, Inc.) was blocked following manufacturer instructions. Briefly, for the blocking/competition, antibody (at the optimal dilution at which consistently achieved positive results) was combined with a five-fold excess (by weight) of blocking peptide (NDUFA4L2 (C-12) P sc-131987P, Santa Cruz Biotechnology, Inc.) in PBS, overnight at 4 °C. Following blocking/competition, the antibody-peptide mixture was diluted into proper blocking buffer and western blot was performed, using also a control condition, with non-blocked antibody.

### 2.2.5 Western Blot

To the protein extract to be analyzed by Western Blot was added a correspondent volume of the 6x Laemmli sample buffer [(0.35 M solution of Tris-HCl with 0.4% SDS (v/v), pH 6.8, 30% glycerol (v/v), 10% SDS (w/v), 9.3% DTT (w/v) and 0.01% bromophenol blue (w/v)] to a 1× final concentration. Proteins were then denatured by boiling at 95 °C for 5 minutes, followed by electrophoretical separation of 15 µg and 30 µg of protein, on a 12.5% SDS-polyacrylamide gel using a Mini-PROTEAN® Tetra Electrophoresis System (Bio-Rad), at 80 V during stacking gel and at 150 V during running gel.

Proteins were then transferred to a polyvinylidene fluoride (PVDF) membrane (Immuno-Blot™ PVDF membrane with 0.2 µm pore size, Bio-Rad), previously activated through brief immersion in methanol and followed by a washing step in deionized water, using a Bio-Rad Trans-Blot Turbo™ Transfer System (30min at 25V). Following transfer, PVDF membranes were blocked, for 1 hour at room temperature, with 5% (w/v) skimmed milk powder in PBS-Tween 20 (PBS-T) [0.1% (v/v)]. Blots were then incubated, overnight at 4 °C followed by 1 hour at room temperature, with primary antibodies (anti-HADHA (sc-374497, Santa Cruz Biotechnology, Inc.), anti-3PGDH (sc-100317, Santa Cruz Biotechnology, Inc.), and anti-NDUFA4L2 (sc-131987, Santa Cruz Biotechnology, Inc.)), either in 1:200 or 1:500 dilutions, in blocking solution. Primary antibodies were then removed, and membranes were extensively washed with PBS-T 3 times for 15 minutes, under agitation. Following washes, membranes were incubated, for 1 hour at room temperature, with the secondary antibodies conjugated with alkaline phosphatase (Table 4) in 5% (w/v) skimmed milk powder dissolved in PBS-T, proceeded by extensive washes with PBS-T, as above.

Protein-immunoreactive bands were developed using the "Enhanced Chemifluorescence (ECF)" detection system (GE Healthcare®) and visualized in a molecular Imager FX System (Bio-Rad). Western blots' images were obtained and analyzed using Image Lab™ Software version 5.7 build 7 (Bio-Rad).

***Table 2.1*** – **List of secondary antibodies conjugated with alkaline phosphatase used in western blot analysis.**

| | Dilution | Source |
|---|---|---|
| **Anti-mouse** | 1:10,000 | Jackson ImmunoResearch Laboratories, Inc. (West Grove, PA, USA) |
| **Anti-goat** | 1:6,000 | |

## 2.3 DJ-1 INTERACTION WITH HADHA AND PGDH

### 2.3.1 HADHA and PGDH Immunoprecipitation

Immunoprecipitation assays were performed using Dynabeads® Co-Immunoprecipitation Kit (Novex® by Life Technologies™), which allows the covalent coupling of the antibodies to the surface of magnetic Dynabeads® M-2710 Epoxy. Once the coupling reaction is finished, the beads-antibodies pair can be used to performed immunoprecipitation (IP), or co-immunoprecipitation assays.

#### 2.3.1.1 Antibody Coupling Protocol Test

Antibody coupling protocol was performed according to the manufacturer protocol, all the buffers used were provided in Dynabeads® Co-Immunoprecipitation Kit (Novex® by Life Technologies™), and the antibodies used in the experience were anti-HADHA (sc-374497, Santa Cruz Biotechnology, Inc.), anti-3PGDH (sc-100317, Santa Cruz Biotechnology, Inc.), and anti-NDUFA4L2 (sc-131987, Santa Cruz Biotechnology, Inc.).

For this, 1 mg of Dynabeads and 1.7 µg of antibodies was used. Beads were washed with 1 mL of C1 buffer, followed by the addition of the appropriate volume of the antibodies, and C1 and C2 buffers in the proportion indicated by the kit manufacturer. The beads were then incubated with the antibodies on a roller at 37 °C overnight (16-24 hours). Following incubation period, the supernatant was collected and for posterior analysis (corresponding to antibody unbound fraction). Antibody-coupled beads were then washed with HB, LB, and SB buffers, as indicated by the kit, and resuspended in 100 µL of SB buffer, to a final concentration of 10 mg antibody-coupled beads/mL (corresponding to antibody bound fraction). For posterior analysis, 30 µL of each fraction was used, plus 30 µL of input fraction (Antibody + C1 + C2) was formulated in the same proportion as in the coupling reaction. The samples were denatured at 95 °C for 5 minutes in 1x Laemmli sample buffer, followed by analysis through western blot (as described in experimental procedure 2.2.5).

#### 2.3.1.2 Cell Sample Preparation

SH-SY5Y (ATTC®) cells were seeded at $75\times10^3$ cells/$cm^2$ in 55 $cm^2$ culture plates with 1:1 MEM-F12 with 10% FBS culture medium. After 24h, serum starvation was induced by changing the culture medium to 1:1 MEM-F12 with 0.1% of FBS, in order to synchronize the cells' activity, by reducing their basal activity, prior to the experiment. Cells were left in starvation and 16h after redox stimulus was applied, by adding 1 mM $H_2O_2$ (hydrogen peroxide) in MEM-F12 with 0.1% FBS solution for 15 and 40 minutes, or adding MEM-F12 with 0.1% FBS without $H_2O_2$ (corresponding to 0 minutes' time point). After incubation was finished, hydrogen peroxide solution was immediately removed, and cells were washed with PBS. To proceed to protein extraction, ice-cold Extraction Solution (ES) (1x IP buffer supplied in the Co-Immunoprecipitation kit; 100 mM of NaCl; Complete Mini protease inhibitor mixture and Complete Mini phosphatase inhibitor mixture) was added to the plate, followed by cells scrapping. Cells lysate was then incubated on ice for 15 minutes, following centrifugation for 5 minutes at 2,600×g and 4 °C. Supernatant was collected, a sample was taken for protein quantification, through BCA assay (experimental procedure 2.3.1.3), and the remaining extract was kept on ice until further need.

#### 2.3.1.3 Protein Quantification – BCA Protein Assay

For this assay, protein content was measured through bicinchoninic acid (BCA) assay, using Pierce™ BCA Protein Assay Kit (ThermoFisher Scientific). This detergent-compatible assay relies primarily in two reactions: 1) the peptides bonds in the protein reduce $Cu^{2+}$ ions from cooper (II) sulfate to $Cu^{+}$, and the amount of $Cu^{2+}$ reduced is proportional to the amount of protein present in solution, 2) next, two molecules of BCA chelate with each $Cu^{+}$ ion, forming a purple-colored product that strongly absorbs light at 562 nm, allowing its colorimetric detection and quantification of total protein.

BSA was used as protein standard and the procedure was developed according to the manufacturer's protocol. Briefly, a set of protein standards was prepared, from a 2.0 mg/mL BSA stock solution, in the same buffer used for protein extraction. Each standard and sample was mixed with BCA working reagent (50:1, Reagent A:B) and then incubated at 37 °C for 30 minutes. Samples, standard and blank solutions were transferred to the wells of a 96 multiwell plate and the absorbance was measured at 562 nm in a Microplate Spectrophotometer (PowerWave XS, BioTek, Bad Friedrichshall, Germany). Finally, results from protein standards were used to design a calibration curve, which allowed the interpolation of protein extract concentration.

#### 2.3.1.4 Immunoprecipitation Method

For the immunoprecipitation assay, 1.5 mg of dynabeads was used, as indicated by the manufacturer, for immunoprecipitations using western blot as detection method. The antibody coupling protocol was performed as described in experimental procedure 2.3.1.1, using 2 μg of HADHA, PGDH and Mouse IgG Isotype Control (10400C, Invitrogen) antibodies.

Remaining immunoprecipitation protocol was performed according to manufacturer's instructions. Briefly, antibody-coupled beads were washed with Sxtraction Solution, followed by

overnight incubation with 900 µg of protein extract (obtained following experimental procedure 2.3.1.2) on a rotator at 4 °C. After incubation, beads were extensively washed with IP buffer and denatured by addition of 1× Laemmli Sample Buffer followed by boiling at 95 °C for 5 minutes. Beads were discarded and eluted proteins/protein complexes were stored at -20 °C until further use. Western Blot was performed to assess immunoprecipitation results (experimental procedure 2.2.5).

### 2.3.2 DJ-1 Pull down

Pull down assays were carried out using His Mag Sepharose™ Ni (Ge Healthcare) magnetic beads used for small-scale purification/screening of histidine-tagged proteins. Such proteins are captured through immobilized nickel ions followed by collection of the beads using a magnetic device.

Pull down assays rely in the use of a "bait" protein, which is bound to the magnetic beads through an affinity tag, that will capture the proteins it interacts with. In this particular case, the "bait" protein used was recombinant WT DJ-1, already existed in the lab. Recombinant DJ-1 was produced using DJ-1_pSKB-3 construct based on a pSKB-3 plasmid, containing either cloned WT DJ-1 human gene, or DJ-1-mutated gene (optimized for *E. coli* expression) between restriction sites. The plasmid consisted on a modified pET-28a plasmid with thrombin alteration to a tobacco etch virus (TEV) recognition site. DJ-1 gene was expressed downstream of a N-terminal hexahistine (His) expressing sequence and TEV recognition site, for the expression of a recombinant DJ-1 with a TEV-cleavable His-tag. The plasmid had a kanamycin resistance gene and also a *lac* repressor and operator genes upstream of the construct site.

#### 2.3.2.1 Cell Sample Preparation

SH-SY5Y (ATTC®) cells were seeded at $75\times10^3$ cells/$cm^2$ in 55 $cm^2$ culture plates with 1:1 MEM-F12 with 10% FBS culture medium. Cells were serum-starved, 24h after plating, by changing the culture medium to 1:1 MEM-F12 with 0.1% FBS. Redox stimulus was then applied, 16h after serum starvation, by the addition of 1 mM of $H_2O_2$ in MEM-F12 with 0.1% FBS culture medium, followed by incubation for 15 and 40 minutes, or addition of MEM-F12 with 0.1% FBS without $H_2O_2$ (corresponding to 0 minutes' time point). As soon as the incubation periods were over, $H_2O_2$ solution was removed and cells were washed with PBS. For protein extraction, ice-cold Extraction Solution was added to the cells, plates were put on ice, cells were scraped with a cell scrapper, and harvested to centrifuge tubes. Cells lysate was then incubated on ice for 15 minutes, followed by centrifugation for 5 minutes at 2,600×g and 4 °C, and collection of the supernatant to a new centrifuge tube. From the extract, a sample was taken and protein content was quantified using BCA method (Experimental procedure 2.3.1.3). Remaining extract was kept on ice until further use.

#### 2.3.2.2 Pull down Assay

For this pull down assay, 15 µL of bead slurry (His Mag Sepharose™ Ni magnetic beads in storage solution [20% ethanol, 5% medium slurry]) and 3 µg of recombinant protein was used. Bead slurry was mixed thoroughly and the amount of volume needed for the whole procedure was extracted. Storage solution was removed and beads were washed with PBS, to equilibrate. Afterwards, beads were resuspended either in a PBS solution containing the recombinant protein, or only in PBS (negative control), and let to incubate for 1h30min at 4 °C using a benchtop shaker. After incubation was finished, beads were washed with PBS and then incubated with 180 µg of protein extract (60 µg of protein extract per 1 µg of recombinant protein) overnight at 4 °C. Afterwards, beads were washed with extraction solution (the same solution used for immunoprecipitation assay). Finally, beads with protein attached were denatured with the addition of 2× Laemmli Buffer, followed by incubation for 15 minutes at 95 °C. Elute fractions were electrophoretically separated using a polyacrylamide gel electrophoresis and results were assessed through Western Blot procedure (experimental procedure 2.2.5), using antibody against HADHA (1:200) and 3PGDH (1:200) proteins as primary antibodies.

### 2.3.3 Colocalization Assays

In order to assess whether DJ-1 and the other two proteins, HADHA and 3PGDH, were interacting within the cell, immunocytochemistry assays, followed by confocal microscopy, were performed.

#### 2.3.3.1 Immunocytochemistry Optimization

Prior to cell's seeding, 96 multi-well plate (Corning) was coated with four different PDL concentrations (10 µg/mL, 1 µg/mL, 0.1 µg/mL and 0.01 µg/mL), let to incubate for 2h in a humidified chamber at 37 °C, 5% $CO_2$. After incubation, wells were washed with sterile $H_2O$ prior to air dry. Plate was either used right away, or kept at 4 °C until further use.

SH-SY5Y (ATTC®) cells were seeded at $40\times10^3$ cells/$cm^2$ in previously-coated wells, in 1:1 MEM-F12 with 10 FBS culture medium, for 24h, after which immunocytochemistry standard protocol was followed. Briefly, culture medium was completely removed, cells were washed with room temperature PBS and fixed in a solution of 4% (w/v) paraformaldehyde (PFA) (Sigma) in PBS, for 20 minutes at room temperature. After fixation, cells were extensively washed with PBS, followed by permeabilization with 0.1% (v/v) Triton X-100 (Sigma-aldrich) in PBS for 20 minute at room temperature. Cells were then washed with PBS and PBS-T. Proteins were then blocked with a solution of 1% (w/v) BSA in PBS, for 30 minutes at room temperature, following incubation with primary antibodies (anti-HADHA and anti-3PGDH) in blocking solution, at three different dilutions (1:25, 1:50 and 1:100), overnight at 4 °C. Cells were then washed again with PBS and PBS-T, followed by incubation with Alexa Fluor® 488 Donkey Anti-Mouse IgG (A-2102, Life Technologies) (1:200) for 1h at room temperature. After incubation with secondary antibody, cells were extensively washed with PBS, fixed in a solution of 4% (w/v) PFA in PBS, for 5 minutes at room temperature, and then washed with PBS. Finally, for nuclear staining, cells were incubated with

200 ng/mL of 4',6-diamidino-2-phenylindole (DAPI) (Life Technologies), for 5 minutes at room temperature. Following incubation with DAPI, cells were lastly washed with PBS and left in PBS until further analyses. In order to assess ideal antibodies dilutions and PDL concentrations, cells were visualized at the Anxiovert 200 M microscope (Zeiss), using 10 Alexa Fluor 489 reflector, FITC (excitation wavelength: 490 nm, emission wavelength: 525 nm) and DAPI (excitation wavelength: 359 nm, emission wavelength: 461 nm) channels, and 40x magnification for images acquisition. Images processing was performed using AxioVision V 4.9.1.0 (Zeiss) software.

#### 2.3.3.2 Immunocytochemistry Assay

For immunocytochemistry assay, to assess colocalization of DJ-1 with HADHA and 3PGDH proteins. First, glass coverslips were put inside each well of a 24 multi-well plate (Corning) and coated with a solution of 1 µg/mL PDL for 2h in a humidified chamber at 37 °C, 5% $CO_2$. Following incubation, coverslips were washed with sterile $H_2O$ prior to air dry.

SH-SY5Y (ATTC®) cells were seeded at $40x10^3$ cells/$cm^2$ in previously-coated coverslips, in 1:1 MEM-F12 with 10 FBS culture medium, for 24h, after which serum starvation protocol was applied by exchanging culture medium to 1:1 MEM-F12 with 0.1% FBS. Afterwards, redox stimulus was applied, 16h after serum starvation, by addition of 1 mM of $H_2O_2$ in MEM-F12 with 0.1% FBS medium, followed by incubation for 15, and 40 minutes, or addition of MEM-F12 with 0.1% FBS without $H_2O_2$ (corresponding to 0 minutes' time point). As soon as the incubation periods were over, solutions were removed and cells were washed with room temperature PBS and then fixed in 4% (w/v) PFA in PBS solution, for 20 minutes at room temperature. Cell were again washed with PBS, followed by permeabilization with 0.1% (v/v) Triton X-100 in PBS for 20 minutes at room temperature. The washing steps were then repeated with PBS and PBS-T. Proteins were blocked with a solution of 1% (w/v) BSA in PBS, for 30 minutes at room temperature, following incubation, in humidity conditions, with antibodies anti-DJ-1 (1:200), anti-HADHA (1:100) and anti-3PGDH (1:100), overnight at 4 °C. Finishing incubation, cells were again washed with PBS and PBS-T, followed by incubation, in humidity conditions, with Alexa Fluor® 488 Donkey Anti-Mouse IgG antibody (1:200) (to mark HADHA and 3PGDH proteins) and Alexa Fluor® 568 Donkey Anti-Goat IgG (1:200) (A-1107, Life Technologies) antibody (to mark DJ-1 protein), for 1h at room temperature. Afterwards, cells were extensively washed with PBS, fixed in a solution of 4% (w/v) PFA in PBS for 5 minutes at room temperature, and then again washed with PBS. Finally, for nuclear staining, cells were incubated with 200 ng/mL of DAPI, for 5 minutes at room temperature, followed by washes with PBS. Coverslips were then mounted on previously washed slides, using Fluorescence Mounting Medium (Dako), and sealed with nail polish. Prepared coverslips were kept at 4 °C until further analyses. Immunocytochemistry analyses were made using Anxiovert 200 M microscope (Zeiss), using proper channels and 63x magnification for images acquisition. Images processing was performed using AxioVision V 4.9.1.0 (Zeiss) software.

To assess colocalization of the proteins, cells were analyzed through confocal microscopy, which allows the visualization of the specimen at different depth levels, scanning images horizontally, through focal planes. This ensures a true analysis of colocalization between proteins, without signal overlapping or background influence [138]. For this, cells were visualized using LSM 780 confocal microscope (Zeiss), with 100x magnification, operated with ZEN 2012 software (Zeiss), and images were acquired using Z-stack mode and selected gain of 180, pinhole opening

of 90.0 and Smart Setup was used. Images were analyzed using BioimageXD 1.0 (r1799) and ImageJ (1.51a), Fiji package, software.

## 2.4 Study of HADHA Dynamic Interactome Under Oxidative Stress Conditions

For the study of HADHA dynamic interactome, SH-SY5Y cells were exposed to $H_2O_2$ stimuli, as described previously, and cell extract was used to perform HADHA IPs, for the different conditions. Moreover, an IP using Mouse IgG Isotype Control antibody was carried out, as a negative control, to assess unspecific binding. Co-immunoprecipitated proteins were then identified and quantified in order to analyze HADHA interactome and the influence of oxidative stress in such interactions.

### 2.4.1 Cell Sample Preparation

SH-SY5Y cells were seeded at $75\times10^3$ cells/cm$^2$ in 55 cm$^2$ plates, followed by serum starvation, 24h after seeding, and exposed to oxidative stress stimuli for different time points, as described previously (throughout experimental procedure 2.3). For this assay, oxidative stress time points assessed were 0, 20, and 40 minutes, in accordance with the main points of DJ-1-regulated ERK and PI3-K/Akt pathways activation on SH-SY5Y cells under oxidative stimuli, optimized in our laboratory in previous work, following methodology previously described by Ruffels *et al*. [139]. As previously performed, stimulation was stopped with the addition of room temperature PBS, followed by addition of ice-cold of Extraction Solution and proteins were extracted as described in experimental procedure 2.2.1.2. A sample of the extract was used to quantify proteins' content (as described in experimental procedure 2.2.1.3) and remaining lysate was kept on ice until further immunoprecipitation.

### 2.4.2 HADHA Immunoprecipitation

For immunoprecipitation assay, 7.5 mg of dynabeads was used in each experiment, as indicated by the manufacturer's instruction for immunoprecipitations to be detected by mass spectrometry. The antibody-coupling protocol was performed as described in Experimental Procedure 2.3.1.1, using 5 µg of HADHA and Mouse IgG Isotype Control (to detect unspecific binding) antibodies. The antibody-coupled beads resuspended in ES were stored at 4 °C until further immunoprecipitation assays.

IP protocol was performed according to the manufacturer's instruction, with some modifications. Briefly, 5,900 µg of protein were added to 7.5 mg of antibody-coupled dynabeads, previously equilibrated in ES, and let to incubate on a rotator at 4 °C overnight. After incubation, three washing steps with 900 µL ES were performed to minimize nonspecific binding. Finally, proteins were eluted with the addition of 30 µL of Laemmli buffer 2x and boilling at 95 °C for 5 minutes. The eluates were kept at -80 °C until further need. Samples preparation for LC-MS/MS

analysis was performed following the Short GeLC-SWATH approach, as described by Anjo, *et al.,* 2015 [140].

### 2.4.3 Gel Separation and Colloidal Coomassie Staining

To the denatured IP eluates, 2 µl of acrylamide/bis-acrylamide 40% solution per 30 µl of sample was added, to promote cysteine alkylation, and 1 µL of GFP was added. Samples were then electrophoretically separated in a pre-cast 4-20% SDS-polyacrylamide gel (Bio-rad) using a Mini-PROTEAN Tetra Electrophoresis System (Bio-rad), for 15 minutes at 110V. Following separation, proteins were stained using Colloidal Coomassie Staining.

The staining was performed based on the previsously work described by Canadiano, *et al.,* 2004 [141]. Briefly, after electrophoresis, gel was washed with distilled water followed by immersion in staining solution (10% (v/v) of 85% solution of phosphoric acid, 10% (w/v) ammonium sulphate, 20% (v/v) methanol). Coomassie Brilliant Blue G-250 (Thermo Scientific) powder was then added to the solution with a filter to allow the formation of colloidal particles under agitation. Gel stained overnight under agitation and extensively washed with distilled water, and maintained in water until further analysis.

### 2.4.4 Gel Bands Processing and Peptides Extraction

After gel staining, entire lanes were sliced, under a flow chamber, into small pieces, of equal sizes, and transferred to microcentrifuge tubes, according to gel lane sections, with 1 mL of LC-Grade water (Fisher), to prevent gel bands dehydration. Gel pieces were destained by exchanging the water for 1 mL of destaining solution (50 mM ammonium bicarbonate and 30% acetonitrile) and placing the tube in a thermomixer for 15 minutes at 850 rpm, following by removal of staining solution. If gel pieces remained blue, the procedure was repeated, otherwise 1 mL of water was added and tubes were placed on the thermomixer to shake for 10 minutes at 850 rpm. Water was removed from the tubes and gel pieces were dehydrated on a Concentrador Plus (Eppendorf) for 1h, followed by addition of 70 µL of trypsin (15 ng/µL in 10 mM ammonium bicarbonate), or enough to cover the dried gel pieces, and in-gel digestion occurred overnight at room temperature, in the dark, to allow the hydrolysis of the proteins. After incubation, excess liquid (containing trypsin and peptides) was collected to low binding microcentrifuge tubes (Eppendorf) and remaining peptides were extracted by sequential addition of 30%, 50%, and 98% of ACN in 1% FA solutions. After the addition of each solution, tubes were agitated in a thermomixer for 15 minutes at 1,050 rpm, and the solution was collected to the same tubes containing initial tryptic solution. Samples containing the peptides were dried on a Concentrator Plus at 60 °C by rotary evaporation under vacuum. Dried peptides were resuspended in 100 µL of 2% ACN and 1% FA, followed by sonication on a Sonics 750W for 2 minutes in a cuphorn (1’’on 1’’ off cycles at 20% amplitude).

Peptide mixture was then desalted using C18 Bond Elut OMIX solid phase extraction pipette tips (Agilent technology). To summarize, tip columns were hydrated with a 50% ACN solution and equilibrated with 2% ACN and 1% FA solution. Peptides were loaded onto the tips, repeating this step five times, followed by washes with 2% ACN and 1% FA solution, and elution

of such peptides to new LoBind microcentrifuge tubes with 70% ACN and 0.1% FA. Eluates were dried using a Concentrator Plus, at 60 °C. Dried samples were then resuspended in 20 µL of 2% ACN and 0.1% FA. Finally, samples were sonicated using a cup-horn (2 minutes with 1'' on 1'' off cycles at 20% amplitude), centrifuged for 5 minutes at 14,100×g, and supernatant was transferred into vials for subsequent LC-MS/MS analysis.

### 2.4.5 Protein Identification and Quantification by LC-MS/MS

Protein identification and relative quantification was carried out on a hybrid quadrupole time-of-flight mass spectrometer (Triple TOF™ 5600 System, ABSciex). Samples were analyzed in two phases: information-dependent acquisition (IDA), for pooled samples, followed by sequential windowed data independent acquisition of the total high-resolution mass spectra (SWATH), for individual samples. Peptides separation was performed using liquid chromatography (nanoLC Ultra 2D, Eksingent) on a MicroLC column ChromXP™ C18CL (300 µm ID × 15cm length, 3 µm particles, 120 Å pore size, Eksigent®) at 5µL/min with a multistep gradient: 0-5 min linear gradient from 5 to 6 %, 5-46 min linear gradient from 6 % to 28 % and, 46-47 min to 35 % of acetonitrile in 0.1 % FA. Peptides were eluted into the mass spectrometer using an electrospray ionization source (DuoSpray™ Source, ABSciex®) with a 50 µm internal diameter (ID) stainless steel emitter (NewObjective). One third of each sample's volume was used for protein identification, using IDA. The mass spectrometer was set for information dependent acquisition scanning full spectra (350-1250 m/z) for 250 ms, followed by up to 100 MS/MS scans (100-1500 m/z from a dynamic accumulation time – minimum 30 ms for precursor above the intensity threshold of 1000 – in order to maintain a cycle time of 3.3 s). Candidate ions with a charge state between +2 and +5 counts above minimum threshold of 10 counts per second were isolated for fragmentation and one MS/MS spectra was collected before adding those ions to the exclusion list for 25 seconds (mass spectrometer operated by Analyst® TF 1.7, ABSciex). Rolling collision was used with a collision energy spread of 5.

Two thirds each sample's volume was used for quantitative analysis by SWATH acquisition mode, using the same chromatographic conditions used as in the IDA analysis described above. For SWATH-MS-based experiments, mass spectrometer was operated in a looped product ion mode [137]. The instrument setup was designed specifically for the samples to be analyzed (Supplementary Table 6.1), in order to adapt the SWATH windows to the complexity of the samples set to be analyzed. Briefly, a set of windows of variable width (containing 1 m/z for windows overlap) was constructed covering the precursor mass range of 350-1250 m/z. A 250 ms survey scan (350-1500 m/z) was acquired at the beginning of each cycle for instrument calibration and SWATH-MS/MS spectra were collected from 100-1500 m/z for 50 ms resulting in a cycle time of 3.25 s from the precursors ranging from 350 to 1250 m/z. The collision energy for each window was determined according to the calculation for a charge +2 ion centered upon the window with variable collision energy spread (CES) according to the window (Supplementary Table 7.1).

## 2.5 DATA ANALYSES

Pull down immunoblots were analyzed by calculating the adjusted volumes (total intensities in a given area with local background subtraction) for each immunoreactive band using Image Lab v5.1 software (Bio-rad Laboratories). All bands were adjusted for the band corresponding to DJ-1, before normalization to maximum amount of HADHA/PGDH. Statistical analysis was performed using GraphPad Prism v6.01 (GraphPad Software, Inc). Statistical significance was considered relevant for $*\rho < 0.05$, $**\rho < 0.01$, and $***\rho < 0.001$, using Kruskal-Walli's test, followed by Dunn's Multiple Comparison *post hoc* test, for comparison among experimental conditions. Parametric assumption, such as data normality, was assessed using Shapuro-Wilk Test. Data presented as mean ± standard deviation (SD). Every experimental condition was tested in four sets of independent experiments.

For proteins identification and library generation Protein Pilot software (v5.1, ABSciex) was used, using the following search parameters: (i) search against a database composed by *Homo Sapiens* from SwissProt (released at May 2016), and malE-GFP; (ii) acrylamide alkylated cysteines as fixed modification; (iii) trypsin as digestion enzyme. An independent False Discovery Rate (FDR) analysis using the target-decoy approach provided with Protein Pilot software was used to assess the quality of the identifications and positive identifications were considered when proteins and peptides reached a 5% local FDR [142,143]. Venn diagrams were designed (using BioVenn application, http://www.cmbi.ru.nl/cdd/biovenn/) to help visualize the number of proteins identified in control IP *versus* HADHA IP, and between the three conditions of HADHA IP (0 minutes, 20 minutes, and 40 minutes).

For SWATH-MS data processing, a specific library of precursor masses and fragment ions was created by combining all files from IDA experiments, using Protein Pilot software with the same parameters as described above. Data processing was performed using SWATH™ processing plug-in for PeakView™ (v2.0.01, ABSciex). Briefly, peptides were selected automatically from the library using the following criteria: (I) the unique peptides for a specific target protein were ranked by the intensity of the precursor ion from IDA analysis as estimated by ProteinPilot, and (ii) peptides with biological modifications and/or shared between different protein entries/isoforms were excluded from selection. Up to 15 peptides were chosen per protein, and SWATH™ quantitation was attempted for all proteins that in the library file were identified below 5% local FDR from ProteinPilot searches. In SWATH™ Acquisition data, peptides are confirmed by finding and scoring peak groups, which are a set of fragment ions for the peptide.

Target fragment ions, up to 5, were automatically selected and peak groups were scored following the criteria described in Lambert *et al*. [144]. Peak group confidence threshold was determined based on a FDR analysis using the target-decoy approach and 1% extraction FDR threshold was used for the analyses. Peptides that met the 1% FDR threshold in at least two of the three biological replicates were retained, and the peak areas of the target fragment ions of those peptides were extracted across the experiments, using an extracted-ion chromatogram (XIC) window of 3 minutes with 100 ppm XIC width.

Human protein levels were estimated by summing all the transitions from all the peptides for a given protein, and normalized to the internal standard (malE-GFP) quantification. To identify true protein interactions, normalized data were compared between the different conditions and the control condition, in which a normal mouse IgG was used. For further analysis, it was only considered proteins with statistical difference among the conditions, and those were considered

the true putative interactors. Statistical significance was considered relevant for $\rho$ <0.1 [145] using Kruskal-Walli's test.

For comparisons across the time points, abundances were normalized with respect to HADHA quantification, already with negative control excluded from the analysis. To analyze the data acquired with AP-MS/MS approach, Graphical Proteomics Data Explorer (GProX) software was used, which allowed clustering analysis and complementary heat maps, as previously performed by Martins-Marques, *et al*., 2015 [145]. Briefly, clustering was performed using the unsupervised clustering fuzzy c-means algorithm implemented in the Mfuzz package, a soft clustering algorithm, noise-robust and well-fitted to the protein file data. Clustering also allowed the tracing of different HADHA interaction profiles throughout the various experimental conditions (using interaction levels – protein levels normalized to HADHA levels – of the previously selected HADHA interactors).

# 3 RESULTS

Parkinson's disease, as the second most common neurodegenerative disorder, has been the object of thorough research. It is considered a sporadic disease, with molecular causes and mechanisms leading to neurodegeneration remaining unknown. Nevertheless, several studies identified different susceptibility genes in a region assigned PARK loci, in which monogenic mutations lead to *Parkinsonism* development, including *dj1* gene.

DJ-1 protein has shown to play a role in neuroprotection, particularly under oxidative stress conditions and mitochondrial damage. However, the mechanisms through which DJ-1 mediates its cytoprotective function are still unclear. Nonetheless, some studies have identified several mutations on *dj1* that have been shown to disrupt DJ-1, by changing its oxidative state for example, affecting previously mentioned function. Although DJ-1 has been unequivocally linked to familial early onset PD, altered oxidation states of the protein were reported in brains of sporadic PD patients.

It is also known that DJ-1 protein accomplishes its functions by interacting with other proteins, being a part of a complex dynamic interactome. Indeed, several DJ-1 binding partners were identified, including HADHA, 3PGDH, NDUFA4 proteins, among others, and reported to have pivotal cell pro-survival functions under oxidative stress conditions. Thus, validation of these binding partners and knowledge on how DJ-1 mutations may influence such interactions would provide important insights into cellular and molecular mechanisms of neurodegeneration caused by oxidative stress in PD.

In this context, the validation of DJ-1 interaction with HADHA, PGDH, and NDUFA4 proteins was performed. To do so, several techniques were employed, such as co-immunoprecipitation, pull down and immunocytochemistry, to assess colocalization of the protein within the cell, in physiological conditions. Moreover, HADHA dynamic interactome under oxidative stress conditions was thoroughly studied, combining affinity purification strategy, through co-immunoprecipitation, with liquid chromatography followed by tandem mass spectrometry (LC-MS/MS). This interactome study should allow a deeper understanding on the mechanisms regulated by HADHA, and possibly an extrapolation of which of those are affected by interaction with DJ-1, allowing an increased knowledge on molecular pathways that lead to PD. The working model chosen was SH-SY5Y neuroblastoma cell line, as it is composed of doparminergic neurons making it a good cell model for PD study [146], and has been widely used in studies with DJ-1, oxidative stress [76], and mitochondrial dysfunction [147] in PD. The oxidative stress conditions were established by exposure to 1 mM of $H_2O_2$, a non-lethal concentration under the experimental conditions used that mimics the ROS burst responsible for the activation of diverse protection mechanisms against such insult [76,139].

## 3.1 ANTIBODIES TESTING

Prior to the start of immunoprecipitation assays for the validation of the interactions the antibodies against HADHA, PGDH, and NDUFA4L2 needed to be assessed for specific binding to the protein of interest. Antibodies proper dilutions and sample's protein amount was tested to defined optimal parameters. Thus, signal of HADHA, PGDH, and NDUFA4 proteins using 15 µg and 30 µg of whole cell lysate with 1:200 and 1:500 antibodies dilution was assessed through western blot (Figure 3.1).

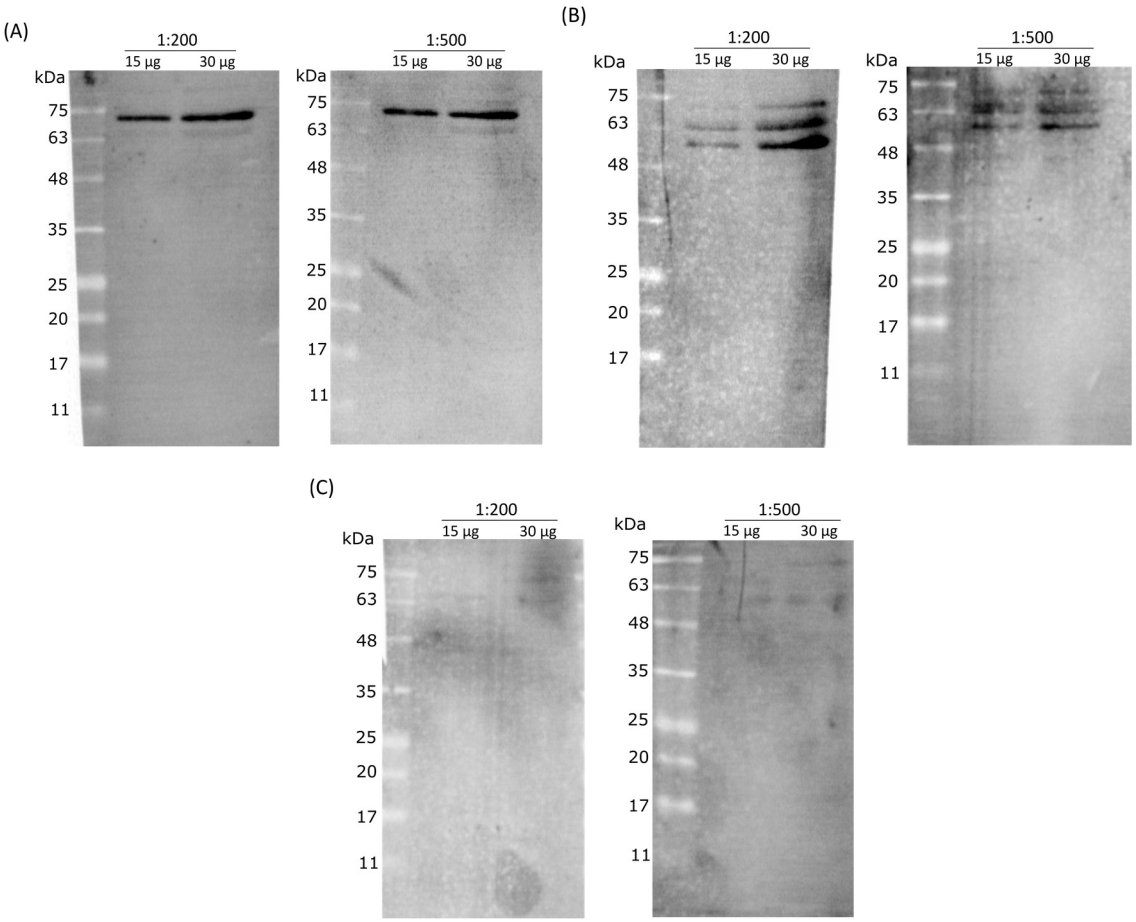


***Figure 3.1*** **–** Immunoblotting analysis of HADHA, PGDH and NDUFA4 proteins expression in SH-SY5Y (ATTC) whole cell lysate. Different protein amount (15 µg and 30 µg) of SH-SY5Y (ATTC) protein extract was subjected to Western Blot procedure, using 1:200 and 1:500 of (A) anti-HADHA, (B) anti-3PGDH, and (C) anti-NDUFA4L2 antibodies dilutions.

The results show that it is possible to observe the presence of a signal in the top four membranes, belonging to both antibodies dilutions and HADHA (Figure 3.1*A*) and PGDH (Figure 3.1*B*) proteins. In anti-HADHA blot membranes, both antibodies dilution (1:200 and 1:500) allowed a detection of a strong signal, even in the lowest amount of protein (15 µg). On the other hand, anti-3PGDH blot membranes show a decreased signal intensity when using a higher antibody dilution (1:500). A similar result is observed when using 1:200 antibody dilution and the lowest amount of protein (15 µg). Overall, the results of these membranes show that both anti-HADHA and anti-3PGDH antibodies are functional and allow the detection of HADHA and PGDH proteins in the extract used for further experimental procedures. On the other hand, analyzing

Figure 3.1*C*, which illustrate immunoblot results for NDUFA4 protein, it is possible to observe the absence of a signal in all the conditions, even when lowest antibody dilution (1:200) and highest protein amount (30 µg) was used. Thus, a variety of tests were performed using anti-NDUFA4L2 antibody, including the use of rat cortex samples, different denaturation methods, HeLa extract (which supplier indicates as antibody positive control), and the use of a blocking peptide to assess whether we were detecting NDUFA4 protein or unspecific binding (details and results depicted within Supplementary Figure 7.1).

## 3.2 VALIDATION OF DJ-1 INTERACTION WITH HADHA AND PGDH

A previous DJ-1 interactome screening performed in our lab identified several binding partners in normal and oxidative stress conditions. From those, proteins belonging to oxidoreductases family were identified, including HADHA, PGDH and NDUFA4 proteins. One major goal of this project was to validate such interactions through different techniques.

To validate the interaction, immunoprecipitation assays, DJ-1 pull downs and colocalization assays were performed in SH-SY5Y cells exposed to 0, 20 and 40 minutes of $H_2O_2$.

### 3.2.1 Immunoprecipitation

Immunoprecipitation assays, as already described in experimental procedures, were performed using Dynabeads® Co-immunoprecipitation Kit. The advantage of this kit relies in the magnetic properties of the beads and the covalent nature of the binding between the antibody and the beads. Such magnetic properties facilitate IP experimental steps: the separation of protein complexes from the extract, the washing, buffer exchanges, and the elution steps. Moreover, the use of magnetic beads allows the discard of centrifugation steps, thus avoiding less disruption of protein complexes throughout the experiment. Therefore, this kit was chosen because it combines a good separation of the protein complexes, higher rate of protein complexes recovery, and, due to the reagents used throughout the experiment, less unspecific binding.

Prior to the IP assay *per se*, the antibody-bead coupling reaction yield was analyzed to assessed whether the bead/antibody ratio used allows a good yield (results are depicted on Supplementary Figure 7.2)

For immunoprecipitation assay, SH-SY5Y serum starved cells were exposed to $H_2O_2$ for 0, 20, and 40 minutes, followed by IP using either HADHA or PGDH antibodies coupled to beads, in each condition, or a normal mouse IgG coupled to the beads (IP control). Eluates were denatured to disrupt the beads-antibody couple, and the protein complexes from the antibody, followed by electrophoretical separation of the proteins through SDS-PAGE. To assess IP results, western blot procedure was performed using anti-DJ-1 antibody, to determine whether the protein was present in immunoprecipitation eluate. If indeed, a DJ-1 signal was detected in the blot membranes, it would mean that the protein was interacting with HADHA and/or PGDH, thus co-purifying with them. Also, immunodetection of HADHA and PGDH using anti-HADHA and anti-3PGDH antibodies was accomplished (Figure 3.2).

DJ-1 protein was not detected in any eluates of the several IP, in any time point (Figure 3.2*A*). However, it was also not detected in HADHA IP input fraction, and in PGDH IP it was detected but with a quite vanished signal, showing its low abundance in such fraction. As this could be due to a problem during the immunoblot procedure, both HADHA and PGDH were immunodetected in the respective membranes (Figure 3.2*B, C*). Figure 3.2*B* shows the presence of a HADHA signal in input fraction of HADHA IP (upper panel) and in the remaining lanes, corresponding to 0, 20 and 40 minutes of $H_2O_2$ exposure, thus confirming the binding of the protein to the antibody. Moreover, the same signal is present in the input fraction of IgG IP (lower panel), but not in the IP eluates fraction, ensuring there was no unspecific binding. The incubation with anti-HADHA antibody allowed the visualization of both heavy chains (HC) and light chains (LC) of the IgG, confirming the presence of the antibodies in each condition. Overall, this means that the lack of DJ-1 signal in HADHA IP eluates is not because antibodies were absent or because HADHA was not binding to its antibody. Figure 3.2*C* shows the presence of PGDH signal in input fraction of PGDH IP, but with low intensity. As PGDH protein is in the same molecular weight range as the heavy chain (HC) of the IgG, it is not possible to say whether the protein is also present, or not, in the IP eluates. For this, different antibodies, raised in a different species, should have been used for IP and WB. Nonetheless, the incubation with anti-3PGDH antibody allowed the visualization of both heavy chains (HC) and light chains (LC) of the IgG, also confirming the presence of the antibody in each condition. Again, this result reinforces that the lack of DJ-1 signal in PGDH IP eluates is not due to the lack of anti-3PGDH-bound beads. The results obtained through this IP experiment did not allowed us a validation of DJ-1 interaction with HADHA and PGDH. However, it would be unwise to state that they do not interact, as there is no DJ-1 signal in the input fractions, meaning there was no protein available in the extract to interact, if indeed interaction occurs, with HADHA and PGDH.

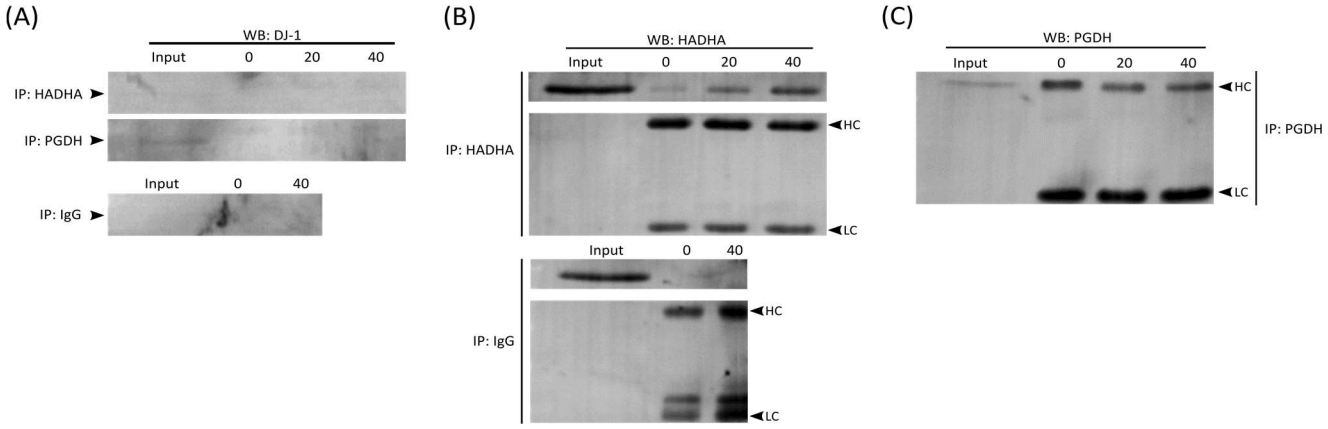


***Figure 3.2 –*** Immunoblot analysis of HADHA and PGDH protein in immunoprecipitation eluates. Serum-starved SH-SY5Y cells were treated with 1 mM of $H_2O_2$ for the indicated periods of time (0, 20, 40 minutes), and equal amounts of protein extract were used for further IP assay. Presence of DJ-1, HADHA, and PGDH proteins in IP eluates were assessed through western blot. (A) Immunodetection of DJ-1 in HADHA IP (upper panel), PGDH IP (middle panel), and Control IP (lower panel). (B) Immunodetection of HADHA and IgGs in HADHA IP (upper panel), and Control IP (lower panel). (C) Immunodetection of PGDH and IgGs in PGDH IP. Input – whole cell extract used for experiment (30 µg); HC – IgG heavy chain; LC – IgG light chain. Anti-mouse (1:10,000) and anti-goat (1:6,000) antibodies were used as secondary antibodies.

### 3.2.2 DJ-1 Pull Down

With the immunoprecipitation method performed in this project, we were not able to validate a physical interaction between DJ-1 the other two proteins focused in this study. However, previous work, accomplished in our lab (unpublished data), successfully identified HADHA and PGDH proteins interaction with endogenous DJ-1, also in SH-SY5Y cells.

A pull down assay was then performed to confirm the interactions previously predicted through co-immunoprecipitation, and to assess interaction of HADHA and PGDH proteins to recombinant WT DJ-1. For that, SH-SY5Y cells were exposed to $H_2O_2$ for different periods (0, 20 and 40 minutes), protein extract was produced and placed in contact with recombinant DJ-1-attached HisMag resin. Recombinant DJ-1 proteins and their interactors were recovered, denatured, electrophoretically separated, and the presence of HADHA and PGDH in pull down eluates was assessed through western blot (Figure 3.3). To evaluate unspecific binding of proteins, an extra pull down experiment was performed in parallel, using HisMag resin with no recombinant proteins attached.

Results show the presence of both HADHA and PGDH proteins in pull down eluates, in all time points of $H_2O_2$ exposure, this is possible to observe in the representative blot membranes (on top) marked with anti-HADHA (Figure 3.3*A*) and anti-3PGDH (Figure 3.3*B*) antibodies, and in the correspondent graphic representation (on bottom). Moreover, and more interestingly, it is possible to distinguish an interaction profile throughout the 40 minutes of oxidative stress.

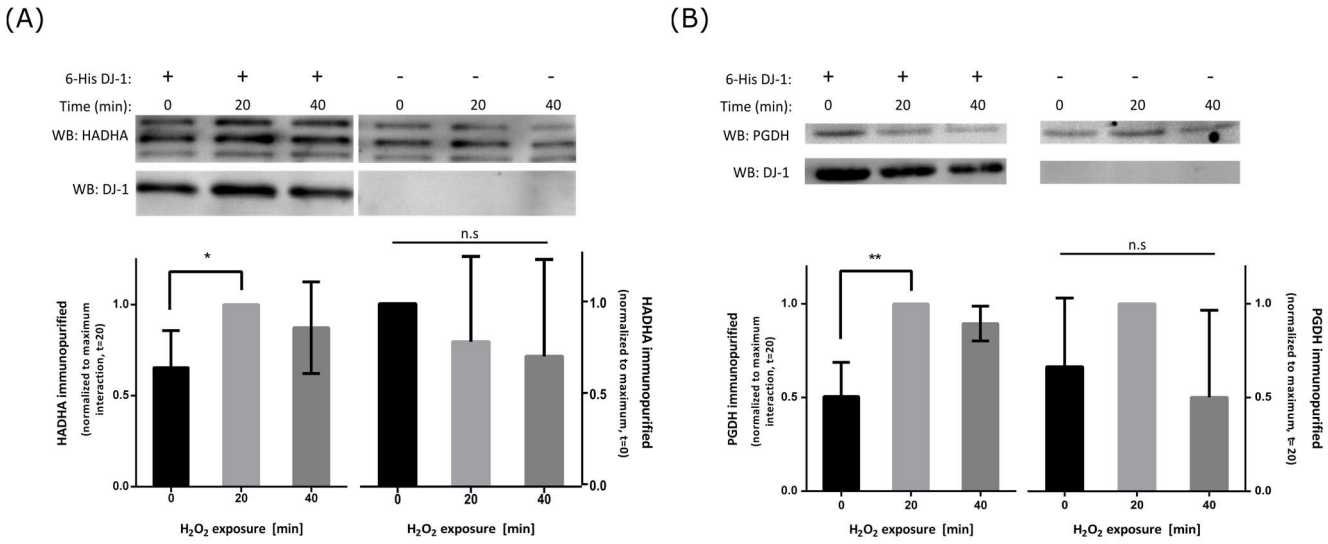


***Figure 3.3 –*** HADHA and PGDH interaction profile with recombinant DJ-1 protein, throughout 40 minutes of SH-SY5Y cells exposure to $H_2O_2$. Serum-starved SH-SY5Y cells were treated with 1 mM of $H_2O_2$ for the indicated periods of time (0, 20 and 40 minutes), and equal amounts of protein extract were placed in contact with recombinant DJ-1-attached HisMag resin. Interaction was assessed by analyzing the presence of HADHA and PGDH in pull down eluates, through western blot. Representative western blot showing (A) HADHA and (B) PGDH presence in the eluates (on top) and graphic representation of the mean ± SD of four independent experiments (n=4) (on bottom) are shown. Data are presented as relative quantification to maximum amount observed. *$p$ <0.05 and **$p$ < 0.01, represent significantly different comparison among experiments, using Krustkal-Wallis followed by Dunn's multiple comparisons post hoc tests; n.s – no statistical difference between the conditions.

Graphic representation shows a significant increase in HADHA and PGDH interaction with recombinant DJ-1 in 20 minutes of $H_2O_2$ exposure, followed by a decrease or maintenance until the 40 minutes of $H_2O_2$ treatment (no significant decrease or increase from 0 minutes to 40 minutes, or from 20 minutes to 40 minutes). One interestingly point worth mention, is that a similar project is being performed in our lab, testing other proteins than HADHA and PGDH, and the same interaction profile is being observed, an increase in the interaction at 20 minutes and a decrease or maintenance at 40 minutes.

Pull down results, however, show a strong presence of HADHA and PGDH signal in the eluates of control experiment, in which no recombinant protein was attached to the beads, and to understand if the previously mentioned profile was nonspecific, and due to unspecific binding to the beads, HADHA and PGDH were quantified in control conditions and the profiles were assessed. The graphical representation shows that no profile was observed in this condition, with no significance difference between the different time points, meaning there was no increase at 20 minutes followed by a decrease or maintenance at 40 minutes. The presence of these proteins in the eluates of pull downs performed with no recombinant protein attached to the beads might be explained by the composition of the resin, as these beads are composed of nickel ($Ni^{2+}$), which is electropositive and confers a high positive charge environment, highly promoting proteins attraction and increase their binding.

Altogether, these results seem to suggest that the profile observed previously occurs due to the presence of the recombinant DJ-1 attached to the HisMag resin, which might mean that HADHA and PGDH proteins are indeed interacting with 6-His DJ-1 protein.

### 3.2.3 DJ-1 Colocalization with HADHA and PGDH

Until now, results from *in vitro* studies, seem to suggest an interaction between HADHA and PGDH with recombinant DJ-1 protein, and previous work performed in our lab suggested such interaction with endogenous DJ-1 protein. However, to determine whether those proteins also associate with DJ-1 *in situ*, immunofluorescence confocal microscopy experiment was performed. Prior to confocal microscopy analysis, some parameters of the immunocytochemistry assay were optimized, such as the optimal antibody dilution and the optimal PDL concentration (details and results on Supplementary Data 7.3). The importance of PDL coating of the surface arises from the fact that SH-SY5Y cells are adherent but hardly adhere to glass, which can be overcome by coating the glass surface with PDL, a positively charged polymer that will maintain cells adherent to the surface.

For confocal microscopy experiments, SH-SY5Y cells were exposed to $H_2O_2$ (0, 20 and 40 minutes), followed by fixation, permeabilization, protein blockage, and incubation with anti-HADHA, or anti-3PGDH, and anti-DJ-1 antibodies and subsequent fluorophore-conjugated secondary antibodies. Cells were then observed under confocal microscope, images were retrieved, and colocalization of the proteins was assessed. Results show that DJ-1 is indeed colocalizing with both proteins in SH-SY5Y cells (Figure 3.4). Colocalization pixel map shows DJ-1 colocalizing with HADHA (upper panel), at 40 minutes of $H_2O_2$ exposure, within the mitochondria around the nucleus, where DJ-1 is being highly expressed, whilst colocalization with PGDH (lower panel), at 0 minutes of $H_2O_2$ exposure, takes place in the cytosol, where both PGDH and DJ-1 are being expressed. Such differential DJ-1 expression in the cell is consistent with studies showing

oxidative stress-induced DJ-1 translocation to the mitochondria [73], and an increase in protein expression in the nucleus, whereas its expression in the cytosol decreases [148].

Altogether, immunofluorescence confocal microscopy results show that DJ-1 in fact interacts with HADHA and PGDH protein *in situ*, strengthening the results previously obtained with the pull down experiments, which suggested an interaction between the proteins. Although the kinetics observed with the recombinant protein (an increase in interaction in 20 minutes of $H_2O_2$ exposure, followed by a decrease or maintenance) was not detected, interaction between the proteins in SH-SY5Y cells was in facto confirmed.

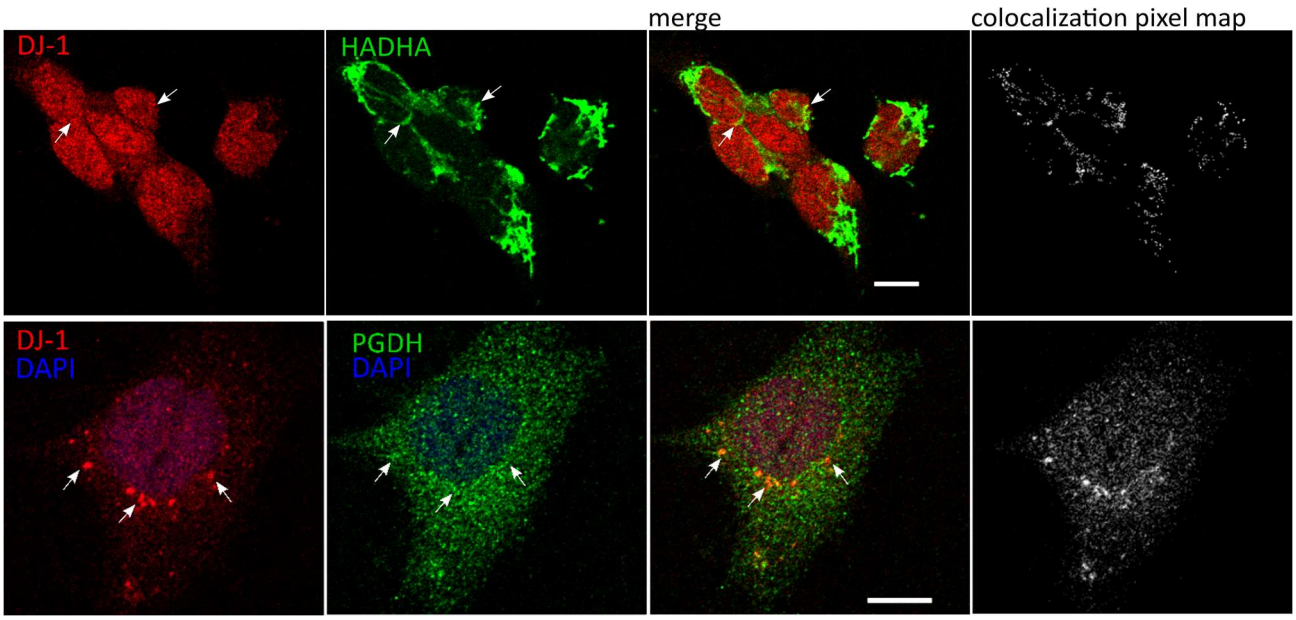


***Figure 3.4 –*** HADHA and PGDH colocalize with DJ-1 in SH-SY5Y cells. Immunostaining of DJ-1 and HADHA, at 40 minutes of $H_2O_2$ exposure (upper panel) and PGDH, at 0 minutes of $H_2O_2$ exposure (lower panel), in SH-SY5Y cells, through confocal microscopy analysis. Nuclei were stained with DAPI (blue), however, staining is not shown in the upper panel as DJ-1 is mainly localized in the nucleus. Scale bars, 10 µm. Arrows indicate examples of colocalization spots. Colocalization pixel map is depicted on the right side.

## 3.3 HADHA Dynamic Interactome in Oxidative Stress Conditions

Results from validation assays seem to corroborate the hypothesis of an interaction between DJ-1 and the other proteins focused on this study. Moreover, those results also seem to indicate that such interactions are regulated by oxidative stress condition, which shows a stress-dependent DJ-1 role in regulation of oxidoreductases proteins, whose function are related with redox reactions, thus being closely linked with cell response to oxidative stress, and subsequent cell death/survival. Therefore, it became of great relevance to study the dynamic interactome of the putative DJ-1 interactors, also in oxidative stress conditions, and assess whether they could be involved in neuroprotection and search for common pathways and roles with the ones previously identified for DJ-1. As mentioned before, HADHA is a mitochondrial protein, and such organelle is not only a major source of ROS as it is much affected by cellular stress [149], thus, the dynamic interactome, under oxidative stress conditions, of this protein was studied, to elucidate its role in such conditions.

To elucidate whether HADHA has an influence in cellular response against oxidative stress, and if so through which mechanisms, the binding partners of the protein were identified in SH-SY5Y cells exposed to different $H_2O_2$ stimulation periods. Oxidative stimuli conditions (0 minutes, 20 minutes and 40 minutes) were chosen based on a previous work with key points of ERK 1/2 and Akt activation, being time zero the resting condition, 20 minutes the maximum activation of such pathways, followed by a drastic decrease (40 minutes). The experimental procedure included immunoprecipitation of HADHA, in the defined conditions, followed by interactome screening through LC-MS/MS. Additionally, a parallel immunoprecipitation was performed using normal mouse IgG (IP negative control), in order to assess non-specific interactors (proteins that bind unspecifically to the beads and the constant regions of the antibody). IDA followed by SWATH acquisitions were used to identify and quantify, respectively, the proteins present in IP eluates. This methodology enabled, not only the identification of HADHA binding partners, but also to trace interaction profiles under the described conditions.

### 3.3.1 Protein Identification and Quantification

With the present approach, it was possible to identify 790 proteins, from which 575 were quantified (Supplementary Table 6.2). Area-proportional Venn diagrams were designed to do a quantitative analysis of proteins identified through IDA acquisition method (Figure 3.5). A first comparison between HADHA IP and negative control IP was performed, and the diagram showed a much higher number of proteins identified in HADHA IP then in the negative control (Figure 3.5*A*). Thus, this might mean that the majority of proteins identified in IP eluates are indeed copurifying with HADHA, interacting with the protein, and not either with the beads or with the constant region of anti-HADHA antibody, i.e. the majority of the proteins identified are not unspecific binders. Then, a second comparison was performed between the conditions in which HADHA IP occurred (0, 20, and 40 minutes of $H_2O_2$ exposure) (Figure 3.5*B*).

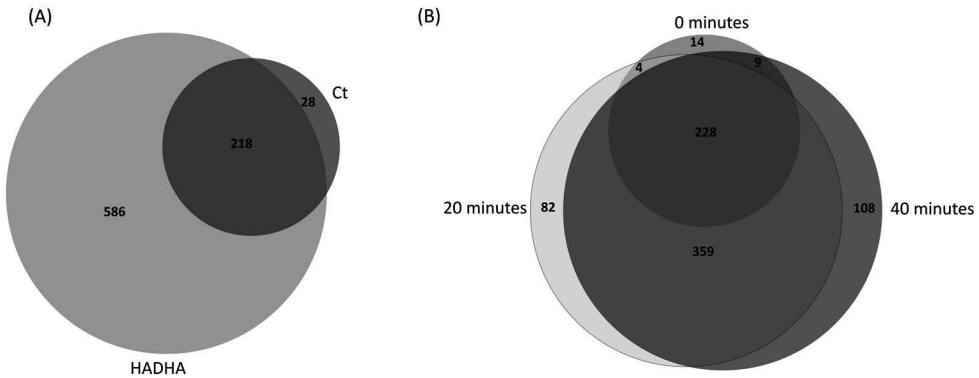


***Figure 3.5 –*** Venn diagrams of identified proteins in all conditions. Area-proportional Venn diagrams showing shared and unique number of proteins identified through IDA acquisition method. (A) comparison between number of proteins identified in HADHA IP (HADHA) and in negative control IP (Ct). (B) comparison between the three conditions used for HADHA IP (0 minutes, 20 minutes, and 40 minutes of $H_2O_2$ exposure).

Venn diagram show that from the total number of proteins, 228 were shared between the 3 conditions, and that the majority of the proteins identified (359) were shared between 20 minutes and 40 minutes of $H_2O_2$ exposure conditions, whereas it was also possible to identify unique proteins in each conditions. However, the most pertinent analysis possible to be made with such results is the notorious increase in the number of proteins identified under oxidative stress conditions (20 and 40 minutes) when compared with the number of proteins identified under resting conditions (0 minutes).

Although results from proteins identification are not conclusive *per se*, the differences in number of proteins identified between the different conditions are suggestive of not only a variation in HADHA interactome as a result of oxidative stress induction, but are also suggestive of a stress-dependent regulation of HADHA protein.

### 3.3.2 Clustering of Profiles and Comparative Analyses

HADHA is a mitochondrial protein that was previously identified, through AP-MS approach, as a putative binding partner of PD-associated DJ-1 protein. The further validations studies, performed in this project, seems to corroborate the previous assumptions and are suggestive of an interaction between the two proteins. Thus, it became of great relevance to study HADHA dynamic interactome to elucidate which cellular mechanisms the protein might possibly influence in oxidative stress conditions. Hence, SWATH strategy was applied to characterize HADHA-interacting network and its dynamics during oxidative stress stimuli.

As mentioned before, from the 790 identified proteins, 575 were quantified and compared between the various experimental conditions (Supplementary Table 7.2). These 575 proteins were further evaluated by complementary analysis to distinguish truly HADHA interactors from nonspecific binding to control IP. Proteins were considered as putative HADHA interactors if they had a *p*-value under 0.1 in the statistical analysis performed (Kruskal-Wallis test). This *p*-value threshold was chosen as this is the first interactome screening of HADHA protein and it's more relevant to evaluate a higher number of proteins. Through this evaluation, it was possible to distinguish 524 proteins considered putative HADHA binding partners. In order to characterize dynamic HADHA-interacting network with those 524 putative binding partners, interaction levels were, by normalizing to the levels of immunopurified HADHA, in each experimental condition. By performing this adjustment, a more accurate measurement of the interactions, in each condition, was achieved. Those interaction values were further subjected to heat map analysis followed by complementary unsupervised clustering analysis. The results show that 523 HADHA-interactors identified display a differential profile of interaction between the three experimental conditions (Figure 3.6*A*). Performing such analysis, it was possible to distinguish seven different interaction profiles: (i) a drastic increase in interaction in the 20 minutes condition, followed by a decrease to basal levels, (ii) a decrease in interaction, from the 0 minutes until the 40 minutes conditions, (iii) a maintenance in the interaction from 0 minutes to 20 minutes, followed by a drastic decrease, (iv) a slight increase in the interaction until the 20 minutes of oxidative stress, followed by a drastic decrease in 40 minutes condition, (v) a drastic increase in interaction until the 20 minutes condition, followed by a slight decrease, (vi) a drastic increase in interactions in the 20 minutes of oxidative stress, followed by a maintenance of such interactions, and (vii) an increase in the interaction throughout the 40 minutes of oxidative stress

stimuli. Moreover, it is possible to observe that the majority of the interactions increase within the 20 minutes of stimuli, followed by a decrease in the 40 minutes' condition (clusters 1, and 5), being cluster 5 the most represented, bearing the highest number of protein (n=216).

To highlight the most representative biological processes associated with each interaction profile, a Gene Ontology (GO) enrichment analysis for each cluster of interactors was performed (Figure 3.6*B*). Overall, the results show that there is an overrepresentation of HADHA-interactors related to gene expression, such as transcription elongation from RNA polymerase II promoter, or DNA replication GO biological processes (cluster 1), positive and negative regulation of gene expression, epigenetics, DNA duplex unwinding, gene silencing by RNA, termination of RNA polymerase II transcription GO biological processes (clusters 1 and 5), or positive and negative regulation of translation, regulation of mRNA stability, DNA recombination, ribosomal large subunit assembly (cluster 5) and many others. Moreover, overrepresentation of interactors related to cytoskeleton was observed, demonstrated by GO biological processes such as extracellular matrix organization (cluster 2), mitotic nuclear envelop disassembly (clusters 1 and 5), or cellular component disassembly involved in execution phase of apoptosis (cluster 5). Also, many HADHA-interactors were found to be involved be associated with mediation of signaling pathways, like ephrin receptor signaling pathway (cluster 6), cytokine-mediated signaling pathway (clusters 1 and 5), or neurotrophin TRK receptor signaling pathway, Wnt signaling pathway, Ras protein signal transduction, activation of MAPKK activity (cluster 5) and many others. Some metabolic processes also seemed to be mediated by HADHA-interacting proteins, such as protein N-linked glycosylation via asparagine (clusters 5 and 6), regulation of glucose transport (clusters 1 and 5), histone mRNA metabolic process, and insulin receptor signaling pathway (cluster 5), for example. Finally, such interactions seem to mediate cellular response to stress through apoptosis, demonstrated by regulation of cellular response to heat (clusters 1 and 5), negative regulation of neuron apoptotic process, positive regulation of apoptotic process (cluster 5) among others.

Altogether, these results demonstrate that HADHA has a quite dynamic interactome that is strongly regulated by oxidative stress. Throughout 40 minutes of oxidative stress stimuli, HADHA interactions with the putative binding partners were modulated. The interactors predicted and analyzed in this project showed implication in several different mechanisms and functions, demonstrating and suggesting HADHA involvement in a myriad of biological processes, and that such implication is strongly influenced by oxidative stress.

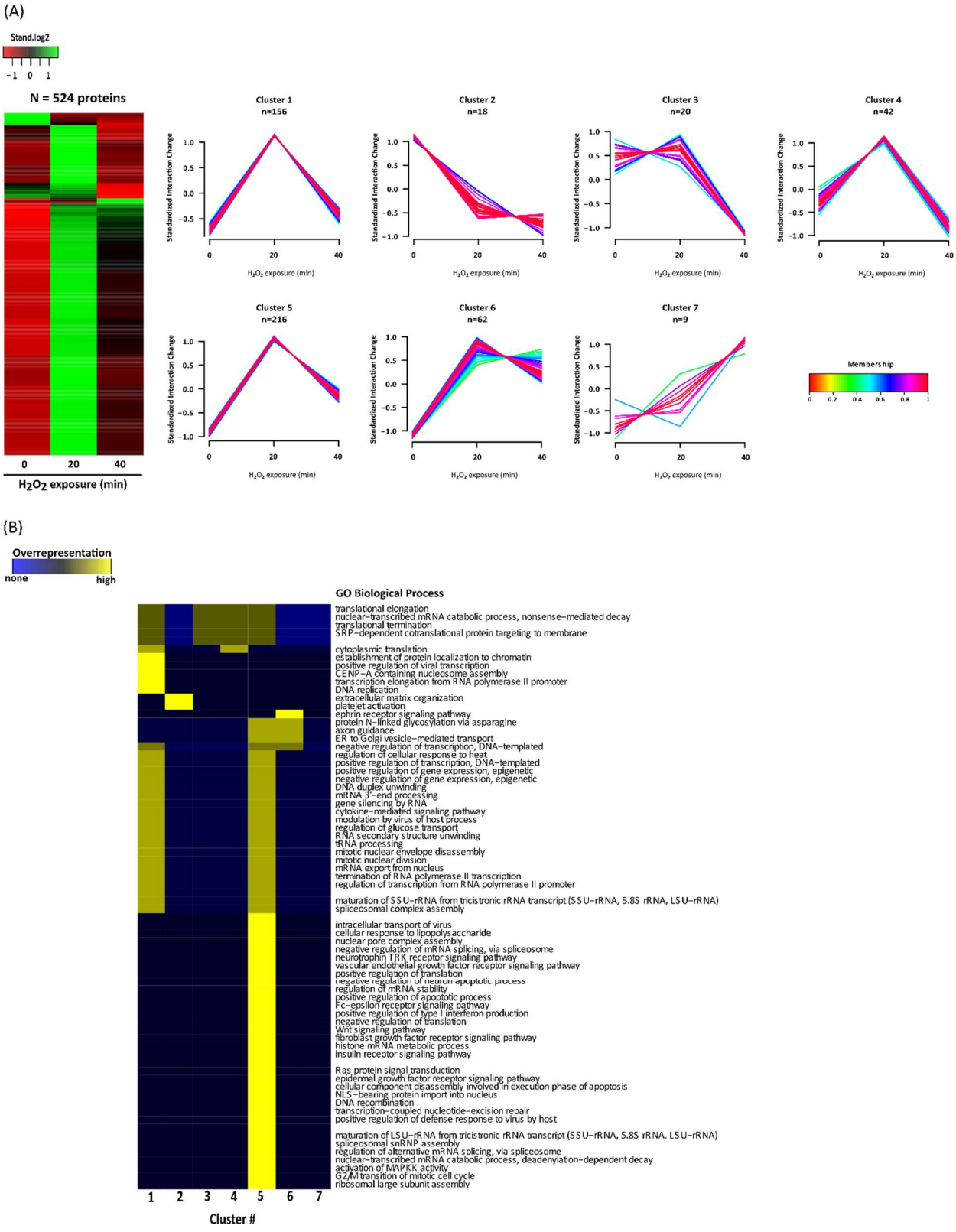


***Figure 3.6*** **–** HADHA-interacting dynamic network in SH-SY5Y cells exposed to oxidative stress for 0, 20, and 40 minutes. (A) dynamic profiles of HADHA interactors among the experimental conditions. Heatmap (left figure) and unsupervised clustering (right figure) were performed for the standardized interaction levels - proteins levels normalized to HADHA – of the 524 putative interactors. An upper and lower ratio limit of $\log_2$ (2) and $\log_2$ (0.5) was used for inclusion into a cluster. "n" represents the number of proteins within each cluster. Membership value represents how well the protein profile fits the average cluster profile. (B) representative overrepresented biological processes of each cluster. Each cluster from (A) was tested for overrepresented GO compared with unregulated proteins using a Bionominal statistical test with Benjamini-Hochberg adjustment and a cut-off of 0.05 *p*-value.

# 4 DISCUSSION

Parkinson's disease, the most common movement disorder and the second most prevalent neurodegenerative disease [2,3], is characterized by a massive loss of dopaminergic neurons in the substantia nigra pars compacta, associated with a depletion of dopamine in the striatum [4], which is the primary hallmark of the disease. The second hallmark is the presence of Lewy Bodies, resulting from insoluble misfolded proteins accumulation [9]. Although PD is considered an idiopathic, sporadic, disease, largely influenced by environmental factors [13], some cases have a genetic background, which arise from mutations in PD-susceptibility genes [5]. Even though the specific etiology and pathophysiology of the disease remain unclear, evidences suggest that both sporadic and genetic forms lead to three types of cellular dysfunctions known to be important in the pathogenesis of PD, independent of the initial insult: misfolding and aggregation of proteins, mitochondrial dysfunction and oxidative stress [9,26]. These dysfunctions are not mutually exclusive, and one of the key aims of current PD research is to understand the sequence in which they act and the points of interaction of these pathways that result in neurodegeneration [26].

*DJ1* has been identified as one of PD-associated genes, causative of autosomal recessive early onset PD [41]. Several functions have been associated to DJ-1 protein [68], from which its neuroprotection role seems to be the most relevant for the disease. The protein is expressed throughout the cytosol [42], showing an oxidation-induced translocation to the nucleus [148] (where it will modulate transcription of antioxidant genes, for example [85]) and to the mitochondria [73], functioning as an oxidative stress sensor and ROS scavenger, which plays an important role in nigral dopamine neurons that are exposed to high levels of oxidative stress [26]. DJ-1 protein seems to be quite influenced by oxidative stress, showing an isoelectric pH shift upon oxidative stress conditions, being this considered its active form that results in neuroprotection [69,73]. However, further oxidation of the protein is thought to cause DJ-1 inactivity, and such oxidized form of the protein has been reported, not only in genetic-background PD patients, but also in patients with sporadic PD [42,77]. Nevertheless, how DJ-1 mediates this neuroprotection is yet not fully understood, thus studies to further elucidate such mechanisms would provide important insights into PD pathophysiology.

Several studies underlying DJ-1 function, show this protein accomplishes its functions by interacting, directly or indirectly, with other proteins, its binding partners [87,92]. Indeed, it has become clear that the majority of the proteins exist in dynamic multiprotein complexes that orchestrate and regulate several biological processes, meaning that binding partners identification of a protein with unknown function might provide important insights into their function, which is of great importance in biological research [123,126]. Since modulation of protein-protein interaction represents an emerging therapeutic paradigm, it is of great interest to identify proteins that bind to certain target protein and help modulate its function. In fact, evidence now suggest that protein interaction interfaces describe a new class of attractive target for drug development [123,127].

In this context, a comprehensive DJ-1 dynamic interactome screening was previously performed in the laboratory, using SH-SY5Y cells, focused on different key points of activation of ERK and PI3-K/Akt pathways, which are known to be modulated by DJ-1 in response to oxidative stress [96,150], condition suggested to be the trigger for DJ-1 neuroprotection. Thus, after defining oxidative stress conditions for the study, an immunoprecipitation assay was performed to isolate endogenous DJ-1 from its molecular environment, coupled with its interactors, and analyzed the IP eluate through LC-MS/MS approaches. With this, several proteins were identified, mainly in stress conditions, which is in agreement with the previously described stress-dependent DJ-1

activation. Most of the proteins identified presented a broad range of biological functions, mainly associated with cellular response to stress, and were reported as DJ-1 binding partners for the first time, meaning validation through complementary assays are needed to ensure their interaction.

From the wide range of proteins identified, oxidoreductase functional group received great attention, due to its association with cellular response to oxidative stress. From those proteins, D-3-phosphoglycerate (PGDH), NADH dehydrogenase [unibiquinone] 1 alpha subcomplex subunit 4 (NDUFA4), and Trifunctional enzyme subunit alpha, mitochondrial (HADHA) proteins were identified as being part of oxidoreductases family. PGDH is a cytosolic protein involved in the early steps of L-serine synthesis in animal cells, which serves as a precursor for the synthesis of proteins, membrane lipids, and the neuromodulators glycine and D-serine [116], playing a central role in cellular proliferation [117]. NDUFA4 is an accessory subunit of cytochrome C oxidase, complex IV of mitochondrial respiratory chain that catalyzes the reduction of oxygen to water [118]. HADHA is a mitochondrial protein that catalyzes mitochondrial β-oxidation of long chain fatty acids, to produce Acetyl-CoA for TCA cycle, resulting in NADH to fuel electron transport chain activity and, consequently, production of ATP needed for cellular basis functions [120]. All three proteins are also known to be involved in the $NAD^+$/NADH balance. The study of DJ-1 cysteine 106 residue demonstrated that its ability to react to hydrogen peroxide by means of oxidation-sensitive Cys residues may allow DJ-1 to act as a sensor of cellular ROS levels, and that oxidized DJ-1 may subsequently acquire new function to defend against ROS-induced cellular damage. Moreover, the identification of such oxidoreductases proteins as putative DJ-1 binding partners, which are associated to oxidative stress, suggested a new mechanism for DJ-1-mediated neuronal protection to such insult. Thus, it became pertinent the physical validation of such interactions, and the study of the dynamic interactome of the interactors, for a deeper knowledge on the effects of oxidative stress on PD pathogenesis.

Thus, an array of complementary strategies was performed to validate the interaction between DJ-1 and the proteins belonging to oxidoreductase family, described before. Prior to validation experiments, some preliminary tests were performed to assess the quality of the antibodies further needed. Such tests showed that NDUFA4 antibody was not detecting the target protein, instead was unspecifically binding to proteins with higher molecular weight. Thus, and as the interaction between DJ-1 and this protein was already validated [151], this protein was no longer used for further validation assays. Co-immunoprecipitations, using the antibodies against HADHA and PGDH proteins, followed by western blot analysis using an antibody against DJ-1, pull-down assays using WT recombinant DJ-1, followed by western blot analysis using antibodies against PGDH, and immunocytochemistry followed by confocal analysis in SH-SY5Y cells were performed as a mean to prove the hypothesis. As the previous DJ-1 interactome screening was performed in oxidative stress conditions, which was the conditions with most proteins identified, the validation experiments were also performed in such conditions, exposing SH-SY5Y cells to 1 mM of $H_2O_2$ for the time points established as the key activation points of the previously described ERK and PI3-K/Akt pathways. Thus, interaction was assessed in resting conditions (0 minutes), in the maximum activation (20 minutes), and a moment after maximum activation, where the phosphorylation levels of Akt and Erk1/2 returned to basal levels (40 minutes).

The results obtained through the IP experiment did not allowed a validation of DJ-1 interaction with HADHA and PGDH. This could be due to some technical errors when performing the experiment, or even with the cell extract where antibody-coupled beads were resuspended

and incubate. This is because there is no DJ-1 signal in the input fractions, meaning no DJ-1 was present, or was present in small amounts, in the extract. However, SH-SY5Y cells have already been extensively used to study DJ-1 protein [76,147], meaning it is highly expressed in those cells, and the amount of the protein shouldn't be a limited step for immunoprecipitation technique. Moreover, it was also not possible to conclude whether the absence of DJ-1 in PGDH IP eluate was because the protein did not bind to the antibody as the protein is in the same molecular weight range as the IgG heavy chain (HC). This is because the antibody used in IP was raised in the same specie as the antibody used in the western blot procedure, to mark PGDH protein, thus, the signal obtained could either be the protein present in the IP eluates and the HC, or only the IgG HC. Therefore, antibodies raised in different species should be used in further attempts. The HADHA IP showed a strong HADHA signal in eluates fractions, meaning the absence of this protein does not explain DJ-1 lack of signal. The fact that HADHA protein was present in IP eluates ensured the immunopurification of the protein, which impelled the choice of this protein to study its interactome, using AP-MS approach.

The second complementary method to validate the interaction *in vitro* was the pull down assay, which allow the extrapolation of the interaction with recombinant protein. WT DJ-1 protein with 6xHis tag was previously produced and purified, and used in the pull down assay to capture the proteins. Results suggested and interaction between PGDH and HADHA with the recombinant protein. Moreover, same results showed an interaction profile throughout the 40 minutes of $H_2O_2$ exposure, with a significant increase in interaction within the 20 minutes time point, followed by a decreased in the 40 minutes time point, which is consistent with stress-dependent activation of DJ-1 and inactivation with further oxidation [77]. A parallel pull down assay was performed using only the beads with no recombinant protein attached, to assess unspecific binding. The result showed the presence of HADHA and PGDH protein in pull down eluates, this could be explained by the fact that beads are composed of nickel, which is electropositive, conferring a high positive environment showing high affinity to proteins, which contain negatively charged regions by nature [152]. The high abundance of such proteins in control pull down, when compared with pull downs in the presence of the recombinant presence, can be explained by the higher availability of fishing sites when beads are alone. Because the amount of recombinant protein added to the bead is enough to saturated, and the binding of the recombinant protein will change the charge in the environmental, thus limiting the sites where proteins can bind unspecifically. Moreover, by observing an interaction profile that only occurs when recombinant protein is present, and which is consistent for both PGDH and HADHA proteins, it suggests that such profile is influenced by the presence of 6xHis-DJ-1. Altogether, these results seem to be indicative of an interaction between recombinant DJ-1, and PGDH and HADHA.

After showing that PGDH and HADHA were interacting *in vitro*, with recombinant WT DJ-1, it became of great relevance to assess such interaction *in situ*, because proteins are normally separated into discrete cellular compartments and get mixed together in *in vitro* IP assays, which result in nonphysiological binding to the target complex, and therefore many potential false interactions. Thus, proving the colocalization of the proteins within the cells would corroborate the previous suggestion of an interaction between the proteins, and would also ensure that such interaction is also occurring *in situ* and is not a nonphysiological reaction derived from cell lysis. Results obtained in this project for immunocytochemistry, followed by confocal analysis of SH-SY5Y cells marked with anti-DJ-1 and anti-HADHA antibodies, or with anti-DJ-1 and anti-PGDH antibodies, showed colocalization of DJ-1 with HADHA and PGDH, thus corroborating the

hypothesis that the proteins might be binding partners. Even though it was not a goal of this project to assess a profile of colocalization, or to measure and compare colocalization intensities between different conditions of oxidative stress, for such immunocytochemistry assays cells were exposed to the same oxidative stress conditions as previous validation experiments, so that we wouldn't misinterpret a lack of colocalization that would only occur in oxidative stress conditions. This procedure came out handful, since colocalization of DJ-1 with HADHA protein was only visible in oxidative stress conditions, at 40 minutes of $H_2O_2$ exposure more specifically, which could be explained by the fact that HADHA is an inner membrane-bound mitochondrial protein, needing DJ-1 oxidation-induced translocation to the mitochondrial previously described [73]. Nevertheless, a mitochondrial marker should be used to confirm such statement, meaning, for further colocalization experiments, this is a point that should be taken into consideration if indeed there's a goal to prove proteins colocalization in the mitochondria. The same should be performed with PGDH protein, as it seems to interact with DJ-1 in the cytosol, however no cytoskeleton marker was used, thus, further experiments should use such markers to prove DJ-1 colocalization with PGDH in the cytosol.

Altogether, validation experiments seem to corroborate the hypothesis of an interaction between DJ-1 and the oxidoreductases proteins studied in this project, PGDH and HADHA, not only *in vitro* but also *in situ*. Moreover, results suggest that this interaction is strongly modulated by oxidative stress, probably explained by oxidative-dependent DJ-1 activation [77]. For further elucidation on how DJ-1 regulates HADHA and PGDH activity under resting and oxidative stress conditions, some functional analysis could be performed, measuring the activity of the enzymes in the presence of WT DJ-1 or PD-associated, or engineered, DJ-1 mutations. Moreover, it would be of quite relevance to study how such mechanisms modulate cell survival in response to oxidative stress, by measuring cell viability in the presence of specific inhibitors of those enzymes, or of the reactions they modulate, in cells transfected, or not, with different DJ-1 mutated forms. This would confer important insights about the importance of such interactions and how this is relevant for PD pathogenesis induced by oxidative stress.

Mitochondria, is not only the major source of endogenous ROS, but also its DNA is particularly susceptible to such insult [149]. Moreover, β-oxidation of long chain fatty acids, which is strongly regulated by HADHA process [153], can also be a source of oxidative stress when impaired, as the accumulation of long chains fatty acids will promote lipotoxicity and consequently altered mitochondrial morphology, bioenergetics dysfunction, induction of permeability transition, and oxidative stress [154]. As previous results seem to suggest an interaction between DJ-1 and HADHA in the mitochondria, and that such interaction is significantly influenced by oxidative stress, it became of great relevance to study the dynamic interactome of HADHA protein, also in resting and oxidative stress conditions, to extrapolate its role in cellular response to oxidative stress. For this first comprehensive HADHA dynamic interactome screening, AP-SWATH approach was used, which allowed the identification of HADHA interactors and, more importantly, to trace interaction profiles under oxidative stress conditions (0, 20, and 40 minutes of oxidative stress stimuli). The results obtained in the current work allowed, not only the identification of several putative HADHA binding partners, but also demonstrated that HADHA-interactome is a very dynamic entity, varying throughout the 40 minutes of oxidative stress. This could be concluded by the highest amount of proteins identified in the 20 and 40 minutes of $H_2O_2$ exposure conditions, 673 and 704 proteins respectively, when comparing with the 255 proteins identified in resting condition, which suggests not only that HADHA has an oxidative stress-modulated dynamic interactome, but also a

stress-dependent regulation of HADHA protein. This was then corroborated with the unsupervised cluster analysis performed for the quantified proteins (n=524) that were suggested to be putative HADHA interactors. Such analysis showed that the majority of the interactions (n=216) increase in the 20 minutes of oxidative stress stimuli, followed by a decrease in the 40 minutes of stimuli, and allowed the grouping of proteins according to their interaction profiles, being possible to distinguish seven different clusters. Overall, oxidative stress seems to modulate HADHA interactions either by enhancing or decreasing the interactions.

Based on the proteins co-purified with HADHA, and the gene ontology enrichment analysis of the clusters, it was possible to infer the influence of the protein in regulation of gene expression. Distinct GO biological processes related to such mechanisms were overrepresented within the several clusters, but more notorious in those in which the interaction with HADHA is increased with oxidative stress stimuli. Moreover, it was possible to quantify distinct proteins involved in gene expression mechanisms, such as ribosomal proteins, histone, transcription factors, and other DNA/RNA-interaction proteins. From those, FACT (Facilitates Chromatin Transcription) complex was highlighted due to its reported role in DNA repair. The complex is constituted by two subunits (SPT16 and SSRP), which were both quantified and considered putative HADHA interactors in this assay, and it is known for its role in reorganization of nucleosomes [155]. Moreover, different reports showed that upon DNA damage, a complex containing FACT complex and casein kinase 2 (CK2) is formed, leading to activation of p53 [156,157]. Activation of p53 leads to transcriptional activation of several genes whose products triggers cell-cycle arrest, apoptosis, and DNA repair [158]. Oxidative stress is frequently associated with DNA damages [159], and strikingly tumor suppressor p53-binding protein 1 (53BP1 protein), whose function will lead to p53 activation [160], was also identified as a putative HADHA interactor. Such interactions seem to be enhanced by oxidative stress stimuli, possibly showing a mechanism of HADHA neuroprotection, involving DNA repair. Furthermore, previous DJ-1 interactome screening performed in our research group, identified FACT complex as a DJ-1 interactor in oxidative conditions, and another study also proved interaction between DJ-1 and p53 [97], suggesting a convergence in both proteins in putative regulation of neuroprotection.

Additionally, mitochondrial proteins and proteins associated with calcium ions transport were also quantified, according with the reported importance of calcium and mitochondrial in oxidative stress and PD [161,162]. Voltage-dependent calcium channel subunit alpha-2/delta-1 protein, that is a part of voltage-dependent calcium channel, responsible for $Ca^{2+}$ influx to cytoplasm [163], was one of the proteins identified as putative HADHA interactor, and such interaction seems to be enhanced by oxidative stress conditions. Calcium ions transport has been associated with PD. Studies have shown that adult SNpc DA neurons are autonomously active, capable of generating slow action potentials in the absence of a synaptic input, which is a result of engagement of voltage-dependent calcium channels (VDCC), allowing $Ca^{2+}$ to enter de cytoplasm. High levels of intracellular calcium will lead to mitochondrial and ER stress in SNpc DA neurons, created by sustained $Ca^{2+}$ entry [162]. Moreover, oxidative stress can also influence calcium homeostasis, in such a way that various oxidants can cause the translocation of $Ca^{2+}$ into the cytoplasm, and consequently into both the mitochondrial and the nucleus. However, if vital protein molecules that form channels are oxidized, it would disrupt their function, resulting in a lower $Ca^{2+}$ concentration in the cytoplasm [161]. Strikingly, Neuroblast differentiation-associated protein (AHNAK) was also shown to co-purify with HADHA. Such protein, has been shown to modulate the voltage-dependent calcium channels to allow $Ca^{2+}$ passage through the channel

[164]. Moreover, AHNAK was reported to be a part of a complex with VDCC, annexin 2, dysferlin, and other proteins, in skeletal muscle repair [165]. With the approach applied in this study, AHNAK, voltage-dependent calcium channel and annexin 2 were identified as putative interactors of HADHA. Such interaction was modulated by oxidative stress, which enhanced HADHA interaction with α-2/δ-1 voltage-dependent calcium channel subunit, but decreased HADHA interaction with AHNAK, within 20 minutes of oxidative conditions. This seems to suggest that HADHA protein may be disrupting the interaction between AHNAK with the VDCC, by interacting more with the channel, perhaps to stop $Ca^{2+}$ accumulation in the cytoplasm, which would lead to neurodegeneration. Although AHNAK functions have been widely attributed to muscle cells, the identification of the same complex in this project, might be indicative that its modulation of VDCC might also be relevant in dopaminergic neurons. Nevertheless, this is just an extrapolation that demands validation, however, if proven to be true, might suggest a neuroprotection mechanisms underlying HADHA protein against oxidative stress.

In line with voltage-dependent ion channels and their association with oxidative stress, voltage-dependent anion channel (VDAC) protein 2 was also identified in the screening as a putative HADHA-interacting protein. This protein forms a pore in the outer mitochondrial membrane, which promotes the passage of metabolites allowing the intercommunication of mitochondria with the remaining cellular components [166]. Reports have shown that VDAC closure can cause intramitochondrial oxidative stress and promote onset of the mitochondrial permeability transition (MTP), by retaining ROS inside the mitochondria [167], which may cause downstream activation of pathways to apoptotic necrotic cell death [168]. The interaction of VDAC with HADHA seems to be promoted in 20 minutes of oxidative stress stimuli exposure, which seems to indicate another mechanism through which HADHA might mediate neuroprotection, possibly by enhancing VDAC opening, thus preventing intramitochondrial oxidative stress and consequent cell death. Additionally, VDAC was also one of the proteins identified as DJ-1 putative binding partner in previous DJ-1 dynamic interactome screening, suggesting another common neuroprotective pathway between this protein and HADHA.

Moreover, several other proteins classes were identified to be associated with signaling pathways that will activate MAPKK signaling pathway, represented by GO biological processes such as neurotrophin TRK signaling pathway, ras protein transduction, or epidermal growth factor signaling pathway, that seem to be enhanced by 20 minutes of redox stimuli, thus indicating a modulation of HADHA in such pathways. Such signaling pathways will be responsible for MAPK signaling pathway that, dependent on the insult, may lead to cell survival or apoptosis [169,170]. Such signaling pathway has also previously been shown to be modulated by DJ-1 [96,114] .

In general, several putative binding partners of HADHA were identified and such interactions seems to be modulated by oxidative stress, and to be associated with neuroprotection. Strikingly, and although DJ-1 did not co-purified with HADHA in this particular study, several proteins identified and several mechanisms of cellular response to oxidative stress seem to be common with the ones previously identified for DJ-1. This indicates that further studies should be performed to highlight the potential points of interaction, which would elucidate possible molecular mechanisms of neuroprotection regarding both proteins. However, as a first HADHA dynamic interactome screening, the validation of such interactions and its significance through complementary and functional analysis should be performed.

However, many interactions are transient and/or dependent on the conditions, and difficult to assess using the described AP-MS approach. Thus, it is expectable that many other

HADHA-interactors are lost in this assay due to the large incubation period. Meaning, posterior studies using additional strategies, such as cross-linking reagents, should be used in order to assess those interactions and acquire a more comprehensive HADHA interactome. Moreover, cross-linking would also allow the elimination of false interactions that are established due to cell lysis and loss of cellular compartmentalization.

# 5 CONCLUSIONS

This project was developed in order to accomplish two interconnected goals. The first goal was to assess whether proteins belonging to oxidoreductases family (PGDH, HADHA, and NDUFA4) could indeed be considered DJ-1 binding partners, as follow up of previous DJ-1 interactome assay. The second goal was to extend the previous dynamic interactome of DJ-1 under oxidative stress to its binding partners, namely HADHA, to assess whether this protein could also be relevant in cellular response to oxidative stress.

To validate the interaction between DJ-1 and the other two oxidoreductases proteins, several complementary methods were performed such as immunoprecipitation, pull down assays, and immunocytochemistry followed by confocal analysis. Although it was not possible to confirm the interaction with the immunoprecipitation approach, the pull down assay suggested an interaction between PGDH and HADH with recombinant WT DJ-1, and that such interaction seems to be modulated by oxidative stress conditions. More importantly, immunocytochemistry followed by confocal analysis allowed the validation of such interaction *in situ*, thus corroborating the hypothesis of PGDH and HADHA as DJ-1 binding partners. Follow up analyses should be performed in cells with PD natural occurring DJ-1 mutations to assess whether such impairment would influence the proteins' interaction *in situ*, which would provide important insights into the relevance of such interaction in the context of PD.

For the HADHA interactome screening, an AP-SWATH-MS approach was performed, which allowed a comprehensive interactomic study in both physiological and pathological conditions, namely in the context of oxidative stress. The study provided the identification and quantification of several HADHA putative binding partners, suggesting a dynamic interactome modulated by stress conditions. Moreover, it suggests that, even though HADHA primary function relies on β-oxidation of free fatty acids, it also seems to modulate cell response to oxidative stress, being implicated in some neuroprotection mechanisms, similarly to DJ-1. Nevertheless, validation of such interactions is required, and future studies are necessary to address the functional relevance and consequence of the identified interactions in regulation of physiological and pathological functions of HADHA.

Many of the quantified proteins in this study are well established in distinct cellular functions in PD. Thus, these results can provide important insights into PD, the distinct pathways involved in the establishment and progression of the disease, highlighting potential new targets for PD prognosis, therapy and prevention.

# 6 REFERENCES

1. Sheikh, S., Haque, E. & Mir, S. Neurodegenerative Diseases: Multifactorial Conformational Diseases and Their Therapeutic Interventions. *J. Neurodegener. Dis.* **2013,** 8 (2012).
2. Davie, C. a. A review of Parkinson's disease. *Br. Med. Bull.* **86,** 109–127 (2008).
3. Bossy-Wetzel, E., Schwarzenbacher, R. & Lipton, S. a. Molecular pathways to neurodegeneration. *Nat. Med.* **10 Suppl,** S2–S9 (2004).
4. Lopiano, L. α -synuclein and Parkinson ' s disease : a proteomic view. *Expert Rev. Proteomics* **5,** 239–248 (2008).
5. Nuytemans, K., Theuns, J., Cruts, M. & Van Broeckhoven, C. Genetic etiology of Parkinson disease associated with mutations in the SNCA, PARK2, PINK1, PARK7, and LRRK2 genes: A mutation update. *Hum. Mutat.* **31,** 763–780 (2010).
6. Winter, Y. *et al.* Longitudinal study of the socioeconomic burden of Parkinson's disease in Germany. *Eur. J. Neurol.* **17,** 1156–63 (2010).
7. Kowal, S. L., Dall, T. M., Chakrabarti, R., Storm, M. V & Jain, A. The current and projected economic burden of Parkinson's disease in the United States. *Mov. Disord.* **28,** 311–8 (2013).
8. Langston, J. W. The Parkinson's complex: Parkinsonism is just the tip of the Iceberg. *Ann. Neurol.* **59,** 591–596 (2006).
9. Dauer, W. & Przedborski, S. Parkinson's Disease: Mechanisms and Models. *Neuron* **39,** 889–909 (2003).
10. Obeso, J. a *et al.* Missing pieces in the Parkinson's disease puzzle. *Nat. Med.* **16,** 653–661 (2010).
11. Braak, H. *et al.* Staging of brain pathology related to sporadic Parkinson's disease. *Neurobiol. Aging* **24,** 197–211 (2003).
12. Vila, M. & Przedborski, S. Genetic clues to the pathogenesis of Parkinson's disease. *Nat. Med.* **10 Suppl,** S58–S62 (2004).
13. Olanow, C. W. & Tatton, W. G. Etiology and Pathogenesis of Parkinson's Disease. *Annu Rev Neurosci* **22,** 123–44 (1999).
14. Xu, J. *et al.* Dopamine-dependent neurotoxicity of alpha-synuclein: a mechanism for selective neurodegeneration in Parkinson disease. *Nat. Med.* **8,** 600–606 (2002).
15. Lev, N. *et al.* A DJ-1 Based Peptide Attenuates Dopaminergic Degeneration in Mice Models of Parkinson's Disease via Enhancing Nrf2. *PLoS One* **10,** e0127549 (2015).
16. Schapira, A. H. & Jenner, P. Etiology and pathogenesis of Parkinson's disease. *Mov. Disord.* **26,** 1049–1055 (2011).
17. Hernán, M. a., Takkouche, B., Caamaño-Isorna, F. & Gestal-Otero, J. J. A meta-analysis of coffee drinking, cigarette smoking, and the risk of Parkinson's disease. *Ann. Neurol.* **52,** 276–284 (2002).
18. Korell, M. & Tanner, C. Epidemiology of Parkinson's Disease: an overview. in *Ebadi M, Pfeiffer RF (eds) Parkinson's disease. New York: CRC Press* 39–50 (2004).
19. Farrer, M. J. Genetics of Parkinson disease: paradigm shifts and future prospects. *Nat. Rev. Genet.* **7,** 306–318 (2006).
20. Mullin, S. & Schapira, A. The genetics of Parkinson ' s disease. *Br. Med. Bull.* 1–14 (2015). doi:10.1093/bmb/ldv022
21. Langston, J., Ballard, P., Tetrud, J. & Irwin, I. Chronic Parkinsonism in humans due to a

product of meperidine-analog synthesis. *Science (80-. ).* **219,** 979–980 (1983).

22. Tanner, C. M. *et al.* Rotenone, paraquat, and Parkinson's disease. *Environ. Health Perspect.* **119,** 866–872 (2011).
23. Javitch, J. a, D'Amato, R. J., Strittmatter, S. M. & Snyder, S. H. Parkinsonism-inducing neurotoxin, N-methyl-4-phenyl-1,2,3,6 -tetrahydropyridine: uptake of the metabolite N-methyl-4-phenylpyridine by dopamine neurons explains selective toxicity. *Proc. Natl. Acad. Sci. U. S. A.* **82,** 2173–2177 (1985).
24. Betarbet, R. *et al.* Chronic systemic pesticide exposure reproduces features of Parkinson's disease. *Nat. Neurosci.* **3,** 1301–1306 (2000).
25. Polymeropoulos, M. H. *et al.* Mutation in the alpha-synuclein gene identified in families with Parkinson's disease. *Science* **276,** 2045–2047 (1997).
26. Bekris, Lynn M. Mata, Ignacio, F. Zabetian, C. P. The Genetics of Parkinson Disease. *J Geriatr Psychiatry Neurol* **23,** 228–242 (2010).
27. Lesage, S. & Brice, A. Parkinson's disease: From monogenic forms to genetic susceptibility factors. *Hum. Mol. Genet.* **18,** 48–59 (2009).
28. Krüger, R. *et al.* Ala30Pro mutation in the gene encoding alpha-synuclein in Parkinson's disease. *Nat. Genet.* **18,** 106–8 (1998).
29. Zarranz, J. J. *et al.* The new mutation, E46K, of alpha-synuclein causes Parkinson and Lewy body dementia. *Ann. Neurol.* **55,** 164–73 (2004).
30. Murphy, D. D., Rueter, S. M., Trojanowski, J. Q. & Lee, V. M. Synucleins are developmentally expressed, and alpha-synuclein regulates the size of the presynaptic vesicular pool in primary hippocampal neurons. *J. Neurosci.* **20,** 3214–3220 (2000).
31. Paisán-Ruíz, C. *et al.* Cloning of the gene containing mutations that cause PARK8-linked Parkinson's disease. *Neuron* **44,** 595–600 (2004).
32. Zimprich, A. *et al.* Mutations in LRRK2 cause autosomal-dominant parkinsonism with pleomorphic pathology. *Neuron* **44,** 601–607 (2004).
33. Dauer, W. & Ho, C. C. Y. The biology and pathology of the familial Parkinson's disease protein LRRK2. *Mov. Disord.* **25,** 2008–2011 (2010).
34. Kitada, T. *et al.* Mutations in the parkin gene cause autosomal recessive juvenile parkinsonism. *Nature* **392,** 605–608 (1998).
35. Shimura, H. *et al.* Familial Parkinson disease gene product, parkin, is a ubiquitin-protein ligase. *Nat. Genet.* **25,** 302–305 (2000).
36. Fitzgerald, J. C. & Plun-Favreau, H. Emerging pathways in genetic Parkinson's disease: Autosomal-recessive genes in Parkinson's disease - A common pathway? *FEBS J.* **275,** 5758–5766 (2008).
37. Valente, E. M. *et al.* Localization of a novel locus for autosomal recessive early-onset parkinsonism, PARK6, on human chromosome 1p35-p36. *Am. J. Hum. Genet.* **68,** 895–900 (2001).
38. Valente, E. M. *et al.* Hereditary early-onset Parkinson's disease caused by mutations in PINK1. *Science* **304,** 1158–1160 (2004).
39. Silvestri, L. *et al.* Mitochondrial import and enzymatic activity of PINK1 mutants associated to recessive parkinsonism. *Hum. Mol. Genet.* **14,** 3477–3492 (2005).
40. van Duijn, C. M. *et al.* Park7, a novel locus for autosomal recessive early-onset parkinsonism, on chromosome 1p36. *Am. J. Hum. Genet.* **69,** 629–634 (2001).

41. Bonifati, V. *et al.* Mutations in the DJ-1 gene associated with autosomal recessive early-onset parkinsonism. *Science* **299,** 256–259 (2003).

42. Bandopadhyay, R. *et al.* The expression of DJ-1 (PARK7) in normal human CNS and idiopathic Parkinson's disease. *Brain* **127,** 420–30 (2004).

43. Waragai, M. *et al.* Increased level of DJ-1 in the cerebrospinal fluids of sporadic Parkinson's disease. *Biochem. Biophys. Res. Commun.* **345,** 967–72 (2006).

44. Waragai, M. *et al.* Plasma levels of DJ-1 as a possible marker for progression of sporadic Parkinson's disease. *Neurosci. Lett.* **425,** 18–22 (2007).

45. Cookson, M. R. Parkinsonism Due to Mutations in PINK1, Parkin, and DJ-1 and Oxidative Stress and Mitochondrial Pathways. *Cold Spring Harb. Perspect. Med.* 1–11 (2012). doi:10.1101/cshperspect.a009415

46. Kumaran, R. & Cookson, M. . Pathways to Parkinsonism Redux: Convergent pathobiological mechanisms in genetics of Parkinson's disease. *Hum Mol Genet.* **pii: ddv23,** (2015).

47. Dexter, D. T. & Jenner, P. Parkinson disease: from pathology to molecular disease mechanisms. *Free Radic. Biol. Med.* **62,** 132–44 (2013).

48. Warrick, J. M. *et al.* Suppression of polyglutamine-mediated neurodegeneration in Drosophila by the molecular chaperone HSP70. *Nat. Genet.* **23,** 425–428 (1999).

49. Hirsch, E. C., Jenner, P. & Przedborski, S. Pathogenesis of Parkinson's disease. *Mov. Disord.* **28,** 24–30 (2013).

50. Stefanis, L. α-Synuclein in Parkinson's disease. *Cold Spring Harb. Perspect. Med.* **2,** a009399 (2012).

51. Dawson, T. M. & Dawson, V. L. Molecular pathways of neurodegeneration in Parkinson's disease. *Science* **302,** 819–822 (2003).

52. Keane, P. C., Kurzawa, M., Blain, P. G. & Morris, C. M. Mitochondrial dysfunction in Parkinson's disease. *Parkinsons. Dis.* **2011,** 716871 (2011).

53. Schapira, a H. *et al.* Mitochondrial complex I deficiency in Parkinson's disease. *J. Neurochem.* **54,** 823–827 (1990).

54. Keeney, P. M., Xie, J., Capaldi, R. a & Bennett, J. P. Parkinson's disease brain mitochondrial complex I has oxidatively damaged subunits and is functionally impaired and misassembled. *J. Neurosci.* **26,** 5256–5264 (2006).

55. Narendra, D., Tanaka, A., Suen, D. F. & Youle, R. J. Parkin-induced mitophagy in the pathogenesis of Parkinson disease. *Autophagy* **5,** 706–708 (2009).

56. Gu, M., Cooper, J. M., Taanman, J. W. & Schapira, a. H. V. Mitochondrial DNA transmission of the mitochondrial defect in Parkinson's disease. *Ann. Neurol.* **44,** 177–186 (1998).

57. Blesa, J. *et al.* Oxidative stress and Parkinson's. *Front. Neuroanat.* **9,** (2015).

58. Hwang, O. Role of oxidative stress in Parkinson's disease. *Exp. Neurobiol.* **22,** 11–7 (2013).

59. Zhang, Y., Dawson, V. L. & Dawson, T. M. Oxidative stress and genetics in the pathogenesis of Parkinson's disease. *Neurobiol. Dis.* **7,** 240–50 (2000).

60. Cao, J. *et al.* The Oxidation States of DJ-1 Dictate the Cell Fate in Response to Oxidative Stress Triggered by 4-HPR: Autophagy or Apoptosis? *Antioxidants Redox Signal.* **21,** 1443–1459 (2014).

61. Nagakubo, D. *et al.* DJ-1, a novel oncogene which transforms mouse NIH3T3 cells in

cooperation with ras. *Biochem. Biophys. Res. Commun.* **231,** 509–513 (1997).

62. Zhong, N. *et al.* DJ-1 transcriptionally up-regulates the human tyrosine hydroxylase by inhibiting the sumoylation of pyrimidine tract-binding protein-associated splicing factor. *J. Biol. Chem.* **281,** 20940–20948 (2006).

63. Xu, J. *et al.* The Parkinson's disease-associated DJ-1 protein is a transcriptional co-activator that protects against neuronal apoptosis. *Hum. Mol. Genet.* **14,** 1231–1241 (2005).

64. Hod, Y., Pentyala, S. N., Whyard, T. C. & El-Maghrabi, M. R. Identification and characterization of a novel protein that regulates RNA-protein interaction. *J. Cell. Biochem.* **72,** 435–444 (1999).

65. Shinbo, Y. *et al.* Proper SUMO-1 conjugation is essential to DJ-1 to exert its full activities. *Cell Death Differ.* **13,** 96–108 (2006).

66. Jin, J. *et al.* Identification of novel proteins associated with both alpha-synuclein and DJ-1. *Mol. Cell. Proteomics* **6,** 845–859 (2007).

67. Junn, E. *et al.* Interaction of DJ-1 with Daxx inhibits apoptosis signal-regulating kinase 1 activity and cell death. *Proc. Natl. Acad. Sci. U. S. A.* **102,** 9691–9696 (2005).

68. Lakshminarasimhan, M., Maldonado, M. T., Zhou, W., Fink, A. L. & Wilson, M. a. Structural impact of three Parkinsonism-associated missense mutations on human DJ-1. *Biochemistry* **47,** 1381–1392 (2008).

69. Wilson, M. a. The role of cysteine oxidation in DJ-1 function and dysfunction. *Antioxid. Redox Signal.* **15,** 111–122 (2011).

70. Wilson, M. a, Collins, J. L., Hod, Y., Ringe, D. & Petsko, G. a. The 1.1-A resolution crystal structure of DJ-1, the protein mutated in autosomal recessive early onset Parkinson's disease. *Proc. Natl. Acad. Sci. U. S. A.* **100,** 9256–9261 (2003).

71. Wagenfeld, A., Gromoll, J. & Cooper, T. G. Molecular cloning and expression of rat contraception associated protein 1 (CAP1), a protein putatively involved in fertilization. *Biochem. Biophys. Res. Commun.* **251,** 545–9 (1998).

72. Kahle, P. J., Waak, J. & Gasser, T. DJ-1 and prevention of oxidative stress in Parkinson's disease and other age-related disorders. *Free Radic. Biol. Med.* **47,** 1354–1361 (2009).

73. Canet-Avilés, R. M. *et al.* The Parkinson's disease protein DJ-1 is neuroprotective due to cysteine-sulfinic acid-driven mitochondrial localization. *Proc. Natl. Acad. Sci. U. S. A.* **101,** 9103–9108 (2004).

74. Quigley, P. M., Korotkov, K., Baneyx, F. & Hol, W. G. J. The 1.6-A crystal structure of the class of chaperones represented by Escherichia coli Hsp31 reveals a putative catalytic triad. *Proc. Natl. Acad. Sci. U. S. A.* **100,** 3137–3142 (2003).

75. Honbou, K. *et al.* The crystal structure of DJ-1, a protein related to male fertility and Parkinson's disease. *J. Biol. Chem.* **278,** 31380–31384 (2003).

76. Miyazaki, S. *et al.* DJ-1-binding compounds prevent oxidative stress-induced cell death and movement defect in Parkinson's disease model rats. *J. Neurochem.* **105,** 2418–2434 (2008).

77. Zhou, W., Zhu, M., Wilson, M. A., Petsko, G. A. & Fink, A. L. The oxidation state of DJ-1 regulates its chaperone activity toward ??-synuclein. *J. Mol. Biol.* **356,** 1036–1048 (2006).

78. Waak, J. *et al.* Oxidizable residues mediating protein stability and cytoprotective interaction of DJ-1 with apoptosis signal-regulating kinase 1. *J. Biol. Chem.* **284,** 14245–14257 (2009).

79. Gorner, K. *et al.* Structural Determinants of the C-terminal Helix-Kink-Helix Motif Essential for Protein Stability and Survival Promoting Activity of DJ-1. *J. Biol. Chem.* **282,** 13680–13691 (2007).

80. Moore, D. J., Zhang, L., Dawson, T. M. & Dawson, V. L. A missense mutation (L166P) in DJ-1, linked to familial Parkinson's disease, confers reduced protein stability and impairs homo-oligomerization. *J. Neurochem.* **87,** 1558–1567 (2003).

81. Olzmann, J. a. *et al.* Familial Parkinson's Disease-associated L166P Mutation Disrupts DJ-1 Protein Folding and Function. *J. Biol. Chem.* **279,** 8506–8515 (2004).

82. Corti, O., Lesage, S. & Brice, a. What Genetics Tells us About the Causes and Mechanisms of Parkinson's Disease. *Physiol. Rev.* **91,** 1161–1218 (2011).

83. Lev, N., Ickowicz, D., Melamed, E. & Offen, D. Oxidative insults induce DJ-1 upregulation and redistribution: implications for neuroprotection. *Neurotoxicology* **29,** 397–405 (2008).

84. Junn, E., Jang, W. H., Zhao, X., Jeong, B. S. & Mouradian, M. M. Mitochondrial localization of DJ-1 leads to enhanced neuroprotection. *J. Neurosci. Res.* **87,** 123–9 (2009).

85. Clements CM, McNally RS, Conti BJ, Mak TW & Ting JP. DJ-1, a cancer- and Parkinson's disease-associated protein, stabilizes the antioxidant transcriptional master regulator Nrf2. *Proc Natl Acad Sci U S A.* **103,** 15091–6 (2006).

86. Milani, P., Ambrosi, G., Gammoh, O., Blandini, F. & Cereda, C. SOD1 and DJ-1 converge at Nrf2 pathway: A clue for antioxidant therapeutic potential in neurodegeneration. *Oxid. Med. Cell. Longev.* **2013,** (2013).

87. Takahashi, K. *et al.* DJ-1 Positively Regulates the Androgen Receptor by Impairing the Binding of PIASx?? to the Receptor. *J. Biol. Chem.* **276,** 37556–37563 (2001).

88. Zhong, N. & Xu, J. Synergistic activation of the human MnSOD promoter by DJ-1 and PGC-1??: Regulation by SUMOylation and oxidation. *Hum. Mol. Genet.* **17,** 3357–3367 (2008).

89. Blackinton, J. *et al.* Effects of DJ-1 mutations and polymorphisms on protein stability and subcellular localization. *Mol. Brain Res.* **134,** 76–83 (2005).

90. Zhang, L. *et al.* Mitochondrial localization of the Parkinson's disease related protein DJ-1: Implications for pathogenesis. *Hum. Mol. Genet.* **14,** 2063–2073 (2005).

91. Takahashi-Niki, K., Niki, T., Taira, T., Iguchi-Ariga, S. M. M. & Ariga, H. Reduced anti-oxidative stress activities of DJ-1 mutants found in Parkinson's disease patients. *Biochem. Biophys. Res. Commun.* **320,** 389–97 (2004).

92. Karunakaran, S. *et al.* Activation of apoptosis signal regulating kinase 1 (ASK1) and translocation of death-associated protein, Daxx, in substantia nigra pars compacta in a mouse model of Parkinson's disease: protection by alpha-lipoic acid. *FASEB J.* **21,** 2226–2236 (2007).

93. Mo, J. S. *et al.* DJ-1 modulates the p38 mitogen-activated protein kinase pathway through physical interaction with apoptosis signal-regulating kinase 1. *J. Cell. Biochem.* **110,** 229–237 (2010).

94. Lev N *et al.* DJ-1 protects against dopamine toxicity: implications for Parkinson's disease and aging. *J Gerontol A Biol Sci Med Sci.* **68,** 215–25 (2013).

95. Mo, J.-S., Kim, M.-Y., Ann, E.-J., Hong, J. & Park, H.-S. DJ-1 modulates UV-induced oxidative stress signaling through the suppression of MEKK1 and cell death. *Cell Death Differ.* **15,** 1030–1041 (2008).

96. Gu, L. *et al.* Involvement of ERK1/2 signaling pathway in DJ-1-induced neuroprotection

against oxidative stress. *Biochem. Biophys. Res. Commun.* **383,** 469–74 (2009).

97. Kato, I. *et al.* Oxidized DJ-1 inhibits p53 by sequestering p53 from promoters in a DNA-binding affinity-dependent manner. *Mol. Cell. Biol.* **33,** 340–59 (2013).

98. Mullett, S. J. & Hinkle, D. a. DJ-1 knock-down in astrocytes impairs astrocyte-mediated neuroprotection against rotenone. *Neurobiol Dis.* **33,** 28–36 (2010).

99. Hulleman, J. D. *et al.* Destabilization of DJ-1 by familial substitution and oxidative modifications: Implications for Parkinson's disease. *Biochemistry* **46,** 5776–5789 (2007).

100. Malgieri, G. & Eliezer, D. Structural effects of Parkinson's disease linked DJ-1 mutations. *Protein Sci.* **17,** 855–868 (2008).

101. Abou-sleiman, P. M., Healy, D. G., Quinn, N., Lees, A. J. & Wood, N. W. The Role of Pathogenic DJ-1 Mutations in Parkinson's Disease. *Ann Neurol 2003;54283–286* **54,** 283–286 (2003).

102. Annesi, G. *et al.* DJ-1 mutations and parkinsonism-dementia-amyotrophic lateral sclerosis complex. *Ann. Neurol.* **58,** 803–807 (2005).

103. Ramsey, C. P. & Giasson, B. I. The E163K DJ-1 mutant shows specific antioxidant deficiency. *Brain Res.* **1239,** 1–11 (2008).

104. Kapp GT, Richardson JS & Oas TG. Kinetic role of helix caps in protein folding is context-dependent. *Biochemistry.* **43,** 3814–23 (2004).

105. Niki, T., Takahashi-Niki, K., Taira, T., Iguchi-Ariga, S. M. M. & Ariga, H. DJBP: a novel DJ-1-binding protein, negatively regulates the androgen receptor by recruiting histone deacetylase complex, and DJ-1 antagonizes this inhibition by abrogation of this complex. *Mol. Cancer Res.* **1,** 247–61 (2003).

106. Moore, D. J. *et al.* Association of DJ-1 and parkin mediated by pathogenic DJ-1 mutations and oxidative stress. *Hum. Mol. Genet.* **14,** 71–84 (2005).

107. Meulener, M. C. *et al.* DJ-1 is present in a large molecular complex in human brain tissue and interacts with alpha-synuclein. *J. Neurochem.* **93,** 1524–32 (2005).

108. Sekito, A. *et al.* DJ-1 interacts with HIPK1 and affects H2O2-induced cell death. *Free Radic. Res.* **40,** 155–65 (2006).

109. Tillman, J. E. *et al.* DJ-1 binds androgen receptor directly and mediates its activity in hormonally treated prostate cancer cells. *Cancer Res.* **67,** 4630–7 (2007).

110. Olzmann, J. A. *et al.* Parkin-mediated K63-linked polyubiquitination targets misfolded DJ-1 to aggresomes via binding to HDAC6. *J. Cell Biol.* **178,** 1025–38 (2007).

111. Kim, Y.-C., Kitaura, H., Taira, T., Iguchi-Ariga, S. M. M. & Ariga, H. Oxidation of DJ-1-dependent cell transformation through direct binding of DJ-1 to PTEN. *Int. J. Oncol.* **35,** 1331–41 (2009).

112. Parsanejad, M. *et al.* DJ-1 Interacts with and Regulates Paraoxonase-2, an Enzyme Critical for Neuronal Survival in Response to Oxidative Stress. *PLoS One* **9,** e106601 (2014).

113. Tang, J. *et al.* PRAK Interacts with DJ-1 and Prevents Oxidative Stress-Induced Cell Death. *Oxid. Med. Cell Longev* **2014,** 735618 (2014).

114. Takahashi-Niki, K. *et al.* Epidermal growth factor-dependent activation of the ERK pathway by DJ-1 through its direct binding to c-Raf. *J. Biol. Chem.* jbc.M115.666271 (2015). doi:10.1074/jbc.M115.666271

115. Knobbe, C. B. *et al.* Choice of biological source material supersedes oxidative stress in its influence on DJ-1 in vivo interactions with Hsp90. *J. Proteome Res.* **10,** 4388–4404 (2011).

116. Furuya, S. *et al.* L-serine and glycine serve as major astroglia-derived trophic factors for cerebellar Purkinje neurons. *Proc. Natl. Acad. Sci. U. S. A.* **97,** 11528–33 (2000).

117. Klomp, L. W. J. *et al.* Molecular Characterization of 3-Phosphoglycerate Dehydrogenase Deficiency—a Neurometabolic Disorder Associated with Reduced L-Serine Biosynthesis. *Am. J. Hum. Genet* **67,** 1389–1399 (2000).

118. Balsa, E. *et al.* NDUFA4 is a subunit of complex IV of the mammalian electron transport chain. *Cell Metab.* **16,** 378–386 (2012).

119. Pitceathly, R. D. S. *et al.* NDUFA4 Mutations Underlie Dysfunction of a Cytochrome c Oxidase Subunit Linked to Human Neurological Disease. *Cell Rep.* **3,** 1795–1805 (2013).

120. Sims, H. F. *et al.* The molecular basis of pediatric long chain 3-hydroxyacyl-CoA dehydrogenase deficiency associated with maternal acute fatty liver of pregnancy. *Proc. Natl. Acad. Sci. USA* **92,** 841–845 (1995).

121. Ibdah, J. A. *et al.* Mild trifunctional protein deficiency is associated with progressive neuropathy and myopathy and suggests a novel genotype-phenotype correlation. *J. Clin. Invest.* **102,** 1193–1199 (1998).

122. Walhout, a J. & Vidal, M. High-throughput yeast two-hybrid assays for large-scale protein interaction mapping. *Methods* **24,** 297–306 (2001).

123. Auerbach, D., Fetchko, M. & Stagljar, I. Proteomic approaches for generating comprehensive protein interaction maps. *Targets* **2,** 85–92 (2003).

124. Cusick, M. E., Klitgord, N., Vidal, M. & Hill, D. E. Interactome: Gateway into systems biology. *Hum. Mol. Genet.* **14,** 171–181 (2005).

125. Gingras, A.-C., Gstaiger, M., Raught, B. & Aebersold, R. Analysis of protein complexes using mass spectrometry. *Nat. Rev. Mol. Cell Biol.* **8,** 645–654 (2007).

126. Monti, M., Orrù, S., Pagnozzi, D. & Pucci, P. Interaction proteomics. *Biosci. Rep.* **25,** 45–56 (2005).

127. Kaake, R. M., Wang, X. & Huang, L. Profiling of protein interaction networks of protein complexes using affinity purification and quantitative mass spectrometry. *Mol. Cell. Proteomics* **9,** 1650–1665 (2010).

128. Walhout, a J., Boulton, S. J. & Vidal, M. Yeast two-hybrid systems and protein interaction mapping projects for yeast and worm. *Yeast* **17,** 88–94 (2000).

129. Ruffner, H., Bauer, A. & Bouwmeester, T. Human protein-protein interaction networks and the value for drug discovery. *Drug Discov. Today* **12,** 709–716 (2007).

130. Fields, S. & Song, O. A novel genetic system to detect protein-protein interactions. *Nature* **340,** 245–246 (1989).

131. Walhout, A. J. . & Boulton, S. J. *Biochemistry and molecular biology*. *WormBook, ed. The C. elegans Research Community* (2006). doi:10.1895/wormbook.1.86.1

132. Rogstad, S. M., Sorkina, T., Sorkin, A. & Wu, C. C. Improved precision of proteomic measurements in immunoprecipitation based purifications using relative quantitation. *Anal. Chem.* **85,** 4301–4306 (2013).

133. Markham, K., Bai, Y. & Schmitt-Ulms, G. Co-immunoprecipitations revisited: An update on experimental concepts and their implementation for sensitive interactome investigations of endogenous proteins. *Anal. Bioanal. Chem.* **389,** 461–473 (2007).

134. Lane, C. S. Mass spectrometry-based proteomics in the life sciences. *Cell. Mol. Life Sci.* **62,** 848–869 (2005).

135. Aebersold, R. & Mann, M. Mass spectrometry-based proteomics. *Nature* **422,** 198–207 (2003).

136. Aebersold, R. & Mann, M. Mass spectrometry-based proteomics. *Nature* **422,** 198–207 (2003).

137. Gillet, L. C. *et al.* Targeted Data Extraction of the MS/MS Spectra Generated by Data-independent Acquisition: A New Concept for Consistent and Accurate Proteome Analysis. *Mol. Cell. Proteomics* **11,** O111.016717–O111.016717 (2012).

138. Wilhelm, S., Gröbler, B., Gluch, M. & Heinz, H. Confocal Laser Scanning Microscopy Principles. *Zeiss Jena* 1–28 (2000). doi:10.1002/9781118382905

139. Ruffels, J., Griffin, M. & Dickenson, J. M. Activation of ERK1/2, JNK and PKB by hydrogen peroxide in human SH-SY5Y neuroblastoma cells: Role of ERK1/2 in H2O2-induced cell death. *Eur. J. Pharmacol.* **483,** 163–173 (2004).

140. Anjo, S. I., Santa, C. & Manadas, B. Short GeLC-SWATH: A fast and reliable quantitative approach for proteomic screenings. *Proteomics* **15,** 757–762 (2015).

141. Candiano, G. *et al.* Blue silver: A very sensitive colloidal Coomassie G-250 staining for proteome analysis. *Electrophoresis* **25,** 1327–1333 (2004).

142. Tang, W. H., Shilov, I. V. & Seymour, S. L. Nonlinear fitting method for determining local false discovery rates from decoy database searches. *J. Proteome Res.* **7,** 3661–3667 (2008).

143. Sennels, L., Bukowski-Wills, J.-C. & Rappsilber, J. Improved results in proteomics by use of local and peptide-class specific false discovery rates. *BMC Bioinformatics* **10,** 179 (2009).

144. Lambert, J.-P. *et al.* Mapping differential interactomes by affinity purification coupled with data-independent mass spectrometry acquisition. *Nat. Methods* **10,** 1239–45 (2013).

145. Martins-Marques, T., Anjo, S. I., Pereira, P., Manadas, B. & Girão, H. Interacting Network of the Gap Junction (GJ) Protein Connexin43 (Cx43) is Modulated by Ischemia and Reperfusion in the Heart. *Mol. Cell. Proteomics* **14,** 3040–55 (2015).

146. Xie, H., Hu, L. & Li, G. SH-SY5Y human neuroblastoma cell line: in vitro cell model of dopaminergic neurons in Parkinson's disease. *Chin. Med. J. (Engl).* **123,** 1086–1092 (2010).

147. Schapira, A. Mitochondrial dysfunction and oxidative stress in Parkinson's disease. *Neurochem. Res.* **107,** 57–64 (2011).

148. Kim, S.-J. *et al.* Nuclear translocation of DJ-1 during oxidative stress-induced neuronal cell death. *Free Radic. Biol. Med.* **53,** 936–50 (2012).

149. Beal, M. F. Aging, energy, and oxidative stress in neurodegenerative diseases. *Ann. Neurol.* **38,** 357–66 (1995).

150. Yang, Y. *et al.* Inactivation of Drosophila DJ-1 leads to impairments of oxidative stress response and phosphatidylinositol 3-kinase/Akt signaling. *Proc. Natl. Acad. Sci. U. S. A.* **102,** 13670–13675 (2005).

151. Hayashi, T. *et al.* DJ-1 binds to mitochondrial complex I and maintains its activity. *Biochem. Biophys. Res. Commun.* **390,** 667–672 (2009).

152. Chikh, G. G., Li, W. M., Schutze-Redelmeier, M.-P., Meunier, J.-C. & Bally, M. B. Attaching histidine-tagged peptides and proteins to lipid-based carriers through use of metal-ion-chelating lipids. *Biochim. Biophys. Acta - Biomembr.* **1567,** 204–212 (2002).

153. Das, A. M. *et al.* Isolated mitochondrial long-chain ketoacyl-CoA thiolase deficiency resulting from mutations in the HADHB gene. *Clin. Chem.* **52,** 530–534 (2006).

154. Wajner, M. & Amaral, A. U. Mitochondrial dysfunction in fatty acid oxidation disorders: insights from human and animal studies. *Biosci. Rep.* BSR20150240 (2015). doi:10.1042/BSR20150240

155. Belotserkovskaya, R. *et al.* FACT facilitates transcription-dependent nucleosome alteration. *Science* **301,** 1090–1093 (2003).

156. Gyenis, L. & Litchfield, D. W. The emerging CK2 interactome: Insights into the regulation and functions of CK2. *Mol. Cell. Biochem.* **316,** 5–14 (2008).

157. Olsten, M. E., Weber, J. E. & Litchfield, D. W. CK2 interacting proteins: Emerging paradigms for CK2 regulation? *Molecular and Cellular Biochemistry* **274,** 115–124 (2005).

158. Lakin, N. D. & Jackson, S. P. Regulation of p53 in response to DNA damage. *Oncogene* **18,** 7644–7655 (1999).

159. Barzilai, A. & Yamamoto, K. I. DNA damage responses to oxidative stress. *DNA Repair* **3,** 1109–1115 (2004).

160. Iwabuchi, K. *et al.* Stimulation of p53-mediated transcriptional activation by the p53-binding proteins, 53BP1 and 53BP2. *J. Biol. Chem.* **273,** 26061–26068 (1998).

161. Ermak, G. & Davies, K. J. Calcium and oxidative stress: from cell signaling to cell death. *Mol Immunol* **38,** 713–721 (2002).

162. Surmeier, D. J., Guzman, J. N., Sanchez-Padilla, J. & Schumacker, P. T. The role of calcium and mitochondrial oxidant stress in the loss of substantia nigra pars compacta dopaminergic neurons in Parkinson's disease. *Neuroscience* **198,** 221–231 (2011).

163. Brust, P. F. *et al.* Human neuronal voltage-dependent calcium channels: Studies on subunit structure and role in channel assembly. *Neuropharmacology* **32,** (1993).

164. Pankonien, I. *et al.* Ahnak1 is a tuneable modulator of cardiac Ca(v)1.2 calcium channel activity. *J. Muscle Res. Cell Motil.* **32,** 281–290 (2011).

165. Huang, Y. *et al.* AHNAK, a novel component of the dysferlin protein complex, redistributes to the cytoplasm with dysferlin during skeletal muscle regeneration. *FASEB J.* **21,** 732–742 (2007).

166. Yu, W. H., Wolfgang, W. & Forte, M. Subcellular localization of human voltage-dependent anion channel isoforms. *J Biol Chem* **270,** 13998–14006 (1995).

167. Tikunov, A. *et al.* Closure of VDAC causes oxidative stress and accelerates the Ca(2+)-induced mitochondrial permeability transition in rat liver mitochondria. *Arch. Biochem. Biophys.* **495,** 174–81 (2010).

168. Lemasters, J. J., Theruvath, T. P., Zhong, Z. & Nieminen, A.-L. Mitochondrial calcium and the permeability transition in cell death. *Biochim. Biophys. Acta* **1787,** 1395–1401 (2009).

169. Bonni, A. Cell Survival Promoted by the Ras-MAPK Signaling Pathway by Transcription-Dependent and -Independent Mechanisms. *Science (80-. ).* **286,** 1358–1362 (1999).

170. Chang, L. & Karin, M. Mammalian MAP kinase signalling cascades. *Nature* **410,** 37–40 (2001).

# 7 SUPPLEMENTARY DATA

## 7.1 SWATH-MS METHOD

***Supplementary Table 7.1*** **– Variable Windows of SWATH-MS Method.** Different SWATH m/z range, windows width, and correspondent collision energy spread (CES).

| | m/z range | Width (Da) | CES |
|---|---|---|---|
| **Window 1** | 350-361.8 | 11.8 | 5 |
| **Window 2** | 360.8-373.4 | 12.6 | 5 |
| **Window 3** | 372.4-385.1 | 12.7 | 5 |
| **Window 4** | 384.1-395.5 | 11.4 | 5 |
| **Window 5** | 394.5-404.5 | 10 | 5 |
| **Window 6** | 403.5-413.5 | 10 | 5 |
| **Window 7** | 412.5-422 | 9.5 | 5 |
| **Window 8** | 421-430.6 | 9.6 | 5 |
| **Window 9** | 429.6-439.1 | 9.5 | 5 |
| **Window 10** | 438.1-447.7 | 9.6 | 5 |
| **Window 11** | 446.7-457.6 | 10.9 | 5 |
| **Window 12** | 456.6-469.3 | 12.7 | 5 |
| **Window 13** | 468.3-481.4 | 13.1 | 5 |
| **Window 14** | 480.4-494.5 | 14.1 | 5 |
| **Window 15** | 493.5-505.3 | 11.8 | 5 |
| **Window 16** | 504.3-515.6 | 11.3 | 5 |
| **Window 17** | 514.6-525.1 | 10.5 | 5 |
| **Window 18** | 524.1-533.6 | 9.5 | 5 |
| **Window 19** | 532.6-541.7 | 9.1 | 5 |
| **Window 20** | 540.7-550.3 | 9.6 | 5 |
| **Window 21** | 549.3-558.4 | 9.1 | 5 |
| **Window 22** | 557.4-567 | 9.6 | 5 |
| **Window 23** | 566-575.1 | 9.1 | 5 |
| **Window 24** | 574.1-583.6 | 9.5 | 5 |
| **Window 25** | 582.6-592.6 | 10 | 5 |
| **Window 26** | 591.6-601.2 | 9.6 | 5 |
| **Window 27** | 600.2-609.3 | 9.1 | 5 |
| **Window 28** | 608.3-617.8 | 9.5 | 5 |
| **Window 29** | 616.8-626.4 | 9.6 | 5 |
| **Window 30** | 625.4-634.9 | 9.5 | 5 |
| **Window 31** | 633.9-643.9 | 10 | 5 |
| **Window 32** | 642.9-652.9 | 10 | 5 |
| **Window 33** | 651.9-662.4 | 10.5 | 5 |
| **Window 34** | 661.4-673.2 | 11.8 | 5 |
| **Window 35** | 672.2-684 | 11.8 | 5 |
| **Window 36** | 683-695.2 | 12.2 | 5 |
| **Window 37** | 694.2-706 | 11.8 | 5 |
| **Window 38** | 705-715 | 10 | 5 |
| **Window 39** | 714-724.5 | 10.5 | 5 |
| **Window 40** | 723.5-733 | 9.5 | 5 |

| | | | |
|---|---|---|---|
| **Window 41** | 732-741.1 | 9.1 | 5 |
| **Window 42** | 740.1-748.8 | 8.7 | 5 |
| **Window 43** | 747.8-756.4 | 8.6 | 5 |
| **Window 44** | 755.4-763.6 | 8.2 | 5 |
| **Window 45** | 762.6-771.3 | 8.7 | 5 |
| **Window 46** | 770.3-779.8 | 9.5 | 5 |
| **Window 47** | 778.8-789.3 | 10.5 | 5 |
| **Window 48** | 788.3-799.2 | 10.9 | 5 |
| **Window 49** | 798.2-810.9 | 12.7 | 5 |
| **Window 50** | 809.9-825.3 | 15.4 | 8 |
| **Window 51** | 824.3-844.6 | 20.3 | 8 |
| **Window 52** | 843.6-868 | 24.4 | 8 |
| **Window 53** | 867-893.2 | 26.2 | 8 |
| **Window 54** | 892.2-920.2 | 28 | 8 |
| **Window 55** | 919.2-949.9 | 30.7 | 8 |
| **Window 56** | 948.9-989.1 | 40.2 | 8 |
| **Window 57** | 988.1-1028.7 | 40.6 | 8 |
| **Window 58** | 1027.7-1068.3 | 40.6 | 10 |
| **Window 59** | 1067.3-1127.2 | 59.9 | 10 |
| **Window 60** | 1126.2-1249.6 | 123.4 | 10 |

## 7.2 ANTI-NDUFA4L2 ANTIBODY TESTING

The western blot analysis previously performed oh SH-SY5Y cells against NDUFA4 antibody (Results 3.1) resulted in the absent of an observed signal. Thus, extra analyses were performed to test anti-NADUFA4L2 antibody.

Since NDUFA4 is a mitochondrial protein, the absence of signal (Figure 3.1*C*) might be due to the protein extraction method that does not allow mitochondrial extraction from cells. Also, NDUFA4 might have a low expression in such cells. To test this, the same immunoblotting analysis was performed using mouse cortex samples stored in our lab, that positively detected mitochondrial proteins, in previous work, and also 30 µg of SH-SY5Y (ATTC) cells extract, and a lower NDUFA4L2 antibody dilution (1:100). Results (Supplementary Figure 6.1*A*) show that it was not possible to detect the protein in the cortex samples. However, a band was detected in SH-SY5Y sample, around 75 kDa, which is in a much higher molecular weight than the one NDUFA4 has (10 kDa). This could be because the denaturation method being was not efficient enough, thus, samples were subjected to different, and more aggressive, denaturation methods (Supplementary Figure 6.1*B*). Different denaturing conditions included (i) increased SDS content to 12% and addition of NaCl (5.13 M), or (ii) addition of Urea (6M) to Laemmli sample buffer. Also, half the samples were denatured at 60 °C for 10 minutes and the other half at 95 °C for 5 minutes. Such conditions were chosen based on optimizations performed in previous work in our lab. Nevertheless, results (Supplementary Figure 6.1*B*) still show the absence of a signal at 10 kDa.

Non-specific binding of an antibody to proteins other than the target antigen can sometime occurs, more frequently when using polyclonal antibodies. A way to detect whether the antibody being used is specifically targeting its antigen, is to perform an immunizing peptide blocking experiment. Such assay allows the neutralization of the antibody, with its specific antigen,

prior to the immunoblotting. Thus, the antibody bound to the blocking peptide is no longer available to bind to the epitope present in the protein in the western blot membrane.

In order to assess whether this could be a sample-specific problem, or if could be a problem with secondary antibody, a western blot assay was performed using 50 µg of HeLa cells' whole cell lysate (cell line that supplier refers as positive control) and anti-DJ-1 antibody (which is a goat polyclonal antibody, like anti-NDUFA4L2 antibody, allowing assessment of secondary antibody (anti-goat) proper function) (Supplementary Figure 6.1*C*). Western blot membrane shows that even though DJ-1 was detected, meaning secondary antibody is properly working, it was still not possible to detect a signal around 10 kDa and remained detecting signal around 50-75 kDa. Thus, in order to evaluate whether those bands belonged to the protein or were unspecific binding, the same western blot procedure was performed but this time using a blocking peptide to block anti-NDUFA4L2 antibody, in the region where it was supposed to bind to its antigen. Meaning, if indeed NDUFA4 protein was being detected, when using this blocked antibody, the bands should disappear. However, analyzing Supplementary Figure 6.1*C*, there is no differences in band profile when using the blocked antibody or unblocked antibody, meaning that the protein of interest was not being detected, but instead unspecific binding of the antibody to other proteins.

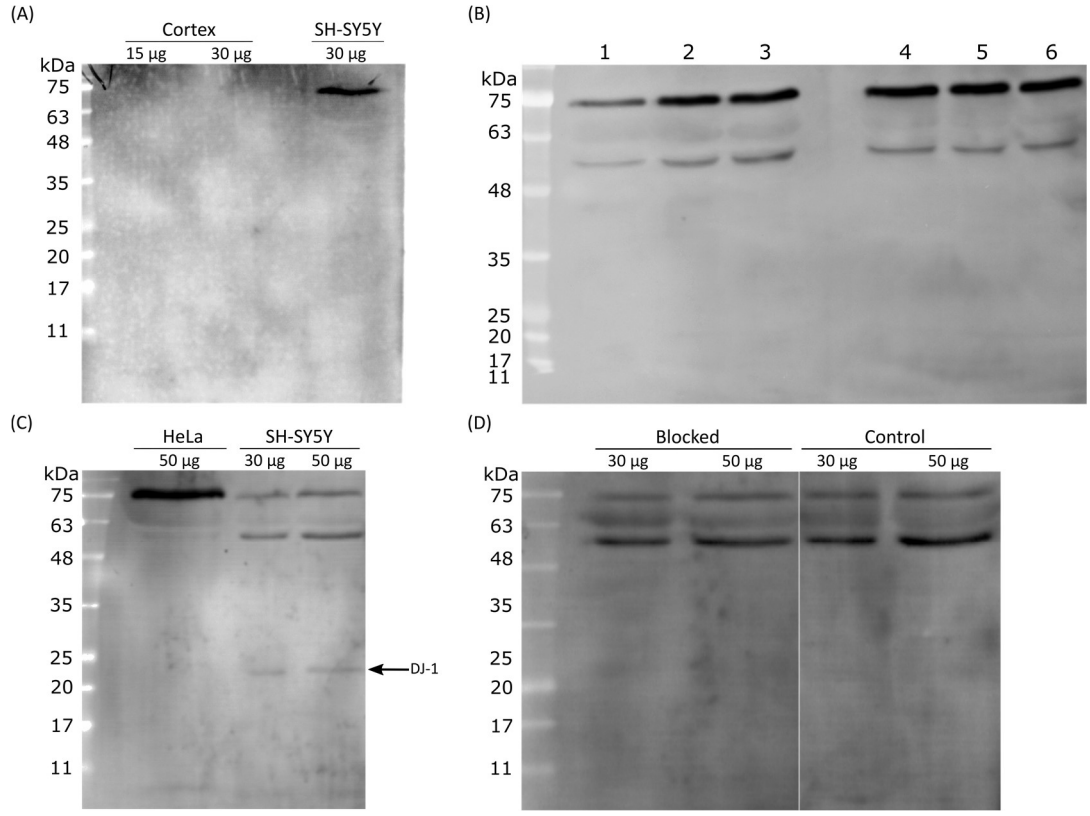


***Supplementary Figure 7.1 –*** Immunoblot analysis of anti-NDUFA4L2 antibody in different conditions. (A) Immunodetection of NDUFA in extracts of rat cortex and SH-SY5Y cells. For cortex 15 µg, 30 µg and 50 µg of proteins were loaded, and for cells samples 30 µg of protein was loaded. NDUFA4L2 antibody dilution used was 1:100 (B) Immunodetection of NDUFA in SH-SY5Y cell extract (30 µg) under different denaturation conditions. Samples from 1-3 were denatured at 60 °C for 10 minutes, and samples from 4-6 were denatured at 95 °C for 5 minutes. 1, 4 - 5.13M Nacl + 12% SDS; 2, 5 – 6 M Urea; 3, 6 – Laemmli sample buffer used in normal protocol. (C) Immunodetection of NDUFA and DJ-1 (1:200) in HeLa and SH-SY5Y whole cell lysates (30 µg and 50 µg). (D) Immunodetection of NDUFA4 using blocked antibody, with a blocking peptide, and unblocked antibody. For each condition, 30 µg and 50 µg of SH-SY5Y whole cell lysate was used.

## 7.3 IMMUNOPRECIPITATION ANTIBODY-COUPLING PROTOCOL TESTING

Different antibodies have different characteristics, even antibody clones raised in the same species against the same antibody can vary in pI, antigen binding affinity, and stability. Meaning, the coupling efficiency can vary slightly between different batches of the same antibody. Thus, prior to immunoprecipitation assay, the amount of antibody needed to ensure a good yield in antibody coupling reaction had to be determined.

Contrary to standard IP procedures, with Dynabeads® Co-immunoprecipitation Kit the antibody (Ab) is first covalently bound to the dynabeads and the Ab-bead pair is then used for the IP experiment. The Ab coupling process was analyzed by checking the presence of the antibody in three different fractions of the coupling reaction: (i) the fraction corresponding to the original amount of Ab added to the beads (input), (ii) the Ab-bead couple fraction (Ab bound), and (iii) fraction corresponding to the supernatant of the reaction (Ab unbound). Immunoglobulins (IgGs) are composed of two heavy chains (HC) and two light chains (LC) linked through disulfide bonds. The approximate molecular weight of an IgG is 148 kDa, from which a single HC has 51 kDa and a single LC has 23 kDa. Thus, this antibody-coupling reaction will be assessed through SDS-PAGE followed by western blot, checking the presence of such HC and LC in the three different fractions mentioned before. In the results obtained for both anti-HADHA and anti-3PGDH antibodies (Supplementary Figure 6.2*A*, *B*) intense bands corresponding to the heavy (HC) and light (LC) chains of the IgGs were observed in the lanes corresponding to the Ab-beads couple (Ab bound), in contrast with the reduced, or absent, signal in the unbound fraction. These results clearly indicate that a higher percentage of Ab used in the reaction was in fact coupled to the beads. On the other hand, in the results obtained for anti-NDUFA4L2 antibody (Supplementary Figure 6.2*C),* although an intense band signal is possible to observe in the input fraction, no signal is visible in the Ab bound fraction, or even in the Ab unbound fraction, meaning that at the end of the coupling reaction no antibody was attached to the beads. As no Ab was detected in the Ab unbound fraction, probably the Ab did bound to the bead, but the subsequent washes disrupted the couple. However, the procedure was performed in parallel for the three antibodies and the protocol was exactly the same, and only with anti-NDUFA4L2 antibody such problems arose, proving once more that the antibody was not properly working in these experiments. The results obtained in this experiment for anti-NDUFA4L2, coupled with the results obtained with the previous tests for this antibody (Supplementary data 6.2), and the fact that NDUFA4 protein was already previously reported to interact with DJ-1 protein [151], are the reason why this protein was left off to subsequent experiments of the project.

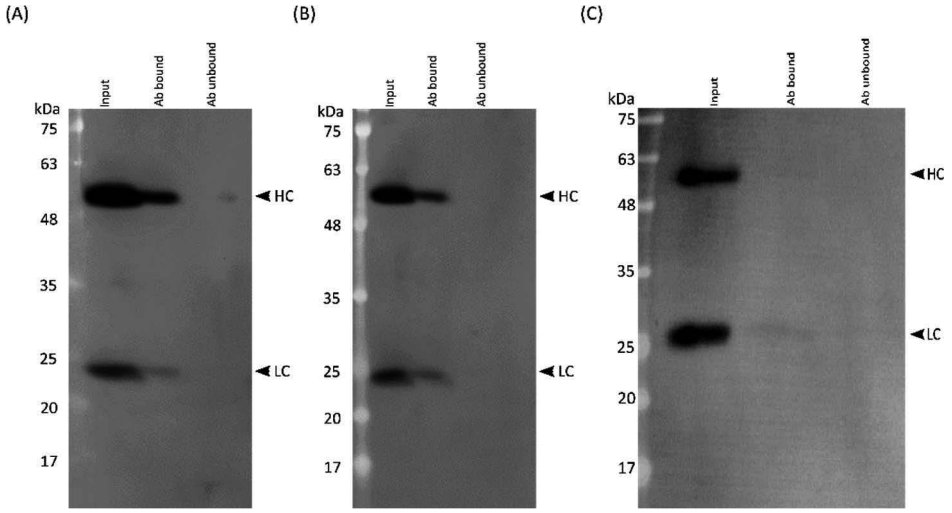


***Supplementary Figure 7.2 –*** Immunoblot analysis of antibody-beads coupling reaction. The antibody-coupling protocol was studied for (A) anti-HADHA antibody, (B) anti-PGDH antibody, and (C) anti-NDUFA4 antibody. Input – initial amount of antibody added to the beads; Ab bound – the coupled Ab-beads; Ab unbound – recovery solution of the coupling reaction, the antibodies that did not bind to the beads. These fractions were denatured and then electrophoretically separated through SDS-PAGE, followed by western blot protocol, using respective antibodies.

## 7.4 IMMUNOCYTOCHEMISTRY OPTIMAL ANTIBODY DILUTION AND PDL CONCENTRATION

In order to perform immunofluorescence confocal microscopy analysis in optimal conditions, different PDL concentration and anti-HADHA and anti-PGDH antibodies dilutions were tested. For that, SH-SY5Y cells were seeded in wells with PDL concentration range from 0.1-10 µg/mL, followed by fixation, permeabilization, protein blockage, incubation with different anti-HADHA, or anti-PGDH antibodies dilutions (1:25, 1:50, 1:100), and subsequent fluorophore-conjugated secondary antibodies. Cells were then observed under fluorescence microscope, images were retrieved, and minimum PDL concentration that still allowed attachment of cells and minimum antibody dilution that still showed a good signal intensity were assessed. Fluorescence microscopy results show no drastic signal intensity reduction when using 1:100 antibody dilution when compared with 1:25 antibody dilution, for both proteins (Supplementary Figure 6.3), therefore, no images were retrieved for 1:50 antibody dilution condition. It is possible to observe an intense green signal, which corresponds to HADHA and PGDH proteins, even when using 1:100 antibody dilution (middle and right panels), thus, this was the dilution chosen for further immunocytochemistry assays. As for PDL concentration, 1 µg/mL was elected as the optimal concentration, since cells seemed to retain their normal conformation, no apparent toxicity occurred, and cells were found in higher density in such condition. Cells seeded in 0.1 µg/mL of PDL wells also showed a normal conformation and some degrees of density, but it was taken in consideration that these tests were performed in 96 MW plates that are made of plastics, to which cells adhere more than glass. Thus, to ensure minimum loss of cells when performing the experiment in glass coverslips, 1 µg/mL of PDL was used. With this assay, it was also possible to visualize the different protein expression. HADHA is a mitochondrial protein and in this assay it seems to be expressed in the mitochondria (although a mitochondrial marker needed to be used to prove this), whereas PGDH seems to be expressing throughout the cytoplasm, which is also in accordance with the fact that it is a cytoplasmic protein.

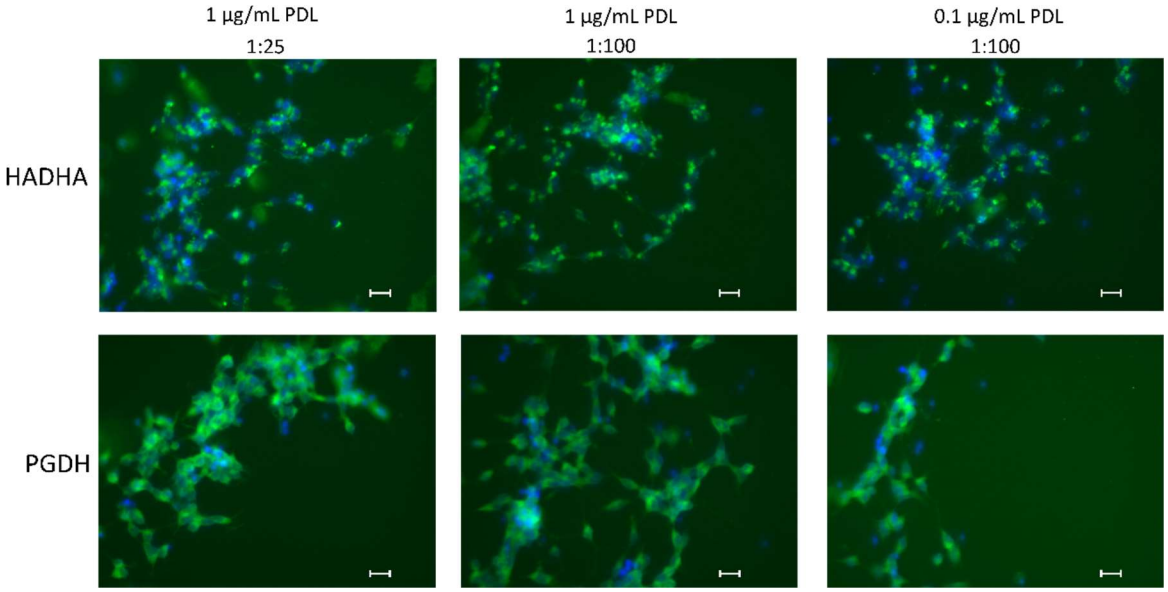


***Supplementary Figure 7.3* –** Fluorescence microscopy analysis of optimal PDL concentration and antibodies dilution. Immunostaining of HADHA (upper row) and PGDH (lower row) proteins, in green, in SH-SY5Y cells, in different antibody dilution (1:25 – left panel, and 1:100 – middle and right panels) and different PDL concentrations (0.1 µg/mL – right panel, and 1 µg/mL – left and middle panels). Nuclei were stained with DAPI (blue). Scale bars, 20 µm.

## 7.5 Proteins Quantified Through SWATH Method

***Supplementary Table 7.2* – Proteins quantified through SWATH acquisition method.** Different proteins that copurified with HADHA in SH-SY5Y cells exposed to $H_2O_2$ (1 mM) for different time points (0, 20 and 40 minutes), their correspondent accession number, name, interaction ratio (quantification median normalized to HADHA quantification median), and *p*-value.

| Accession Number | Protein name | Quantification | | | *p*-value |
|---|---|---|---|---|---|
| | | 0 min | 20 min | 40 min | |
| | ***p*-value < 0.1** | | | | |
| **A6NHR9** | Structural maintenance of chromosomes flexible hinge domain-containing protein 1 | 4.34E-02 | 3.03E-01 | 1.10E-01 | 0.019 |
| **O00139** | Kinesin-like protein KIF2A | 1.98E-03 | 9.20E-02 | 4.77E-02 | 0.019 |
| **O00159** | Unconventional myosin-Ic | 6.25E-02 | 3.30E-01 | 1.54E-01 | 0.019 |
| **O00422** | Histone deacetylase complex subunit SAP18 | 3.88E-02 | 1.13E-01 | 3.85E-02 | 0.019 |
| **O00541** | Pescadillo homolog | 1.51E-02 | 1.52E-01 | 5.35E-02 | 0.019 |
| **O00567** | Nucleolar protein 56 | 8.33E-02 | 1.09E+00 | 3.39E-01 | 0.019 |
| **O00571** | ATP-dependent RNA helicase DDX3X | 2.25E-01 | 1.04E+00 | 4.87E-01 | 0.019 |
| **O14880** | Microsomal glutathione S-transferase 3 | 9.24E-03 | 4.79E-02 | 1.95E-02 | 0.022 |
| **O14979** | Heterogeneous nuclear ribonucleoprotein D-like | 6.00E-02 | 5.86E-01 | 1.33E-01 | 0.022 |
| **O14980** | Exportin-1 | 2.93E-03 | 7.31E-02 | 2.94E-02 | 0.022 |
| **O15027** | Protein transport protein Sec16A | 1.06E-01 | 5.03E-01 | 4.02E-01 | 0.022 |
| **O15042** | U2 snRNP-associated SURP motif-containing protein | 3.14E-03 | 4.54E-02 | 1.74E-02 | 0.022 |
| **O15144** | Actin-related protein 2/3 complex subunit 2 | 2.88E-03 | 3.93E-02 | 1.22E-02 | 0.022 |

| | | | | | |
|---|---|---|---|---|---|
| **O15145** | Actin-related protein 2/3 complex subunit 3 | 6.13E-03 | 5.98E-02 | 1.99E-02 | 0.022 |
| **O15213** | WD repeat-containing protein 46 | 2.61E-02 | 1.09E-01 | 4.03E-02 | 0.022 |
| **O15240** | Neurosecretory protein VGF [Cleaved into: Neuroendocrine regulatory peptide-1 | 7.25E-02 | 5.58E-01 | 3.03E-01 | 0.022 |
| **O43143** | Pre-mRNA-splicing factor ATP-dependent RNA helicase DHX15 | 2.87E-01 | 2.48E+00 | 9.41E-01 | 0.022 |
| **O43172** | U4/U6 small nuclear ribonucleoprotein Prp4 | 4.97E-03 | 3.85E-02 | 1.73E-02 | 0.022 |
| **O43290** | U4/U6.U5 tri-snRNP-associated protein 1 | 4.15E-03 | 6.47E-02 | 1.86E-02 | 0.022 |
| **O43390** | Heterogeneous nuclear ribonucleoprotein R | 2.91E-01 | 1.85E+00 | 6.57E-01 | 0.022 |
| **O43660** | Pleiotropic regulator 1 | 1.24E-02 | 9.48E-02 | 3.17E-02 | 0.022 |
| **O43707** | Alpha-actinin-4 | 2.78E-03 | 7.09E-02 | 3.42E-02 | 0.022 |
| **O43795** | Unconventional myosin-Ib | 1.01E-01 | 9.92E-01 | 6.86E-01 | 0.022 |
| **O43809** | Cleavage and polyadenylation specificity factor subunit 5 | 8.32E-02 | 6.88E-02 | 3.03E-02 | 0.022 |
| **O60216** | Double-strand-break repair protein rad21 homolog | 6.88E-03 | 9.65E-02 | 2.69E-02 | 0.022 |
| **O60264** | SWI/SNF-related matrix-associated actin-dependent regulator of chromatin subfamily A member 5 | 2.82E-01 | 1.37E+00 | 5.28E-01 | 0.022 |
| **O60287** | Nucleolar pre-ribosomal-associated protein 1 | 1.91E-02 | 5.91E-02 | 2.32E-02 | 0.022 |
| **O60318** | Germinal-center associated nuclear protein | 1.05E-02 | 4.45E-02 | 1.83E-02 | 0.022 |
| **O60341** | Lysine-specific histone demethylase 1A | 5.82E-03 | 2.43E-02 | 8.96E-03 | 0.022 |
| **O60506** | Heterogeneous nuclear ribonucleoprotein Q | 1.38E-01 | 9.84E-01 | 2.73E-01 | 0.022 |
| **O60832** | H/ACA ribonucleoprotein complex subunit 4 | 7.04E-02 | 5.47E-01 | 1.65E-01 | 0.022 |
| **O75131** | Copine-3 | 4.25E-03 | 4.03E-02 | 2.41E-02 | 0.022 |
| **O75152** | Zinc finger CCCH domain-containing protein 11A | 1.18E-03 | 4.46E-02 | 1.34E-02 | 0.022 |
| **O75367** | Core histone macro-H2A.1 | 6.48E-01 | 3.92E+00 | 1.30E+00 | 0.022 |
| **O75369** | Filamin-B | 2.09E-03 | 8.10E-03 | 8.97E-04 | 0.022 |
| **O75400** | Pre-mRNA-processing factor 40 homolog A | 1.58E-02 | 1.06E-01 | 4.10E-02 | 0.023 |
| **O75431** | Metaxin-2 | 5.60E-03 | 4.93E-02 | 1.79E-02 | 0.023 |
| **O75475** | PC4 and SFRS1-interacting protein | 1.43E-01 | 7.18E-01 | 2.13E-01 | 0.024 |
| **O75494** | Serine/arginine-rich splicing factor 10 | 8.15E-03 | 7.39E-02 | 1.83E-02 | 0.024 |
| **O75525** | KH domain-containing, RNA-binding, signal transduction-associated protein 3 | 1.52E-02 | 1.86E-01 | 6.21E-02 | 0.024 |
| **O75531** | Barrier-to-autointegration factor | 5.97E-02 | 1.25E-01 | 4.49E-02 | 0.024 |
| **O75533** | Splicing factor 3B subunit 1 | 1.90E-01 | 6.79E-01 | 2.51E-01 | 0.024 |
| **O75643** | U5 small nuclear ribonucleoprotein 200 kDa helicase | 1.47E-01 | 9.81E-01 | 3.16E-01 | 0.024 |
| **O75691** | Small subunit processome component 20 homolog | 9.87E-02 | 2.01E-01 | 6.60E-02 | 0.024 |
| **O75694** | Nuclear pore complex protein Nup155 | 1.84E-01 | 4.67E-01 | 1.74E-01 | 0.024 |
| **O76021** | Ribosomal L1 domain-containing protein 1 | 8.07E-02 | 9.41E-01 | 3.19E-01 | 0.024 |
| **O94901** | SUN domain-containing protein 1 | 4.34E-03 | 4.28E-02 | 1.59E-02 | 0.024 |
| **O94906** | Pre-mRNA-processing factor 6 | 2.96E-02 | 3.05E-01 | 9.67E-02 | 0.024 |
| **O95478** | Ribosome biogenesis protein NSA2 homolog | 1.84E-03 | 2.61E-02 | 1.08E-02 | 0.024 |
| **O95487** | Protein transport protein Sec24B | 8.98E-04 | 1.00E-02 | 4.27E-03 | 0.024 |
| **O95602** | DNA-directed RNA polymerase I subunit RPA1 | 1.38E-03 | 1.97E-02 | 7.92E-03 | 0.024 |

| | | | | | |
|---|---|---|---|---|---|
| **O95793** | Double-stranded RNA-binding protein Staufen homolog 1 | 1.13E-02 | 3.09E-02 | 1.17E-02 | 0.024 |
| **O96019** | Actin-like protein 6A | 3.08E-02 | 2.24E-01 | 8.42E-02 | 0.024 |
| **P01023** | Alpha-2-macroglobulin | 6.35E-02 | 3.47E-02 | 1.33E-02 | 0.024 |
| **P02461** | Collagen alpha-1 | 3.65E-01 | 6.81E-02 | 6.68E-02 | 0.024 |
| **P02545** | Prelamin-A/C [Cleaved into: Lamin-A/C | 4.21E-01 | 5.03E+00 | 1.75E+00 | 0.024 |
| **P02768** | Serum albumin | 1.18E-01 | 8.45E-02 | 6.01E-02 | 0.024 |
| **P04004** | Vitronectin | 1.10E-02 | 1.03E-02 | 7.33E-03 | 0.024 |
| **P04406** | Glyceraldehyde-3-phosphate dehydrogenase | 3.57E-01 | 5.30E-01 | 3.04E-01 | 0.024 |
| **P05141** | ADP/ATP translocase 2 | 6.60E-02 | 2.59E-01 | 8.92E-02 | 0.024 |
| **P05388** | 60S acidic ribosomal protein P0 | 4.06E-02 | 9.85E-02 | 3.29E-02 | 0.024 |
| **P06748** | Nucleophosmin | 1.64E-01 | 2.42E+00 | 6.07E-01 | 0.024 |
| **P06753** | Tropomyosin alpha-3 chain | 1.02E-02 | 9.33E-02 | 4.14E-02 | 0.024 |
| **P07196** | Neurofilament light polypeptide | 1.29E-02 | 1.51E-01 | 4.61E-02 | 0.024 |
| **P07197** | Neurofilament medium polypeptide | 1.49E-02 | 7.33E-02 | 2.58E-02 | 0.024 |
| **P07305** | Histone H1.0 | 1.73E-01 | 4.55E-01 | 1.18E-01 | 0.024 |
| **P07355** | Annexin A2 | 4.15E-02 | 4.25E-02 | 2.16E-02 | 0.024 |
| **P07437** | Tubulin beta chain | 3.23E-02 | 1.18E-01 | 5.17E-02 | 0.024 |
| **P07910** | Heterogeneous nuclear ribonucleoproteins C1/C2 | 1.23E+00 | 9.85E+00 | 2.37E+00 | 0.024 |
| **P08123** | Collagen alpha-2 | 7.71E-01 | 1.33E-01 | 1.74E-01 | 0.024 |
| **P08238** | Heat shock protein HSP 90-beta | 1.19E-01 | 2.10E-01 | 1.03E-01 | 0.024 |
| **P08579** | U2 small nuclear ribonucleoprotein B'' | 1.65E-02 | 1.05E-01 | 3.88E-02 | 0.024 |
| **P08670** | Vimentin | 2.68E+00 | 4.91E+01 | 1.78E+01 | 0.024 |
| **P09651** | Heterogeneous nuclear ribonucleoprotein A1 | 7.50E-01 | 3.60E+00 | 1.02E+00 | 0.024 |
| **P09661** | U2 small nuclear ribonucleoprotein A' | 5.72E-02 | 2.65E-01 | 9.05E-02 | 0.024 |
| **P09874** | Poly [ADP-ribose] polymerase 1 | 1.06E+00 | 1.74E+00 | 9.07E-01 | 0.024 |
| **P11021** | 78 kDa glucose-regulated protein | 1.04E-01 | 1.33E-01 | 7.35E-02 | 0.024 |
| **P11142** | Heat shock cognate 71 kDa protein | 4.42E-01 | 7.20E-01 | 4.88E-01 | 0.024 |
| **P11387** | DNA topoisomerase 1 | 1.36E-02 | 1.57E-01 | 5.58E-02 | 0.024 |
| **P11388** | DNA topoisomerase 2-alpha | 5.00E-01 | 2.71E-01 | 2.10E-01 | 0.024 |
| **P11940** | Polyadenylate-binding protein 1 | 8.99E-02 | 1.56E-01 | 1.10E-01 | 0.024 |
| **P12236** | ADP/ATP translocase 3 | 6.39E-02 | 7.18E-02 | 3.48E-02 | 0.024 |
| **P12270** | Nucleoprotein TPR | 8.55E-02 | 4.10E-01 | 1.76E-01 | 0.024 |
| **P12814** | Alpha-actinin-1 | 1.77E-02 | 1.07E-01 | 4.68E-02 | 0.024 |
| **P12956** | X-ray repair cross-complementing protein 6 | 2.00E-02 | 1.45E-01 | 5.94E-02 | 0.024 |
| **P13010** | X-ray repair cross-complementing protein 5 | 1.62E-02 | 1.15E-01 | 4.71E-02 | 0.024 |
| **P14678** | Small nuclear ribonucleoprotein-associated proteins B and B' | 1.83E-01 | 5.96E-01 | 2.29E-01 | 0.024 |
| **P14866** | Heterogeneous nuclear ribonucleoprotein L | 1.58E-01 | 1.64E+00 | 5.20E-01 | 0.024 |
| **P15880** | 40S ribosomal protein S2 | 4.72E-02 | 1.38E-01 | 5.97E-02 | 0.024 |
| **P16401** | Histone H1.5 | 4.97E-01 | 3.43E+00 | 9.89E-01 | 0.024 |
| **P16402** | Histone H1.3 | 7.25E-01 | 4.32E+00 | 1.37E+00 | 0.024 |
| **P17480** | Nucleolar transcription factor 1 | 2.91E-02 | 1.01E-01 | 4.07E-02 | 0.024 |
| **P17844** | Probable ATP-dependent RNA helicase DDX5 | 3.05E-01 | 1.18E+00 | 4.88E-01 | 0.024 |
| **P18085** | ADP-ribosylation factor 4 | 3.44E-03 | 1.18E-02 | 4.81E-03 | 0.024 |

| | | | | | |
|---|---|---|---|---|---|
| **P18124** | 60S ribosomal protein L7 | 2.03E-01 | 5.10E-01 | 1.87E-01 | 0.024 |
| **P18583** | Protein SON | 2.03E-02 | 1.10E-01 | 3.74E-02 | 0.024 |
| **P19105** | Myosin regulatory light chain 12A | 1.74E-02 | 4.19E-02 | 3.89E-02 | 0.024 |
| **P19338** | Nucleolin | 2.94E-02 | 3.00E-01 | 6.40E-02 | 0.024 |
| **P19387** | DNA-directed RNA polymerase II subunit RPB3 | 2.09E-03 | 2.33E-02 | 8.39E-03 | 0.024 |
| **P19525** | Interferon-induced, double-stranded RNA-activated protein kinase | 3.66E-02 | 1.07E-01 | 3.66E-02 | 0.024 |
| **P20700** | Lamin-B1 | 3.29E-01 | 2.45E+00 | 9.09E-01 | 0.024 |
| **P21333** | Filamin-A | 6.18E-02 | 2.70E-01 | 1.17E-01 | 0.024 |
| **P22061** | Protein-L-isoaspartate | 8.86E-02 | 1.06E-02 | 3.85E-03 | 0.024 |
| **P22087** | rRNA 2'-O-methyltransferase fibrillarin | 4.11E-01 | 2.10E+00 | 7.13E-01 | 0.024 |
| **P22626** | Heterogeneous nuclear ribonucleoproteins A2/B1 | 1.12E+00 | 7.18E+00 | 2.09E+00 | 0.024 |
| **P23246** | Splicing factor, proline- and glutamine-rich | 7.83E-02 | 3.60E-01 | 1.59E-01 | 0.025 |
| **P23396** | 40S ribosomal protein S3 | 3.89E-02 | 7.05E-02 | 1.02E-01 | 0.025 |
| **P23528** | Cofilin-1 | 6.43E-02 | 1.04E-01 | 4.24E-02 | 0.025 |
| **P24928** | DNA-directed RNA polymerase II subunit RPB1 | 7.39E-02 | 1.90E-01 | 7.71E-02 | 0.025 |
| **P25705** | ATP synthase subunit alpha, mitochondrial | 1.02E-02 | 4.47E-02 | 2.05E-02 | 0.025 |
| **P26368** | Splicing factor U2AF 65 kDa subunit | 4.94E-02 | 2.56E-01 | 8.93E-02 | 0.025 |
| **P26373** | 60S ribosomal protein L13 | 5.31E-02 | 1.27E-01 | 4.19E-02 | 0.025 |
| **P26378** | ELAV-like protein 4 | 2.99E-02 | 2.07E-01 | 6.94E-02 | 0.025 |
| **P26599** | Polypyrimidine tract-binding protein 1 | 4.29E-01 | 2.21E+00 | 8.39E-01 | 0.025 |
| **P27635** | 60S ribosomal protein L10 | 2.99E-02 | 1.05E-01 | 2.66E-02 | 0.025 |
| **P28288** | ATP-binding cassette sub-family D member 3 | 8.17E-03 | 4.26E-02 | 1.78E-02 | 0.025 |
| **P28289** | Tropomodulin-1 | 3.39E-03 | 1.80E-02 | 8.52E-03 | 0.025 |
| **P28370** | Probable global transcription activator SNF2L1 | 5.07E-03 | 3.89E-02 | 1.37E-02 | 0.025 |
| **P30050** | 60S ribosomal protein L12 | 2.72E-02 | 6.40E-02 | 2.51E-02 | 0.025 |
| **P30876** | DNA-directed RNA polymerase II subunit RPB2 | 5.57E-02 | 3.22E-01 | 1.24E-01 | 0.025 |
| **P31943** | Heterogeneous nuclear ribonucleoprotein H | 8.04E-02 | 8.44E-01 | 2.97E-01 | 0.025 |
| **P32119** | Peroxiredoxin-2 | 2.26E-03 | 6.01E-02 | 1.60E-02 | 0.025 |
| **P32969** | 60S ribosomal protein L9 | 4.81E-02 | 1.27E-01 | 5.02E-02 | 0.025 |
| **P33176** | Kinesin-1 heavy chain | 1.95E-02 | 2.53E-02 | 1.03E-02 | 0.025 |
| **P33240** | Cleavage stimulation factor subunit 2 | 3.65E-03 | 1.14E-02 | 3.11E-03 | 0.025 |
| **P33992** | DNA replication licensing factor MCM5 | 4.24E-03 | 3.93E-02 | 1.89E-02 | 0.025 |
| **P35222** | Catenin beta-1 | 4.71E-03 | 2.30E-02 | 1.08E-02 | 0.025 |
| **P35251** | Replication factor C subunit 1 | 2.69E-03 | 1.08E-02 | 4.81E-03 | 0.025 |
| **P35268** | 60S ribosomal protein L22 | 3.23E-02 | 7.36E-02 | 2.60E-02 | 0.025 |
| **P35579** | Myosin-9 | 1.18E-01 | 3.61E-01 | 6.26E-01 | 0.025 |
| **P35580** | Myosin-10 | 6.01E-02 | 2.65E-01 | 1.91E-01 | 0.025 |
| **P36578** | 60S ribosomal protein L4 | 3.86E-01 | 1.28E+00 | 4.88E-01 | 0.025 |
| **P36873** | Serine/threonine-protein phosphatase PP1-gamma catalytic subunit | 2.97E-03 | 4.53E-02 | 2.71E-02 | 0.025 |
| **P37108** | Signal recognition particle 14 kDa protein | 4.61E-02 | 9.59E-02 | 3.86E-02 | 0.025 |
| **P37198** | Nuclear pore glycoprotein p62 | 6.69E-03 | 3.75E-02 | 5.25E-03 | 0.025 |
| **P38159** | RNA-binding motif protein, X chromosome | 1.40E-01 | 1.08E+00 | 3.55E-01 | 0.025 |
| **P38432** | Coilin | 8.61E-03 | 7.11E-02 | 2.35E-02 | 0.025 |

| | | | | | |
|---|---|---|---|---|---|
| **P38646** | Stress-70 protein, mitochondrial | 9.71E-03 | 3.37E-02 | 1.70E-02 | 0.025 |
| **P38919** | Eukaryotic initiation factor 4A-III | 1.80E-01 | 8.98E-01 | 3.54E-01 | 0.025 |
| **P39023** | 60S ribosomal protein L3 | 1.70E-02 | 5.87E-02 | 2.44E-02 | 0.025 |
| **P40429** | 60S ribosomal protein L13a | 7.41E-02 | 1.54E-01 | 4.55E-02 | 0.025 |
| **P40939** | Trifunctional enzyme subunit alpha, mitochondrial | 1.00E+00 | 1.00E+00 | 1.00E+00 | 0.025 |
| **P41219** | Peripherin | 1.17E-02 | 1.31E-01 | 5.10E-02 | 0.025 |
| **P42166** | Lamina-associated polypeptide 2, isoform alpha | 2.09E-03 | 1.43E-02 | 3.94E-03 | 0.025 |
| **P42167** | Lamina-associated polypeptide 2, isoforms beta/gamma | 3.62E-02 | 5.25E-02 | 2.08E-02 | 0.025 |
| **P42285** | Superkiller viralicidic activity 2-like 2 | 5.65E-02 | 1.89E-01 | 6.84E-02 | 0.025 |
| **P42677** | 40S ribosomal protein S27 | 1.63E-02 | 2.10E-02 | 9.92E-03 | 0.025 |
| **P42766** | 60S ribosomal protein L35 | 4.48E-02 | 7.06E-02 | 2.21E-02 | 0.025 |
| **P43243** | Matrin-3 | 3.40E-01 | 2.34E+00 | 8.26E-01 | 0.025 |
| **P43363** | Melanoma-associated antigen 10 | 3.37E-03 | 1.51E-02 | 5.43E-03 | 0.025 |
| **P45880** | Voltage-dependent anion-selective channel protein 2 | 4.80E-02 | 3.40E-01 | 1.46E-01 | 0.025 |
| **P46013** | Antigen KI-67 | 4.27E-02 | 9.59E-02 | 4.56E-02 | 0.025 |
| **P46060** | Ran GTPase-activating protein 1 | 2.68E-02 | 2.41E-01 | 8.85E-02 | 0.025 |
| **P46087** | Probable 28S rRNA | 6.73E-02 | 5.28E-01 | 1.54E-01 | 0.025 |
| **P46100** | Transcriptional regulator ATRX | 4.17E-03 | 4.66E-02 | 1.68E-02 | 0.025 |
| **P46776** | 60S ribosomal protein L27a | 4.92E-02 | 1.18E-01 | 3.98E-02 | 0.025 |
| **P46781** | 40S ribosomal protein S9 | 4.30E-02 | 1.28E-01 | 3.61E-02 | 0.025 |
| **P46783** | 40S ribosomal protein S10 | 1.27E-02 | 2.81E-02 | 1.36E-02 | 0.025 |
| **P47755** | F-actin-capping protein subunit alpha-2 | 1.59E-02 | 6.98E-02 | 2.96E-02 | 0.025 |
| **P47756** | F-actin-capping protein subunit beta | 3.39E-03 | 4.22E-02 | 1.80E-02 | 0.025 |
| **P48047** | ATP synthase subunit O, mitochondrial | 1.50E-03 | 9.74E-03 | 6.36E-03 | 0.025 |
| **P48681** | Nestin | 1.87E-01 | 1.34E+00 | 5.56E-01 | 0.025 |
| **P49750** | YLP motif-containing protein 1 | 8.98E-04 | 3.62E-02 | 1.24E-02 | 0.025 |
| **P49756** | RNA-binding protein 25 | 2.39E-02 | 2.40E-01 | 7.30E-02 | 0.025 |
| **P49790** | Nuclear pore complex protein Nup153 | 5.62E-02 | 1.47E-01 | 7.34E-02 | 0.025 |
| **P49792** | E3 SUMO-protein ligase RanBP2 | 4.05E-02 | 4.95E-01 | 2.23E-01 | 0.025 |
| **P50454** | Serpin H1 | 2.70E+00 | 2.60E-01 | 4.38E-01 | 0.025 |
| **P50914** | 60S ribosomal protein L14 | 7.99E-02 | 1.56E-01 | 5.38E-02 | 0.025 |
| **P51114** | Fragile X mental retardation syndrome-related protein 1 | 7.65E-03 | 4.63E-02 | 2.03E-02 | 0.025 |
| **P51532** | Transcription activator BRG1 | 7.03E-03 | 1.02E-01 | 3.32E-02 | 0.025 |
| **P51610** | Host cell factor 1 | 2.94E-03 | 5.26E-02 | 2.01E-02 | 0.025 |
| **P51991** | Heterogeneous nuclear ribonucleoprotein A3 | 2.04E-01 | 2.29E+00 | 7.14E-01 | 0.025 |
| **P52272** | Heterogeneous nuclear ribonucleoprotein M | 5.98E-01 | 4.78E+00 | 1.81E+00 | 0.025 |
| **P52292** | Importin subunit alpha-1 | 2.45E-02 | 1.60E-01 | 6.91E-02 | 0.025 |
| **P52294** | Importin subunit alpha-5 | 2.61E-03 | 3.78E-02 | 1.79E-02 | 0.025 |
| **P52597** | Heterogeneous nuclear ribonucleoprotein F | 3.24E-02 | 4.36E-01 | 1.53E-01 | 0.025 |
| **P52948** | Nuclear pore complex protein Nup98-Nup96 [Cleaved into: Nuclear pore complex protein Nup98 | 4.97E-02 | 4.46E-01 | 1.43E-01 | 0.025 |
| **P53992** | Protein transport protein Sec24C | 1.29E-02 | 2.16E-01 | 1.45E-01 | 0.025 |

| | | | | | |
|---|---|---|---|---|---|
| **P54289** | Voltage-dependent calcium channel subunit alpha-2/delta-1 | 4.04E-03 | 1.81E-02 | 9.30E-03 | 0.025 |
| **P55084** | Trifunctional enzyme subunit beta, mitochondrial | 5.73E-02 | 7.06E-02 | 3.81E-02 | 0.025 |
| **P55265** | Double-stranded RNA-specific adenosine deaminase | 1.03E-01 | 1.00E+00 | 3.40E-01 | 0.025 |
| **P55735** | Protein SEC13 homolog | 1.48E-02 | 1.20E-01 | 5.69E-02 | 0.025 |
| **P55769** | NHP2-like protein 1 | 4.08E-03 | 2.30E-02 | 7.33E-03 | 0.025 |
| **P55795** | Heterogeneous nuclear ribonucleoprotein H2 | 2.35E-02 | 1.70E-01 | 4.84E-02 | 0.025 |
| **P56134** | ATP synthase subunit f, mitochondrial | 1.94E-02 | 2.71E-02 | 1.25E-02 | 0.025 |
| **P56182** | Ribosomal RNA processing protein 1 homolog A | 1.75E-02 | 1.82E-02 | 6.04E-03 | 0.025 |
| **P56537** | Eukaryotic translation initiation factor 6 | 4.95E-03 | 4.88E-02 | 1.70E-02 | 0.025 |
| **P57088** | Transmembrane protein 33 | 1.84E-02 | 2.36E-02 | 1.36E-02 | 0.025 |
| **P57740** | Nuclear pore complex protein Nup107 | 3.21E-02 | 4.61E-01 | 1.60E-01 | 0.025 |
| **P59998** | Actin-related protein 2/3 complex subunit 4 | 1.00E-02 | 6.05E-02 | 2.06E-02 | 0.025 |
| **P60660** | Myosin light polypeptide 6 | 1.14E-02 | 7.28E-02 | 4.88E-02 | 0.025 |
| **P60842** | Eukaryotic initiation factor 4A-I | 1.40E-02 | 1.24E-01 | 6.21E-02 | 0.025 |
| **P61158** | Actin-related protein 3 | 8.75E-03 | 4.33E-02 | 1.61E-02 | 0.025 |
| **P61247** | 40S ribosomal protein S3a | 2.37E-02 | 8.34E-02 | 3.01E-02 | 0.025 |
| **P61313** | 60S ribosomal protein L15 | 3.96E-02 | 1.30E-01 | 3.07E-02 | 0.025 |
| **P61353** | 60S ribosomal protein L27 | 7.19E-02 | 1.72E-01 | 6.39E-02 | 0.025 |
| **P61956** | Small ubiquitin-related modifier 2 | 4.58E-03 | 3.79E-01 | 1.22E-01 | 0.025 |
| **P61962** | DDB1- and CUL4-associated factor 7 | 3.42E-03 | 1.68E-02 | 7.85E-03 | 0.025 |
| **P61964** | WD repeat-containing protein 5 | 3.17E-02 | 7.49E-02 | 2.84E-02 | 0.025 |
| **P61978** | Heterogeneous nuclear ribonucleoprotein K | 4.10E-01 | 3.38E+00 | 1.25E+00 | 0.025 |
| **P62081** | 40S ribosomal protein S7 | 9.07E-02 | 2.69E-01 | 1.04E-01 | 0.025 |
| **P62136** | Serine/threonine-protein phosphatase PP1-alpha catalytic subunit | 1.98E-02 | 5.93E-02 | 2.65E-02 | 0.025 |
| **P62140** | Serine/threonine-protein phosphatase PP1-beta catalytic subunit | 1.98E-03 | 4.58E-02 | 1.72E-02 | 0.025 |
| **P62241** | 40S ribosomal protein S8 | 1.04E-02 | 4.02E-02 | 1.53E-02 | 0.025 |
| **P62244** | 40S ribosomal protein S15a | 1.02E-01 | 3.06E-01 | 1.06E-01 | 0.025 |
| **P62249** | 40S ribosomal protein S16 | 1.22E-01 | 3.03E-01 | 1.16E-01 | 0.025 |
| **P62263** | 40S ribosomal protein S14 | 4.46E-02 | 6.96E-02 | 4.25E-02 | 0.025 |
| **P62266** | 40S ribosomal protein S23 | 3.82E-02 | 8.28E-02 | 2.92E-02 | 0.025 |
| **P62269** | 40S ribosomal protein S18 | 1.91E-02 | 4.05E-02 | 1.41E-02 | 0.025 |
| **P62277** | 40S ribosomal protein S13 | 7.30E-02 | 1.96E-01 | 6.34E-02 | 0.026 |
| **P62280** | 40S ribosomal protein S11 | 4.13E-02 | 1.10E-01 | 4.22E-02 | 0.026 |
| **P62304** | Small nuclear ribonucleoprotein E | 2.02E-02 | 1.22E-01 | 4.33E-02 | 0.026 |
| **P62308** | Small nuclear ribonucleoprotein G | 5.20E-03 | 3.03E-02 | 1.29E-02 | 0.026 |
| **P62314** | Small nuclear ribonucleoprotein Sm D1 | 2.76E-02 | 2.25E-01 | 7.35E-02 | 0.026 |
| **P62316** | Small nuclear ribonucleoprotein Sm D2 | 5.37E-02 | 2.01E-01 | 6.45E-02 | 0.026 |
| **P62318** | Small nuclear ribonucleoprotein Sm D3 | 8.81E-02 | 3.24E-01 | 1.07E-01 | 0.026 |
| **P62424** | 60S ribosomal protein L7a | 9.46E-03 | 5.63E-02 | 1.89E-02 | 0.026 |
| **P62701** | 40S ribosomal protein S4, X isoform | 1.03E-01 | 3.14E-01 | 1.18E-01 | 0.027 |
| **P62750** | 60S ribosomal protein L23a | 5.71E-02 | 8.98E-02 | 3.44E-02 | 0.027 |

| | | | | | |
|---|---|---|---|---|---|
| **P62753** | 40S ribosomal protein S6 | 6.08E-03 | 6.16E-02 | 2.39E-02 | 0.027 |
| **P62805** | Histone H4 | 1.35E+01 | 3.81E+01 | 1.56E+01 | 0.029 |
| **P62826** | GTP-binding nuclear protein Ran | 5.32E-02 | 2.66E-01 | 8.74E-02 | 0.029 |
| **P62847** | 40S ribosomal protein S24 | 3.11E-02 | 1.21E-01 | 4.07E-02 | 0.029 |
| **P62851** | 40S ribosomal protein S25 | 1.14E-02 | 5.41E-02 | 2.64E-02 | 0.029 |
| **P62899** | 60S ribosomal protein L31 | 5.64E-02 | 1.27E-01 | 4.25E-02 | 0.029 |
| **P62906** | 60S ribosomal protein L10a | 3.11E-02 | 8.19E-02 | 3.61E-02 | 0.029 |
| **P62913** | 60S ribosomal protein L11 | 7.85E-02 | 1.77E-01 | 6.47E-02 | 0.029 |
| **P62917** | 60S ribosomal protein L8 | 3.17E-02 | 9.56E-02 | 3.40E-02 | 0.029 |
| **P62937** | Peptidyl-prolyl cis-trans isomerase A | 1.57E-02 | 1.84E-02 | 1.24E-02 | 0.029 |
| **P62987** | Ubiquitin-60S ribosomal protein L40 | 7.46E-01 | 6.68E+00 | 2.31E+00 | 0.029 |
| **P62995** | Transformer-2 protein homolog beta | 1.91E-02 | 1.39E-01 | 4.28E-02 | 0.029 |
| **P63261** | Actin, cytoplasmic 2 | 6.82E-01 | 5.21E+00 | 2.29E+00 | 0.029 |
| **P67809** | Nuclease-sensitive element-binding protein 1 | 2.11E-02 | 1.21E-01 | 3.61E-02 | 0.029 |
| **P68371** | Tubulin beta-4B chain | 1.62E-02 | 5.42E-02 | 2.30E-02 | 0.029 |
| **P78316** | Nucleolar protein 14 | 7.02E-03 | 5.31E-02 | 1.48E-02 | 0.029 |
| **P78347** | General transcription factor II-I | 4.33E-02 | 4.04E-01 | 1.51E-01 | 0.029 |
| **P78406** | mRNA export factor | 8.04E-03 | 5.55E-02 | 2.54E-02 | 0.029 |
| **P78527** | DNA-dependent protein kinase catalytic subunit | 5.60E-02 | 2.87E-01 | 1.20E-01 | 0.029 |
| **P83731** | 60S ribosomal protein L24 | 2.94E-02 | 1.25E-01 | 4.51E-02 | 0.029 |
| **P84103** | Serine/arginine-rich splicing factor 3 | 1.47E-02 | 2.50E-01 | 9.76E-02 | 0.029 |
| **P84243** | Histone H3.3 | 2.54E-01 | 1.22E-01 | 7.06E-02 | 0.03 |
| **Q00325** | Phosphate carrier protein, mitochondrial | 6.71E-02 | 1.26E-01 | 5.83E-02 | 0.03 |
| **Q00610** | Clathrin heavy chain 1 | 1.02E-01 | 7.02E-01 | 4.39E-01 | 0.03 |
| **Q00839** | Heterogeneous nuclear ribonucleoprotein U | 4.24E-01 | 4.73E+00 | 1.86E+00 | 0.03 |
| **Q01082** | Spectrin beta chain, non-erythrocytic 1 | 1.62E-02 | 1.97E-01 | 1.12E-01 | 0.03 |
| **Q01780** | Exosome component 10 | 1.78E-01 | 9.82E-02 | 4.01E-02 | 0.03 |
| **Q02809** | Procollagen-lysine,2-oxoglutarate 5-dioxygenase 1 | 1.00E+00 | 6.46E-01 | 4.90E-01 | 0.03 |
| **Q02878** | 60S ribosomal protein L6 | 1.18E-01 | 3.87E-01 | 6.73E-02 | 0.03 |
| **Q02880** | DNA topoisomerase 2-beta | 2.75E-01 | 1.13E+00 | 4.11E-01 | 0.03 |
| **Q03252** | Lamin-B2 | 4.93E-01 | 7.22E-01 | 2.54E-01 | 0.03 |
| **Q03701** | CCAAT/enhancer-binding protein zeta | 1.01E-01 | 7.40E-01 | 2.58E-01 | 0.03 |
| **Q06265** | Exosome complex component RRP45 | 1.19E-02 | 6.64E-02 | 2.14E-02 | 0.03 |
| **Q06830** | Peroxiredoxin-1 | 1.41E-01 | 3.38E-01 | 1.22E-01 | 0.03 |
| **Q07020** | 60S ribosomal protein L18 | 1.62E-01 | 4.36E-01 | 1.10E-01 | 0.03 |
| **Q07021** | Complement component 1 Q subcomponent-binding protein, mitochondrial | 2.69E-03 | 3.40E-02 | 1.04E-02 | 0.03 |
| **Q07666** | KH domain-containing, RNA-binding, signal transduction-associated protein 1 | 2.18E-02 | 1.63E-01 | 6.02E-02 | 0.03 |
| **Q07955** | Serine/arginine-rich splicing factor 1 | 4.31E-02 | 1.73E-01 | 6.32E-02 | 0.03 |
| **Q08211** | ATP-dependent RNA helicase A | 6.43E-01 | 4.32E+00 | 1.57E+00 | 0.03 |
| **Q08830** | Fibrinogen-like protein 1 | 1.78E-02 | 2.29E-02 | 1.96E-02 | 0.03 |
| **Q08945** | FACT complex subunit SSRP1 | 1.47E-01 | 5.38E-01 | 1.74E-01 | 0.03 |
| **Q09028** | Histone-binding protein RBBP4 | 1.13E-01 | 9.92E-01 | 3.64E-01 | 0.03 |

| | | | | | |
|---|---|---|---|---|---|
| **Q09161** | Nuclear cap-binding protein subunit 1 | 2.18E-02 | 1.31E-01 | 4.64E-02 | 0.03 |
| **Q09666** | Neuroblast differentiation-associated protein AHNAK | 1.02E+01 | 2.02E+00 | 2.69E+00 | 0.03 |
| **Q12769** | Nuclear pore complex protein Nup160 | 7.52E-02 | 3.46E-01 | 1.36E-01 | 0.03 |
| **Q12788** | Transducin beta-like protein 3 | 5.61E-02 | 4.89E-01 | 1.74E-01 | 0.03 |
| **Q12874** | Splicing factor 3A subunit 3 | 2.02E-02 | 1.36E-01 | 4.59E-02 | 0.03 |
| **Q12888** | Tumor suppressor p53-binding protein 1 | 2.48E-02 | 1.19E-01 | 5.59E-02 | 0.03 |
| **Q12905** | Interleukin enhancer-binding factor 2 | 3.06E-01 | 2.60E+00 | 8.34E-01 | 0.03 |
| **Q12906** | Interleukin enhancer-binding factor 3 | 4.46E-01 | 3.29E+00 | 9.48E-01 | 0.03 |
| **Q13045** | Protein flightless-1 homolog | 1.41E-03 | 1.65E-02 | 1.08E-02 | 0.03 |
| **Q13123** | Protein Red | 1.00E-02 | 1.28E-01 | 4.17E-02 | 0.03 |
| **Q13148** | TAR DNA-binding protein 43 | 1.93E-02 | 1.45E-01 | 4.88E-02 | 0.03 |
| **Q13151** | Heterogeneous nuclear ribonucleoprotein A0 | 2.67E-01 | 5.57E-01 | 1.76E-01 | 0.03 |
| **Q13185** | Chromobox protein homolog 3 | 6.36E-02 | 2.41E-01 | 6.94E-02 | 0.03 |
| **Q13206** | Probable ATP-dependent RNA helicase DDX10 | 8.98E-04 | 3.81E-02 | 1.25E-02 | 0.03 |
| **Q13242** | Serine/arginine-rich splicing factor 9 | 1.52E-02 | 1.22E-01 | 3.27E-02 | 0.03 |
| **Q13247** | Serine/arginine-rich splicing factor 6 | 2.11E-02 | 8.50E-02 | 3.42E-02 | 0.03 |
| **Q13263** | Transcription intermediary factor 1-beta | 8.67E-02 | 7.67E-01 | 3.40E-01 | 0.03 |
| **Q13330** | Metastasis-associated protein MTA1 | 2.12E-02 | 1.05E-01 | 3.00E-02 | 0.03 |
| **Q13435** | Splicing factor 3B subunit 2 | 1.60E-01 | 3.57E-01 | 1.12E-01 | 0.03 |
| **Q13547** | Histone deacetylase 1 | 6.98E-03 | 5.30E-02 | 1.68E-02 | 0.03 |
| **Q13573** | SNW domain-containing protein 1 | 9.58E-03 | 9.14E-02 | 2.60E-02 | 0.03 |
| **Q13595** | Transformer-2 protein homolog alpha | 3.97E-03 | 8.91E-02 | 3.46E-02 | 0.03 |
| **Q13601** | KRR1 small subunit processome component homolog | 2.04E-02 | 6.65E-02 | 2.30E-02 | 0.03 |
| **Q13769** | THO complex subunit 5 homolog | 1.58E-02 | 3.03E-02 | 6.41E-03 | 0.03 |
| **Q13813** | Spectrin alpha chain, non-erythrocytic 1 | 1.09E-01 | 3.91E-01 | 2.23E-01 | 0.03 |
| **Q13868** | Exosome complex component RRP4 | 3.02E-02 | 3.59E-02 | 1.32E-02 | 0.03 |
| **Q13895** | Bystin | 9.72E-03 | 7.87E-02 | 2.32E-02 | 0.03 |
| **Q14103** | Heterogeneous nuclear ribonucleoprotein D0 | 4.35E-02 | 5.20E-01 | 1.40E-01 | 0.03 |
| **Q14137** | Ribosome biogenesis protein BOP1 | 6.11E-03 | 4.01E-02 | 1.60E-02 | 0.03 |
| **Q14146** | Unhealthy ribosome biogenesis protein 2 homolog | 2.66E-03 | 1.82E-02 | 6.93E-03 | 0.03 |
| **Q14151** | Scaffold attachment factor B2 | 1.01E-02 | 6.65E-02 | 1.77E-02 | 0.03 |
| **Q14562** | ATP-dependent RNA helicase DHX8 | 1.98E-03 | 1.74E-02 | 4.68E-03 | 0.03 |
| **Q14576** | ELAV-like protein 3 | 8.35E-03 | 3.74E-02 | 1.46E-02 | 0.03 |
| **Q14683** | Structural maintenance of chromosomes protein 1A | 6.05E-02 | 3.00E-01 | 1.05E-01 | 0.03 |
| **Q14684** | Ribosomal RNA processing protein 1 homolog B | 7.61E-03 | 1.24E-01 | 3.74E-02 | 0.03 |
| **Q14690** | Protein RRP5 homolog | 1.32E-01 | 8.31E-01 | 3.29E-01 | 0.03 |
| **Q14839** | Chromodomain-helicase-DNA-binding protein 4 | 7.64E-02 | 3.83E-01 | 1.43E-01 | 0.03 |
| **Q14974** | Importin subunit beta-1 | 1.14E-01 | 6.67E-01 | 2.77E-01 | 0.03 |
| **Q14978** | Nucleolar and coiled-body phosphoprotein 1 | 1.88E-02 | 6.03E-02 | 1.71E-02 | 0.03 |
| **Q14980** | Nuclear mitotic apparatus protein 1 | 1.92E-01 | 1.61E+00 | 6.56E-01 | 0.03 |
| **Q15007** | Pre-mRNA-splicing regulator WTAP | 1.13E-03 | 2.36E-02 | 5.54E-03 | 0.03 |

| | | | | | |
|---|---|---|---|---|---|
| **Q15029** | 116 kDa U5 small nuclear ribonucleoprotein component | 1.35E-01 | 1.07E+00 | 3.32E-01 | 0.031 |
| **Q15050** | Ribosome biogenesis regulatory protein homolog | 3.30E-02 | 1.66E-01 | 5.91E-02 | 0.032 |
| **Q15061** | WD repeat-containing protein 43 | 4.51E-02 | 3.87E-01 | 1.04E-01 | 0.033 |
| **Q15149** | Plectin | 2.68E-01 | 1.36E+00 | 6.26E-01 | 0.033 |
| **Q15233** | Non-POU domain-containing octamer-binding protein | 7.00E-02 | 3.19E-01 | 1.41E-01 | 0.033 |
| **Q15269** | Periodic tryptophan protein 2 homolog | 2.48E-01 | 3.88E-01 | 1.30E-01 | 0.033 |
| **Q15287** | RNA-binding protein with serine-rich domain 1 | 5.57E-03 | 2.39E-02 | 9.91E-03 | 0.033 |
| **Q15291** | Retinoblastoma-binding protein 5 | 1.71E-03 | 4.82E-02 | 1.76E-02 | 0.033 |
| **Q15365** | Poly(rC)-binding protein 1 | 1.50E-02 | 9.37E-02 | 3.88E-02 | 0.033 |
| **Q15366** | Poly(rC)-binding protein 2 | 5.56E-02 | 1.47E-01 | 6.17E-02 | 0.033 |
| **Q15393** | Splicing factor 3B subunit 3 | 1.32E-01 | 1.10E+00 | 4.38E-01 | 0.033 |
| **Q15397** | Pumilio homolog 3 | 6.37E-03 | 8.07E-02 | 2.69E-02 | 0.033 |
| **Q15424** | Scaffold attachment factor B1 | 1.20E-01 | 6.32E-01 | 2.15E-01 | 0.033 |
| **Q15427** | Splicing factor 3B subunit 4 | 1.70E-03 | 2.15E-02 | 1.06E-02 | 0.033 |
| **Q15428** | Splicing factor 3A subunit 2 | 1.62E-02 | 8.64E-02 | 3.35E-02 | 0.033 |
| **Q15436** | Protein transport protein Sec23A | 2.83E-03 | 2.47E-02 | 1.38E-02 | 0.033 |
| **Q15437** | Protein transport protein Sec23B | 1.56E-02 | 1.86E-01 | 1.14E-01 | 0.033 |
| **Q15459** | Splicing factor 3A subunit 1 | 6.99E-02 | 3.01E-01 | 1.15E-01 | 0.033 |
| **Q15717** | ELAV-like protein 1 | 6.88E-01 | 1.04E+00 | 4.62E-01 | 0.033 |
| **Q16352** | Alpha-internexin | 2.90E-01 | 2.59E+00 | 1.05E+00 | 0.033 |
| **Q16531** | DNA damage-binding protein 1 | 4.68E-02 | 3.06E-01 | 1.04E-01 | 0.033 |
| **Q16629** | Serine/arginine-rich splicing factor 7 | 5.83E-02 | 2.32E-01 | 7.05E-02 | 0.033 |
| **Q16643** | Drebrin | 1.09E-01 | 1.37E+00 | 6.14E-01 | 0.033 |
| **Q16891** | MICOS complex subunit MIC60 | 1.19E-01 | 1.20E+00 | 4.31E-01 | 0.033 |
| **Q1KMD3** | Heterogeneous nuclear ribonucleoprotein U-like protein 2 | 1.52E-01 | 1.97E+00 | 5.10E-01 | 0.033 |
| **Q29RF7** | Sister chromatid cohesion protein PDS5 homolog A | 3.12E-03 | 1.29E-02 | 4.53E-03 | 0.033 |
| **Q2TAY7** | WD40 repeat-containing protein SMU1 | 2.75E-02 | 2.82E-01 | 9.36E-02 | 0.033 |
| **Q49A26** | Putative oxidoreductase GLYR1 | 4.64E-03 | 4.12E-02 | 1.64E-02 | 0.033 |
| **Q53GS9** | U4/U6.U5 tri-snRNP-associated protein 2 | 3.14E-02 | 3.94E-02 | 1.46E-02 | 0.033 |
| **Q5BKZ1** | DBIRD complex subunit ZNF326 | 3.26E-02 | 1.26E-01 | 4.10E-02 | 0.034 |
| **Q5JRA6** | Melanoma inhibitory activity protein 3 | 4.88E-02 | 2.46E-01 | 1.52E-01 | 0.034 |
| **Q5JTH9** | RRP12-like protein | 8.43E-03 | 3.13E-01 | 1.17E-01 | 0.034 |
| **Q5JWF2** | Guanine nucleotide-binding protein G | 1.95E-02 | 9.75E-02 | 4.28E-02 | 0.034 |
| **Q5QJE6** | Deoxynucleotidyltransferase terminal-interacting protein 2 | 8.12E-02 | 1.25E-01 | 4.11E-02 | 0.034 |
| **Q5RKV6** | Exosome complex component MTR3 | 3.98E-03 | 3.73E-02 | 1.43E-02 | 0.034 |
| **Q5SRE5** | Nucleoporin NUP188 homolog | 7.07E-03 | 8.38E-02 | 3.89E-02 | 0.034 |
| **Q5SSJ5** | Heterochromatin protein 1-binding protein 3 | 5.34E-02 | 7.68E-01 | 2.28E-01 | 0.034 |
| **Q5SY16** | Polynucleotide 5'-hydroxyl-kinase NOL9 | 1.53E-02 | 1.79E-01 | 5.82E-02 | 0.034 |
| **Q5T280** | Putative methyltransferase C9orf114 | 1.66E-02 | 2.65E-02 | 7.88E-03 | 0.034 |
| **Q5T9A4** | ATPase family AAA domain-containing protein 3B | 3.35E-03 | 3.06E-02 | 7.95E-03 | 0.034 |

| | | | | | |
|---|---|---|---|---|---|
| **Q5TA45** | Integrator complex subunit 11 | 2.25E-03 | 3.80E-02 | 1.57E-02 | 0.034 |
| **Q5VTE0** | Putative elongation factor 1-alpha-like 3 | 2.95E-01 | 6.52E-01 | 3.43E-01 | 0.034 |
| **Q68CQ4** | Digestive organ expansion factor homolog | 1.80E-03 | 3.42E-02 | 8.41E-03 | 0.034 |
| **Q68E01** | Integrator complex subunit 3 | 5.98E-04 | 3.02E-02 | 9.71E-03 | 0.034 |
| **Q69YN4** | Protein virilizer homolog | 3.03E-03 | 2.76E-02 | 1.14E-02 | 0.034 |
| **Q6DKI1** | 60S ribosomal protein L7-like 1 | 6.88E-03 | 4.78E-02 | 1.63E-02 | 0.034 |
| **Q6DRA6** | Putative histone H2B type 2-D | 1.06E+00 | 4.72E+00 | 1.56E+00 | 0.034 |
| **Q6FI13** | Histone H2A type 2-A | 4.49E-03 | 5.33E-02 | 1.61E-02 | 0.034 |
| **Q6P1J9** | Parafibromin | 3.79E-03 | 3.91E-02 | 1.46E-02 | 0.034 |
| **Q6P2Q9** | Pre-mRNA-processing-splicing factor 8 | 1.98E-01 | 1.41E+00 | 5.31E-01 | 0.034 |
| **Q6PL18** | ATPase family AAA domain-containing protein 2 | 7.56E-03 | 3.72E-02 | 1.53E-02 | 0.034 |
| **Q6UN15** | Pre-mRNA 3'-end-processing factor FIP1 | 1.29E-01 | 8.43E-02 | 5.64E-02 | 0.034 |
| **Q6UXN9** | WD repeat-containing protein 82 | 6.37E-03 | 4.85E-02 | 1.96E-02 | 0.034 |
| **Q6ZRI8** | Rho GTPase-activating protein 36 | 5.56E-03 | 5.94E-02 | 2.60E-02 | 0.034 |
| **Q71DI3** | Histone H3.2 | 9.17E-02 | 2.03E-01 | 9.41E-02 | 0.034 |
| **Q71U36** | Tubulin alpha-1A chain | 4.78E-02 | 1.31E-01 | 6.02E-02 | 0.034 |
| **Q71UI9** | Histone H2A.V | 4.19E-01 | 1.45E+00 | 5.44E-01 | 0.034 |
| **Q7KZ85** | Transcription elongation factor SPT6 | 1.45E-02 | 9.71E-02 | 3.88E-02 | 0.034 |
| **Q7L2E3** | Putative ATP-dependent RNA helicase DHX30 | 8.98E-04 | 1.20E-02 | 6.82E-03 | 0.034 |
| **Q7Z3B4** | Nucleoporin p54 | 4.79E-03 | 8.54E-02 | 2.83E-02 | 0.034 |
| **Q7Z3K3** | Pogo transposable element with ZNF domain | 2.30E-02 | 3.13E-01 | 1.09E-01 | 0.034 |
| **Q7Z7K6** | Centromere protein V | 5.03E-03 | 9.72E-02 | 3.32E-02 | 0.034 |
| **Q86U42** | Polyadenylate-binding protein 2 | 6.73E-02 | 1.80E-01 | 5.62E-02 | 0.034 |
| **Q86U86** | Protein polybromo-1 | 3.43E-02 | 2.81E-01 | 1.08E-01 | 0.034 |
| **Q86W42** | THO complex subunit 6 homolog | 1.08E-02 | 1.15E-01 | 4.27E-02 | 0.034 |
| **Q8IUE6** | Histone H2A type 2-B | 2.72E-01 | 8.76E-01 | 3.48E-01 | 0.034 |
| **Q8IWA0** | WD repeat-containing protein 75 | 4.76E-03 | 1.35E-01 | 4.87E-02 | 0.034 |
| **Q8IWX8** | Calcium homeostasis endoplasmic reticulum protein | 6.73E-03 | 2.74E-02 | 9.72E-03 | 0.034 |
| **Q8IX01** | SURP and G-patch domain-containing protein 2 | 1.64E-02 | 5.41E-02 | 1.61E-02 | 0.034 |
| **Q8IX12** | Cell division cycle and apoptosis regulator protein 1 | 2.81E-03 | 2.18E-02 | 7.98E-03 | 0.034 |
| **Q8IXT5** | RNA-binding protein 12B | 1.30E-02 | 1.33E-01 | 4.55E-02 | 0.034 |
| **Q8IY81** | pre-rRNA processing protein FTSJ3 | 6.78E-02 | 2.46E-01 | 5.57E-02 | 0.034 |
| **Q8IZL8** | Proline-, glutamic acid- and leucine-rich protein 1 | 4.46E-02 | 3.26E-01 | 1.04E-01 | 0.034 |
| **Q8N163** | Cell cycle and apoptosis regulator protein 2 | 6.07E-02 | 5.90E-01 | 1.68E-01 | 0.034 |
| **Q8N1F7** | Nuclear pore complex protein Nup93 | 8.14E-02 | 4.76E-01 | 1.88E-01 | 0.034 |
| **Q8N684** | Cleavage and polyadenylation specificity factor subunit 7 | 6.52E-03 | 4.91E-02 | 2.12E-02 | 0.034 |
| **Q8NEJ9** | Neuroguidin | 3.14E-03 | 2.40E-02 | 4.93E-03 | 0.034 |
| **Q8NFH4** | Nucleoporin Nup37 | 9.54E-03 | 7.93E-02 | 2.54E-02 | 0.034 |
| **Q8NI27** | THO complex subunit 2 | 5.48E-02 | 3.54E-01 | 1.32E-01 | 0.034 |
| **Q8NI36** | WD repeat-containing protein 36 | 7.63E-02 | 6.16E-01 | 2.35E-01 | 0.034 |
| **Q8TDD1** | ATP-dependent RNA helicase DDX54 | 4.19E-03 | 3.51E-02 | 1.25E-02 | 0.034 |
| **Q8TDN6** | Ribosome biogenesis protein BRX1 homolog | 4.05E-02 | 3.81E-01 | 1.24E-01 | 0.034 |

| | | | | | |
|---|---|---|---|---|---|
| **Q8TED0** | U3 small nucleolar RNA-associated protein 15 homolog | 1.61E-02 | 1.97E-01 | 6.66E-02 | 0.034 |
| **Q8TEM1** | Nuclear pore membrane glycoprotein 210 | 1.71E-01 | 8.82E-01 | 3.58E-01 | 0.034 |
| **Q8WTT2** | Nucleolar complex protein 3 homolog | 2.22E-02 | 1.17E-01 | 3.76E-02 | 0.034 |
| **Q8WUM0** | Nuclear pore complex protein Nup133 | 7.67E-02 | 4.99E-01 | 1.75E-01 | 0.034 |
| **Q8WWQ0** | PH-interacting protein | 4.51E-02 | 1.08E-01 | 4.04E-02 | 0.034 |
| **Q8WWY3** | U4/U6 small nuclear ribonucleoprotein Prp31 | 6.10E-03 | 3.68E-02 | 1.22E-02 | 0.034 |
| **Q8WXH0** | Nesprin-2 | 2.45E-02 | 5.86E-02 | 2.85E-02 | 0.034 |
| **Q8WYP5** | Protein ELYS | 7.41E-03 | 1.01E-01 | 3.97E-02 | 0.034 |
| **Q92481** | Transcription factor AP-2-beta | 6.23E-03 | 8.00E-02 | 3.18E-02 | 0.036 |
| **Q92499** | ATP-dependent RNA helicase DDX1 | 1.51E-02 | 8.35E-02 | 3.01E-02 | 0.036 |
| **Q92621** | Nuclear pore complex protein Nup205 | 1.05E-01 | 6.82E-01 | 2.80E-01 | 0.036 |
| **Q92747** | Actin-related protein 2/3 complex subunit 1A | 5.52E-04 | 1.13E-02 | 3.74E-03 | 0.036 |
| **Q92769** | Histone deacetylase 2 | 1.38E-02 | 9.47E-02 | 2.67E-02 | 0.036 |
| **Q92797** | Symplekin | 3.94E-03 | 2.31E-02 | 7.54E-03 | 0.036 |
| **Q92841** | Probable ATP-dependent RNA helicase DDX17 | 7.78E-02 | 5.88E-01 | 2.09E-01 | 0.036 |
| **Q92922** | SWI/SNF complex subunit SMARCC1 | 3.69E-02 | 7.77E-02 | 3.23E-02 | 0.036 |
| **Q92945** | Far upstream element-binding protein 2 | 2.06E-01 | 1.03E+00 | 3.63E-01 | 0.038 |
| **Q92979** | Ribosomal RNA small subunit methyltransferase NEP1 | 1.22E-02 | 1.24E-01 | 4.63E-02 | 0.038 |
| **Q93009** | Ubiquitin carboxyl-terminal hydrolase 7 | 2.94E-03 | 9.69E-03 | 4.37E-03 | 0.038 |
| **Q969G3** | SWI/SNF-related matrix-associated actin-dependent regulator of chromatin subfamily E member 1 | 8.32E-03 | 1.23E-01 | 3.88E-02 | 0.038 |
| **Q969X6** | U3 small nucleolar RNA-associated protein 4 homolog | 6.33E-03 | 1.13E-01 | 4.56E-02 | 0.038 |
| **Q96A72** | Protein mago nashi homolog 2 | 9.39E-03 | 6.93E-02 | 2.03E-02 | 0.038 |
| **Q96DI7** | U5 small nuclear ribonucleoprotein 40 kDa protein | 1.94E-02 | 1.13E-01 | 4.18E-02 | 0.038 |
| **Q96E39** | RNA binding motif protein, X-linked-like-1 | 1.04E-02 | 1.55E-01 | 4.31E-02 | 0.038 |
| **Q96EE3** | Nucleoporin SEH1 | 3.54E-03 | 3.73E-02 | 1.53E-02 | 0.038 |
| **Q96GM5** | SWI/SNF-related matrix-associated actin-dependent regulator of chromatin subfamily D member 1 | 4.45E-03 | 3.15E-02 | 1.53E-03 | 0.038 |
| **Q96GQ7** | Probable ATP-dependent RNA helicase DDX27 | 2.14E-01 | 3.59E-01 | 1.11E-01 | 0.038 |
| **Q96HA1** | Nuclear envelope pore membrane protein POM 121 | 1.61E-03 | 1.53E-02 | 4.58E-03 | 0.038 |
| **Q96HS1** | Serine/threonine-protein phosphatase PGAM5, mitochondrial | 1.21E-02 | 1.14E-01 | 4.26E-02 | 0.038 |
| **Q96HW7** | Integrator complex subunit 4 | 8.49E-04 | 1.67E-02 | 7.06E-03 | 0.038 |
| **Q96J01** | THO complex subunit 3 | 6.40E-03 | 4.90E-02 | 1.58E-02 | 0.038 |
| **Q96JM2** | Zinc finger protein 462 | 3.40E-03 | 2.74E-03 | 2.66E-03 | 0.038 |
| **Q96KR1** | Zinc finger RNA-binding protein | 2.51E-02 | 7.83E-02 | 2.34E-02 | 0.038 |
| **Q96L91** | E1A-binding protein p400 | 1.20E-03 | 7.87E-03 | 4.93E-03 | 0.04 |
| **Q96ME7** | Zinc finger protein 512 | 3.03E-02 | 1.23E-01 | 4.52E-02 | 0.04 |
| **Q96MU7** | YTH domain-containing protein 1 | 8.22E-03 | 5.05E-02 | 1.80E-02 | 0.041 |
| **Q96PK6** | RNA-binding protein 14 | 1.27E-02 | 7.15E-02 | 2.64E-02 | 0.041 |

| | | | | | |
|---|---|---|---|---|---|
| **Q96QC0** | Serine/threonine-protein phosphatase 1 regulatory subunit 10 | 1.81E-01 | 6.28E-02 | 1.83E-02 | 0.041 |
| **Q96S97** | Myeloid-associated differentiation marker | 6.13E-03 | 6.11E-02 | 2.70E-02 | 0.041 |
| **Q96SI9** | Spermatid perinuclear RNA-binding protein | 1.47E-01 | 6.71E-02 | 5.21E-02 | 0.041 |
| **Q96ST3** | Paired amphipathic helix protein Sin3a | 2.55E-03 | 6.00E-02 | 2.03E-02 | 0.041 |
| **Q96T23** | Remodeling and spacing factor 1 | 1.48E-02 | 3.87E-02 | 1.65E-02 | 0.041 |
| **Q99453** | Paired mesoderm homeobox protein 2B | 3.36E-02 | 2.19E-01 | 7.23E-02 | 0.041 |
| **Q99459** | Cell division cycle 5-like protein | 3.58E-02 | 2.55E-01 | 9.49E-02 | 0.041 |
| **Q99496** | E3 ubiquitin-protein ligase RING2 | 9.28E-03 | 7.10E-02 | 2.57E-02 | 0.041 |
| **Q99567** | Nuclear pore complex protein Nup88 | 8.35E-03 | 1.20E-01 | 4.53E-02 | 0.041 |
| **Q99729** | Heterogeneous nuclear ribonucleoprotein A/B | 3.99E-02 | 6.19E-01 | 1.51E-01 | 0.041 |
| **Q99848** | Probable rRNA-processing protein EBP2 | 7.72E-03 | 7.57E-02 | 1.99E-02 | 0.041 |
| **Q99873** | Protein arginine N-methyltransferase 1 | 1.88E-02 | 8.09E-02 | 4.19E-02 | 0.041 |
| **Q99880** | Histone H2B type 1-L | 6.66E+00 | 2.29E+01 | 7.76E+00 | 0.043 |
| **Q9BQ39** | ATP-dependent RNA helicase DDX50 | 7.67E-03 | 8.27E-02 | 2.72E-02 | 0.043 |
| **Q9BQE3** | Tubulin alpha-1C chain | 3.81E-02 | 1.17E-01 | 4.98E-02 | 0.043 |
| **Q9BQG0** | Myb-binding protein 1A | 9.49E-02 | 9.18E-01 | 3.50E-01 | 0.043 |
| **Q9BSC4** | Nucleolar protein 10 | 5.83E-03 | 9.15E-02 | 2.89E-02 | 0.043 |
| **Q9BUQ8** | Probable ATP-dependent RNA helicase DDX23 | 2.45E-03 | 5.78E-02 | 1.84E-02 | 0.043 |
| **Q9BV38** | WD repeat-containing protein 18 | 7.75E-02 | 2.56E-01 | 9.45E-02 | 0.043 |
| **Q9BVA1** | Tubulin beta-2B chain | 5.13E-03 | 2.86E-02 | 1.81E-02 | 0.043 |
| **Q9BVI4** | Nucleolar complex protein 4 homolog | 6.81E-03 | 6.53E-02 | 2.75E-02 | 0.043 |
| **Q9BVJ6** | U3 small nucleolar RNA-associated protein 14 homolog A | 2.11E-02 | 2.38E-01 | 6.71E-02 | 0.044 |
| **Q9BVL2** | Nucleoporin p58/p45 | 5.78E-03 | 3.98E-02 | 1.57E-02 | 0.044 |
| **Q9BVP2** | Guanine nucleotide-binding protein-like 3 | 2.25E-02 | 1.22E-01 | 3.75E-02 | 0.044 |
| **Q9BW27** | Nuclear pore complex protein Nup85 | 3.59E-02 | 3.03E-01 | 8.38E-02 | 0.044 |
| **Q9BXP5** | Serrate RNA effector molecule homolog | 5.23E-03 | 4.95E-02 | 2.92E-02 | 0.048 |
| **Q9BYG3** | MKI67 FHA domain-interacting nucleolar phosphoprotein | 1.55E-02 | 1.00E-01 | 3.00E-02 | 0.048 |
| **Q9BZE4** | Nucleolar GTP-binding protein 1 | 3.62E-02 | 3.03E-01 | 1.00E-01 | 0.048 |
| **Q9BZF1** | Oxysterol-binding protein-related protein 8 | 2.69E-03 | 4.72E-02 | 1.89E-02 | 0.048 |
| **Q9BZJ0** | Crooked neck-like protein 1 | 7.10E-03 | 2.47E-02 | 7.42E-03 | 0.048 |
| **Q9GZL7** | Ribosome biogenesis protein WDR12 | 2.31E-02 | 1.24E-01 | 4.46E-02 | 0.048 |
| **Q9GZR2** | RNA exonuclease 4 | 1.78E-03 | 1.29E-02 | 5.76E-03 | 0.048 |
| **Q9GZR7** | ATP-dependent RNA helicase DDX24 | 1.19E-02 | 6.37E-02 | 2.30E-02 | 0.048 |
| **Q9H0A0** | RNA cytidine acetyltransferase | 1.65E-01 | 8.04E-01 | 2.83E-01 | 0.048 |
| **Q9H0D6** | 5'-3' exoribonuclease 2 | 2.21E-03 | 4.85E-02 | 1.48E-02 | 0.049 |
| **Q9H0S4** | Probable ATP-dependent RNA helicase DDX47 | 2.34E-02 | 3.08E-01 | 1.06E-01 | 0.049 |
| **Q9H2P0** | Activity-dependent neuroprotector homeobox protein | 8.98E-04 | 2.61E-02 | 7.06E-03 | 0.049 |
| **Q9H307** | Pinin | 1.20E-03 | 5.14E-02 | 1.81E-02 | 0.05 |
| **Q9H4L4** | Sentrin-specific protease 3 | 2.39E-02 | 6.29E-02 | 2.90E-02 | 0.05 |
| **Q9H583** | HEAT repeat-containing protein 1 | 6.78E-02 | 5.37E-01 | 2.09E-01 | 0.05 |
| **Q9H6R4** | Nucleolar protein 6 | 5.65E-02 | 2.84E-01 | 1.06E-01 | 0.05 |
| **Q9H7B2** | Ribosome production factor 2 homolog | 1.77E-02 | 2.19E-01 | 6.23E-02 | 0.05 |

| | | | | | |
|---|---|---|---|---|---|
| **Q9H8H0** | Nucleolar protein 11 | 1.36E-02 | 2.37E-01 | 8.11E-02 | 0.05 |
| **Q9HCD5** | Nuclear receptor coactivator 5 | 5.77E-03 | 9.07E-02 | 2.14E-02 | 0.05 |
| **Q9NPE3** | H/ACA ribonucleoprotein complex subunit 3 | 3.12E-02 | 2.10E-02 | 7.62E-03 | 0.052 |
| **Q9NQT4** | Exosome complex component RRP46 | 5.09E-03 | 4.06E-02 | 1.48E-02 | 0.052 |
| **Q9NQZ2** | Something about silencing protein 10 | 4.04E-03 | 2.37E-02 | 6.49E-03 | 0.053 |
| **Q9NR30** | Nucleolar RNA helicase 2 | 2.91E-01 | 3.04E+00 | 9.66E-01 | 0.053 |
| **Q9NRG9** | Aladin | 1.63E-02 | 2.34E-01 | 8.55E-02 | 0.053 |
| **Q9NRX1** | RNA-binding protein PNO1 | 4.42E-03 | 2.75E-02 | 1.00E-02 | 0.053 |
| **Q9NTI5** | Sister chromatid cohesion protein PDS5 homolog B | 1.77E-03 | 7.06E-03 | 4.56E-03 | 0.053 |
| **Q9NU22** | Midasin | 1.80E-03 | 8.15E-03 | 3.78E-03 | 0.053 |
| **Q9NV06** | DDB1- and CUL4-associated factor 13 | 6.12E-03 | 2.52E-02 | 9.15E-03 | 0.053 |
| **Q9NV31** | U3 small nucleolar ribonucleoprotein protein IMP3 | 2.04E-02 | 1.21E-01 | 3.03E-02 | 0.055 |
| **Q9NVI7** | ATPase family AAA domain-containing protein 3A | 5.17E-02 | 6.20E-02 | 2.25E-02 | 0.055 |
| **Q9NVP1** | ATP-dependent RNA helicase DDX18 | 2.08E-01 | 6.77E-01 | 2.52E-01 | 0.055 |
| **Q9NW13** | RNA-binding protein 28 | 3.10E-02 | 1.89E-01 | 6.32E-02 | 0.055 |
| **Q9NWH9** | SAFB-like transcription modulator | 6.67E-03 | 1.02E-01 | 2.99E-02 | 0.055 |
| **Q9NWX6** | Probable tRNA | 3.84E-01 | 1.89E-01 | 1.46E-01 | 0.055 |
| **Q9NX24** | H/ACA ribonucleoprotein complex subunit 2 | 7.18E-03 | 3.25E-02 | 9.60E-03 | 0.055 |
| **Q9NX63** | MICOS complex subunit MIC19 | 6.43E-03 | 8.27E-02 | 2.74E-02 | 0.057 |
| **Q9NXF1** | Testis-expressed sequence 10 protein | 2.82E-02 | 1.24E-01 | 3.74E-02 | 0.057 |
| **Q9NY12** | H/ACA ribonucleoprotein complex subunit 1 | 4.67E-02 | 1.77E-01 | 6.83E-02 | 0.057 |
| **Q9NY93** | Probable ATP-dependent RNA helicase DDX56 | 4.53E-02 | 9.25E-02 | 3.64E-02 | 0.057 |
| **Q9NYF8** | Bcl-2-associated transcription factor 1 | 9.90E-03 | 5.58E-02 | 1.97E-02 | 0.057 |
| **Q9NYH9** | U3 small nucleolar RNA-associated protein 6 homolog | 3.22E-02 | 1.39E-01 | 5.62E-02 | 0.057 |
| **Q9P0M6** | Core histone macro-H2A.2 | 1.46E-01 | 1.02E+00 | 3.45E-01 | 0.059 |
| **Q9P2I0** | Cleavage and polyadenylation specificity factor subunit 2 | 5.25E-03 | 2.73E-02 | 1.21E-02 | 0.06 |
| **Q9P2K5** | Myelin expression factor 2 | 7.43E-03 | 6.51E-02 | 2.51E-02 | 0.063 |
| **Q9UBU9** | Nuclear RNA export factor 1 | 2.96E-02 | 2.42E-01 | 8.82E-02 | 0.063 |
| **Q9UHB6** | LIM domain and actin-binding protein 1 | 2.49E-02 | 1.68E-01 | 6.60E-02 | 0.063 |
| **Q9UHX1** | Poly(U)-binding-splicing factor | 5.09E-03 | 1.80E-02 | 9.56E-03 | 0.063 |
| **Q9UIG0** | Tyrosine-protein kinase BAZ1B | 8.85E-02 | 9.61E-01 | 3.60E-01 | 0.063 |
| **Q9UKF6** | Cleavage and polyadenylation specificity factor subunit 3 | 1.65E-03 | 8.00E-02 | 3.01E-02 | 0.063 |
| **Q9UKM9** | RNA-binding protein Raly | 3.75E-01 | 2.55E+00 | 6.68E-01 | 0.066 |
| **Q9UKN8** | General transcription factor 3C polypeptide 4 | 8.27E-03 | 1.85E-02 | 1.11E-02 | 0.066 |
| **Q9UKX7** | Nuclear pore complex protein Nup50 | 3.73E-03 | 2.37E-02 | 9.33E-03 | 0.066 |
| **Q9ULH0** | Kinase D-interacting substrate of 220 kDa | 1.20E-03 | 9.14E-03 | 3.46E-03 | 0.066 |
| **Q9ULV4** | Coronin-1C | 6.13E-03 | 1.22E-01 | 5.42E-02 | 0.066 |
| **Q9UM54** | Unconventional myosin-VI | 7.98E-03 | 2.82E-02 | 2.64E-02 | 0.07 |
| **Q9UMS4** | Pre-mRNA-processing factor 19 | 2.01E-01 | 1.10E+00 | 3.84E-01 | 0.075 |
| **Q9UMS6** | Synaptopodin-2 | 1.18E-01 | 4.47E-01 | 2.04E-01 | 0.075 |
| **Q9UNX3** | 60S ribosomal protein L26-like 1 | 6.24E-02 | 1.86E-01 | 4.69E-02 | 0.075 |

| | | | | | |
|---|---|---|---|---|---|
| **Q9UNX4** | WD repeat-containing protein 3 | 5.22E-02 | 5.85E-01 | 2.01E-01 | 0.075 |
| **Q9UQE7** | Structural maintenance of chromosomes protein 3 | 9.34E-02 | 3.10E-01 | 1.06E-01 | 0.077 |
| **Q9Y224** | UPF0568 protein C14orf166 | 2.26E-03 | 3.43E-02 | 1.14E-02 | 0.079 |
| **Q9Y230** | RuvB-like 2 | 9.59E-02 | 8.37E-01 | 3.02E-01 | 0.079 |
| **Q9Y265** | RuvB-like 1 | 1.43E-01 | 6.54E-01 | 2.41E-01 | 0.08 |
| **Q9Y2H5** | Pleckstrin homology domain-containing family A member 6 | 6.50E-03 | 4.47E-02 | 2.25E-02 | 0.082 |
| **Q9Y2P8** | RNA 3'-terminal phosphate cyclase-like protein | 1.70E-03 | 2.10E-02 | 7.41E-03 | 0.082 |
| **Q9Y2R4** | Probable ATP-dependent RNA helicase DDX52 | 2.09E-03 | 2.90E-02 | 3.89E-03 | 0.082 |
| **Q9Y2W1** | Thyroid hormone receptor-associated protein 3 | 4.46E-03 | 3.49E-02 | 1.20E-02 | 0.084 |
| **Q9Y2X3** | Nucleolar protein 58 | 1.00E-01 | 8.11E-01 | 2.46E-01 | 0.086 |
| **Q9Y3B4** | Splicing factor 3B subunit 6 | 1.16E-02 | 2.82E-02 | 8.93E-03 | 0.086 |
| **Q9Y3I0** | tRNA-splicing ligase RtcB homolog | 2.39E-03 | 4.36E-02 | 1.54E-02 | 0.086 |
| **Q9Y3T9** | Nucleolar complex protein 2 homolog | 1.69E-02 | 2.83E-01 | 8.94E-02 | 0.086 |
| **Q9Y4A5** | Transformation/transcription domain-associated protein | 3.01E-03 | 3.87E-02 | 1.49E-02 | 0.086 |
| **Q9Y4W2** | Ribosomal biogenesis protein LAS1L | 5.34E-02 | 2.59E-01 | 7.42E-02 | 0.092 |
| **Q9Y512** | Sorting and assembly machinery component 50 homolog | 1.26E-02 | 2.15E-01 | 9.97E-02 | 0.092 |
| **Q9Y5B9** | FACT complex subunit SPT16 | 2.27E-01 | 1.07E+00 | 3.48E-01 | 0.092 |
| **Q9Y5J1** | U3 small nucleolar RNA-associated protein 18 homolog | 4.93E-02 | 1.49E-01 | 4.75E-02 | 0.094 |
| **Q9Y5Q9** | General transcription factor 3C polypeptide 3 | 1.50E-03 | 2.21E-02 | 4.43E-03 | 0.094 |
| **Q9Y5S9** | RNA-binding protein 8A | 1.27E-02 | 1.64E-01 | 3.03E-02 | 0.094 |
| **Q9Y6K1** | DNA (cytosine-5)-methyltransferase 3A | 2.06E-02 | 1.47E-01 | 5.48E-02 | 0.094 |
| | ***p*-value > 0.1** | | | | |
| **P13645** | Keratin, type I cytoskeletal 10 | 8.08E+00 | 2.47E+00 | 2.71E+00 | 0.101 |
| **P04264** | Keratin, type II cytoskeletal 1 | 9.54E+00 | 3.10E+00 | 3.76E+00 | 0.101 |
| **Q14498** | RNA-binding protein 39 | 3.28E-02 | 5.03E-02 | 2.05E-02 | 0.108 |
| **P62829** | 60S ribosomal protein L23 | 1.55E-01 | 1.41E-01 | 6.92E-02 | 0.108 |
| **P62487** | DNA-directed RNA polymerase II subunit RPB7 | 3.95E-02 | 6.54E-02 | 1.39E-02 | 0.11 |
| **P62875** | DNA-directed RNA polymerases I, II, and III subunit RPABC5 | 3.11E-03 | 6.82E-03 | 7.87E-03 | 0.11 |
| **Q13838** | Spliceosome RNA helicase DDX39B | 1.50E-03 | 2.63E-02 | 8.65E-03 | 0.113 |
| **Q03164** | Histone-lysine N-methyltransferase 2A | 1.41E-03 | 5.94E-03 | 8.97E-04 | 0.113 |
| **Q92522** | Histone H1x | 2.99E-03 | 2.31E-02 | 6.04E-03 | 0.113 |
| **Q9NQT5** | Exosome complex component RRP40 | 3.82E-03 | 1.86E-02 | 5.06E-03 | 0.113 |
| **P31942** | Heterogeneous nuclear ribonucleoprotein H3 | 5.06E-02 | 1.37E-01 | 6.86E-02 | 0.118 |
| **P13639** | Elongation factor 2 | 9.33E-03 | 2.36E-02 | 1.30E-02 | 0.118 |
| **P35908** | Keratin, type II cytoskeletal 2 epidermal | 1.78E+00 | 1.17E+00 | 1.12E+00 | 0.123 |
| **P45973** | Chromobox protein homolog 5 | 3.44E-02 | 2.69E-02 | 7.28E-03 | 0.123 |
| **P01859** | Ig gamma-2 chain C region | 5.47E-01 | 1.40E-01 | 1.81E-01 | 0.123 |
| **Q12789** | General transcription factor 3C polypeptide 1 | 1.91E-02 | 1.88E-02 | 9.38E-03 | 0.129 |
| **P69905** | Hemoglobin subunit alpha | 3.79E-02 | 6.08E-02 | 3.95E-02 | 0.129 |
| **O43818** | U3 small nucleolar RNA-interacting protein 2 | 2.14E-03 | 4.44E-02 | 2.06E-03 | 0.129 |
| **P35658** | Nuclear pore complex protein Nup214 | 1.64E-02 | 3.15E-02 | 1.19E-02 | 0.132 |

| | | | | | |
|---|---|---|---|---|---|
| **P08779** | Keratin, type I cytoskeletal 16 | 6.18E-02 | 2.37E-02 | 4.14E-02 | 0.132 |
| **P07900** | Heat shock protein HSP 90-alpha | 4.19E-02 | 2.84E-02 | 3.55E-03 | 0.132 |
| **P02452** | Collagen alpha-1 | 5.30E+00 | 1.01E+00 | 1.12E+00 | 0.135 |
| **O00425** | Insulin-like growth factor 2 mRNA-binding protein 3 | 3.86E-02 | 3.59E-02 | 2.10E-02 | 0.135 |
| **Q9P258** | Protein RCC2 | 1.74E-03 | 4.52E-02 | 1.50E-02 | 0.147 |
| **P41223** | Protein BUD31 homolog | 4.88E-03 | 1.64E-02 | 5.65E-03 | 0.154 |
| **Q8NBJ5** | Procollagen galactosyltransferase 1 | 3.89E-01 | 1.25E-01 | 6.84E-02 | 0.157 |
| **Q04837** | Single-stranded DNA-binding protein, mitochondrial | 3.19E-02 | 5.66E-02 | 2.03E-02 | 0.172 |
| **Q68CP9** | AT-rich interactive domain-containing protein 2 | 3.96E-03 | 7.54E-03 | 1.03E-02 | 0.183 |
| **P35637** | RNA-binding protein FUS | 1.32E-01 | 1.75E-01 | 9.64E-02 | 0.183 |
| **O15226** | NF-kappa-B-repressing factor | 1.20E-03 | 3.84E-02 | 2.78E-03 | 0.183 |
| **P46778** | 60S ribosomal protein L21 | 8.14E-03 | 4.82E-02 | 1.56E-02 | 0.192 |
| **P02538** | Keratin, type II cytoskeletal 6A | 1.49E-01 | 2.77E-02 | 2.71E-02 | 0.2 |
| **P13646** | Keratin, type I cytoskeletal 13 | 6.59E-03 | 2.47E-02 | 3.63E-03 | 0.204 |
| **Q96JM3** | Chromosome alignment-maintaining phosphoprotein 1 | 3.56E-02 | 1.32E-01 | 1.65E-02 | 0.209 |
| **Q96G21** | U3 small nucleolar ribonucleoprotein protein IMP4 | 4.02E-02 | 4.76E-02 | 1.04E-02 | 0.218 |
| **P35232** | Prohibitin | 2.92E-03 | 9.24E-03 | 3.36E-03 | 0.218 |
| **Q02413** | Desmoglein-1 | 8.23E-03 | 9.86E-03 | 1.01E-02 | 0.223 |
| **O60568** | Procollagen-lysine,2-oxoglutarate 5-dioxygenase 3 | 2.48E+00 | 7.98E-01 | 5.29E-01 | 0.243 |
| **Q9UKV3** | Apoptotic chromatin condensation inducer in the nucleus | 2.68E-01 | 8.75E-02 | 4.16E-02 | 0.248 |
| **Q99943** | 1-acyl-sn-glycerol-3-phosphate acyltransferase alpha | 4.34E-01 | 1.49E-01 | 9.86E-02 | 0.264 |
| **P19474** | E3 ubiquitin-protein ligase TRIM21 | 2.20E-01 | 2.59E-01 | 1.88E-01 | 0.282 |
| **Q02543** | 60S ribosomal protein L18a | 2.39E-01 | 1.22E-01 | 3.65E-02 | 0.282 |
| **P07477** | Trypsin-1 | 3.52E-01 | 1.15E-01 | 8.77E-02 | 0.333 |
| **P02751** | Fibronectin | 1.37E-02 | 8.01E-03 | 7.37E-03 | 0.34 |
| **Q5D862** | Filaggrin-2 | 8.13E-02 | 1.77E-02 | 1.76E-02 | 0.369 |
| **P11216** | Glycogen phosphorylase, brain form | 3.76E-01 | 1.83E-01 | 4.34E-02 | 0.408 |
| **P81605** | Dermcidin | 5.61E-02 | 1.46E-02 | 1.62E-02 | 0.442 |
| **P01621** | Ig kappa chain V-III region NG9 | 4.02E-02 | 1.83E-02 | 1.08E-02 | 0.459 |
| **O15061** | Synemin | 3.35E-03 | 2.58E-03 | 8.38E-04 | 0.536 |
| **Q10570** | Cleavage and polyadenylation specificity factor subunit 1 | 1.69E+00 | 5.92E-01 | 1.33E-01 | 0.644 |